

# NAVAL POSTGRADUATE SCHOOL

## Monterey, California



### THESIS

**AVIONICS SYSTEM DEVELOPMENT  
FOR A ROTARY WING  
UNMANNED AERIAL VEHICLE**

by

Daniel S. Greer

June 1998

Thesis Advisor:

Russ W. Duren

Approved for public release; distribution is unlimited.

DTIC QUALITY INSPECTED 1

19980807 040

# REPORT DOCUMENTATION PAGE

Form Approved  
OMB No. 0704-0188

Public reporting burden for this collection of information is estimated to average 1 hour per response, including the time for reviewing instruction, searching existing data sources, gathering and maintaining the data needed, and completing and reviewing the collection of information. Send comments regarding this burden estimate or any other aspect of this collection of information, including suggestions for reducing this burden, to Washington headquarters Services, Directorate for Information Operations and Reports, 1215 Jefferson Davis Highway, Suite 1204, Arlington, VA 22202-4302, and to the Office of Management and Budget, Paperwork Reduction Project (0704-0188) Washington DC 20503.

1. AGENCY USE ONLY (Leave blank)

2. REPORT DATE  
June 1998

3. REPORT TYPE AND DATES COVERED  
Master's Thesis

4. TITLE AND SUBTITLE  
AVIONICS SYSTEM DEVELOPMENT FOR A ROTARY WING UNMANNED  
AERIAL VEHICLE

5. FUNDING NUMBERS

6. AUTHOR(S)  
Greer, Daniel S.

7. PERFORMING ORGANIZATION NAME(S) AND ADDRESS(ES)  
Naval Postgraduate School  
Monterey, CA 93943-5000

8. PERFORMING  
ORGANIZATION REPORT  
NUMBER

9. SPONSORING / MONITORING AGENCY NAME(S) AND ADDRESS(ES)

10. SPONSORING /  
MONITORING  
AGENCY REPORT NUMBER

## 11. SUPPLEMENTARY NOTES

The views expressed in this thesis are those of the author and do not reflect the official policy or position of the Department of Defense or the U.S. Government.

## 12a. DISTRIBUTION / AVAILABILITY STATEMENT

Approved for public release; distribution is unlimited.

## 12b. DISTRIBUTION CODE

## 13. ABSTRACT (maximum 200 words)

The Naval Postgraduate School has developed a successful Rapid Flight Test Prototyping System (RFTPS) for the development of software for remote computer control of fixed wing Unmanned Aerial Vehicles (UAV). This thesis reviews the work accomplished to mount sensors on a small remote controlled helicopter with instrumentation compatible with the RFTPS: an inertial measurement unit, a Global Positioning System (GPS) receiver, an altitude sensor and associated power supply and telemetry equipment. A helicopter with sufficient lift capability was selected and a lightweight aluminum structure was built to serve as both an avionics platform for the necessary equipment and also as a landing skid. Since the altitude sensors used for fixed wing UAV's, such as barometric sensors and GPS, do not provide sufficient accuracy for low altitude hover control, a lightweight, precision altimeter was developed using ultrasound technology. Circuitry was developed to drive a Polaroid 6500 Series Ranging Module and process the output data in a form compatible with the RFTPS avionics architecture. Flight testing revealed severe vibrations throughout the helicopter. An alternative avionics package of reduced size was constructed to house the sonic altimeter and a three-axis accelerometer. Subsequent test flight results and recommendations for further research are provided.

## 14. SUBJECT TERMS

Unmanned Aerial Vehicles, avionics, sonic altimeter

15. NUMBER OF  
PAGES  
122

16. PRICE CODE

17. SECURITY  
CLASSIFICATION OF REPORT  
Unclassified

18. SECURITY CLASSIFICATION OF  
THIS PAGE  
Unclassified

19. SECURITY CLASSIFI- CATION  
OF ABSTRACT  
Unclassified

20. LIMITATION  
OF ABSTRACT  
UL



Approved for public release; distribution is unlimited

**AVIONICS SYSTEM DEVELOPMENT FOR A ROTARY WING  
UNMANNED AERIAL VEHICLE**

Daniel S. Greer  
Commander, United States Navy  
B.S., University of Texas, 1981

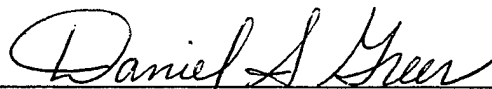
Submitted in partial fulfillment of the  
requirements for the degree of

**MASTER OF SCIENCE IN AERONAUTICAL ENGINEERING**

from the

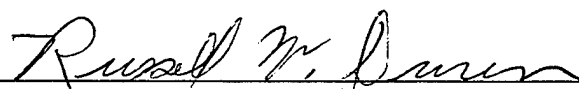
**NAVAL POSTGRADUATE SCHOOL  
June 1998**

Author:



Daniel S. Greer

Approved by:



Russ W. Duren, Thesis Advisor



Isaac I. Kaminer, Second Reader



Gerald H. Lindsey, Chairman  
Department of Aeronautics and Astronautics



## ABSTRACT

The Naval Postgraduate School has developed a successful Rapid Flight Test Prototyping System (RFTPS) for the development of software for remote computer control of fixed wing Unmanned Aerial Vehicles (UAV). This thesis reviews the work accomplished to mount sensors on a small remote controlled helicopter with instrumentation compatible with the RFTPS: an inertial measurement unit, a Global Positioning System (GPS) receiver, an altitude sensor and associated power supply and telemetry equipment. A helicopter with sufficient lift capability was selected and a lightweight aluminum structure was built to serve as both an avionics platform for the necessary equipment and also as a landing skid. Since the altitude sensors used for fixed wing UAV's, such as barometric sensors and GPS, do not provide sufficient accuracy for low altitude hover control, a lightweight, precision altimeter was developed using ultrasound technology. Circuitry was developed to drive a Polaroid 6500 Series Ranging Module and process the output data in a form compatible with the RFTPS avionics architecture. Flight testing revealed severe vibrations throughout the helicopter. An alternative avionics package of reduced size was constructed to house the sonic altimeter and a three-axis accelerometer. Subsequent test flight results and recommendations for further research are provided.



# TABLE OF CONTENTS

<b>I. INTRODUCTION .....</b>	<b>1</b>
A. BACKGROUND .....	1
B. BERGEN INDUSTRIAL HELICOPTER DESCRIPTION.....	2
1. General Arrangement.....	3
2. Flight Control System .....	4
<b>II. AVIONCS SUITE DESIGN.....</b>	<b>11</b>
A. RAPID PROTOTYPING SYSTEM .....	11
1. Overview of RFTPS.....	11
2. Ground Station Hardware Modifications.....	13
B. HELICOPTER AVIONIC SYSTEM DEFINITION .....	14
C. INERTIAL MEASUREMENT UNIT.....	15
D. DIFFERENTIAL GLOBAL POSITIONING SYSTEM RECEIVER .....	19
E. TELEMETRY .....	20
<b>III. SONAR ALTIMETER DESIGN AND CONSTRUCTION.....</b>	<b>23</b>
A. REQUIREMENTS .....	23
B. POLAROID 6500 SERIES RANGING MODULE.....	24
1. Transducer Selection.....	25
2. Ranging Module Theory of Operation.....	26
C. SONALT POWER SUPPLY .....	29
D. DRIVE OSCILLATOR .....	32
E. OUTPUT SIGNAL PROCESSING.....	35
1. PWM Waveform Creation.....	36
2. PWM Waveform to Voltage Conversion.....	37
F. TRANSDUCER MOUNTING.....	40
G. SONALT TESTING.....	40
<b>IV. AVIONICS RACK AND POWER SUPPLY DESIGN .....</b>	<b>43</b>
A. REQUIREMENTS.....	43
B. SKID DESIGN .....	43
C. COMPONENT PLACEMENT .....	44
D. POWER SUPPLY SYSTEM.....	46
E. VIBRATION ISOLATION.....	48
<b>V. INITIAL FLIGHT TESTING AND SYSTEM MODIFICATION .....</b>	<b>55</b>
A. INITIAL FLIGHT TESTING.....	55
B. SYSTEM MODIFICATION .....	56
C. PWM TO BLADE ANGLE CORRESPONDENCE.....	60
D. REALSIM SOFTWARE MODIFICATIONS .....	62
<b>VI. AVIONIC SYSTEM TESTING.....</b>	<b>65</b>
A. FLIGHT TESTING .....	65
B. DATA QUALITY.....	66
1. Vertical Doublets .....	67
2. Lateral and Longitudinal Doublets.....	70



C. COMPLEMENTARY DATA FILTERING TO PRODUCE VELOCITY AND ALTITUDE ESTIMATES .....	72
<b>VII. CONCLUSIONS AND RECOMMENDATIONS.....</b>	<b>75</b>
A. OVERVIEW .....	75
B. SPECIFIC COMMENTS.....	75
1. <i>Sonic Altimeter</i> .....	75
2. <i>Avionics Mounting and Vibration Control</i> .....	75
3. <i>Avionics Package Weight Reduction</i> .....	76
4. <i>Data Quality First Priority</i> .....	77
5. <i>Controller Design</i> .....	77
6. <i>RFTPS Ground Station</i> .....	77
C. SUMMARY.....	77
<b>LIST OF REFERENCES.....</b>	<b>79</b>
<b>APPENDIX A. SONALT CALIBRATION DATA .....</b>	<b>81</b>
<b>APPENDIX B. WEIGHT AND BALANCE LOG .....</b>	<b>85</b>
<b>APPENDIX C. AVIONICS SYSTEM WIRING DIAGRAMS .....</b>	<b>87</b>
<b>APPENDIX D. MODIFIED AVIONICS PACKAGE WIRING .....</b>	<b>91</b>
<b>APPENDIX E. BLADE ANGLE VS. PULSE WIDTH DATA .....</b>	<b>93</b>
<b>APPENDIX F. REALSIM SUPERBLOCK DIAGRAMS .....</b>	<b>97</b>
<b>APPENDIX G. FLIGHT TEST DATA.....</b>	<b>99</b>
<b>INITIAL DISTRIBUTION LIST.....</b>	<b>111</b>

## ACKNOWLEDGEMENTS

This work was heavily involved in hardware development, and unlike some theoretical work that could be attempted, all ideas were "submitted" to Newton and Maxwell at flight test for evaluation against the basic laws of nature. Some of my ideas, thought to be so elegant and clever, proved somewhat lacking under such scrutiny, but such is the nature of a fledgling engineering development exercise. I learned a great deal from the successes and more from the failures. Perhaps the most valuable learning experience involved the trials and difficulties in any project moving from the initial concept on the back of the envelope to fruition. Many have helped make this work profitable. Any deficiencies can be traced to me, but behind our several successes are those who mentored, guided and assisted me. Special thanks to Professor Duren whose patience and steadfast support, advice and counsel were greatly appreciated. Professor Kaminer graciously allowed me to use his flight test ground control equipment. Mr. Jerry Lentz spent many hours working with me on the electronic components used in this project. I absorbed only a small fraction of his considerable expertise with electronics. His desire to see the project succeed is greatly appreciated. Mr. Don Meeks, our flight test pilot at the UAV laboratory performed above and beyond the call of duty. He never failed to provide assistance as I put together various hardware components, and graciously allowed access to his tools and offered his experience with remote control aircraft. Thanks go to Mr. John Moulton who fabricated the aluminum avionics mounting frame, and who responded on short notice to urgent engine starter modifications. Finally, while I spent the hours drilling holes, bending metal, and crunching data, my wife Gigi provided her constant support. Thanks.



# I. INTRODUCTION

## A. BACKGROUND

The Naval Postgraduate School has fostered a highly successful Unmanned Aerial Vehicle (UAV) program across several years, primarily supporting research involving avionics and flight control system development. The remarkable advances in computer hardware and software technology over the past decade have allowed engineers to develop control algorithms using high-level intuitive constructions, such as block-diagrams, that may be converted to executable code for implementation.

The most recent effort in the evolving UAV program is the Rapid Flight Test Prototyping System (RFTPS) [Ref. 7,8]. RFTPS allows the engineer to design, test, and implement a control system using the MATRIX<sub>x</sub> family of software. A sophisticated ground station implements this software in the field and controls a fixed-wing UAV named FROG. This small airplane is equipped with sensors whose data is communicated to the ground station via wireless modems. Control signals are then computed by the ground station and transmitted to the flight control actuators on the FROG using a Futaba remote control (RC) transmitter similar to that used by RC hobbyists. The RFTPS is a proven system that continues to evolve.

Of special value to this thesis work, the RFTPS system was developed with an open software architecture, to allow the ground station hardware to control most any fixed-wing UAV using the same sensor suite, provided the software is updated to reflect the new vehicle's aerodynamic qualities.

This thesis reviews the work accomplished to mount sensors on a small remote controlled helicopter with instrumentation compatible with the RFTPS: an inertial measurement unit, a Global Positioning System (GPS) receiver, an altitude sensor and associated power supply and telemetry equipment. The following chapters discuss the design of the avionics suite, including one of the principal sensors, and the support structure needed to allow the helicopter to operate with the RFTPS.

In developing a design for the avionics suite, the sensors required to provide the necessary information to the ground station were determined and their individual requirements assessed. Areas investigated when studying these sensors were: power requirements, interface requirements, size, weight, susceptibility to noise, environmental

limitations, and so forth. Secondly, telemetry equipment was studied to determine how sensor data is transmitted to the ground station. As discussed in Chapter II, the avionics system was then defined to meet these requirements.

As detailed in Chapter III, an improved altitude data source was required to control the helicopter. The helicopter operates within 20 feet of the ground and accuracy within just a few inches is required at a relatively high data rate. Barometric altimeters are not sensitive enough to discern differences of a few inches. A lightweight, inexpensive sonar altimeter (SONALT) was developed and tested to meet the need for precise altitude information.

With the components of the avionics package now defined, a method was devised to mount the components on the vehicle, since the basic helicopter does not provide any location to carry additional payload. Factors such as component weight, vehicle center-of-gravity, component vibration isolation, component placement, and ease of construction are discussed in Chapter IV. The balance of these factors, through several design iterations, resulted in a very lightweight, yet sturdy aluminum structure to replace the landing skid of the basic helicopter. This structure would serve as both landing skid and avionics platform.

The SONALT and on-board avionics were developed concurrently with the construction of the avionics platform on which the avionics were to be mounted. Unfortunately, initial flight testing of the avionics platform revealed that vibrations of the rotors excited a particular resonant mode in the newly created composite chassis/aluminum frame system. Efforts at controlling these vibrations and subsequent modifications to the avionics system are detailed in Chapter V.

Follow-on testing of the modified avionics system and test results are presented in Chapter VI, while conclusions and recommendations are offered in Chapter VII.

## **B. BERGEN INDUSTRIAL HELICOPTER DESCRIPTION**

The Bergen Industrial Twin Helicopter manufactured by Bergen Machine and Tools, Inc., was chosen for this project. It is a remote control helicopter, but is more capable than helicopters flown by weekend hobbyists. The Bergen Twin, shown in Figure 1.1, was developed specifically to provide a stable platform for cameras and also to serve as the internal machinery inside scale models of full-sized helicopters. Bergen provided this vehicle with the power and stability needed to support these extra loads.

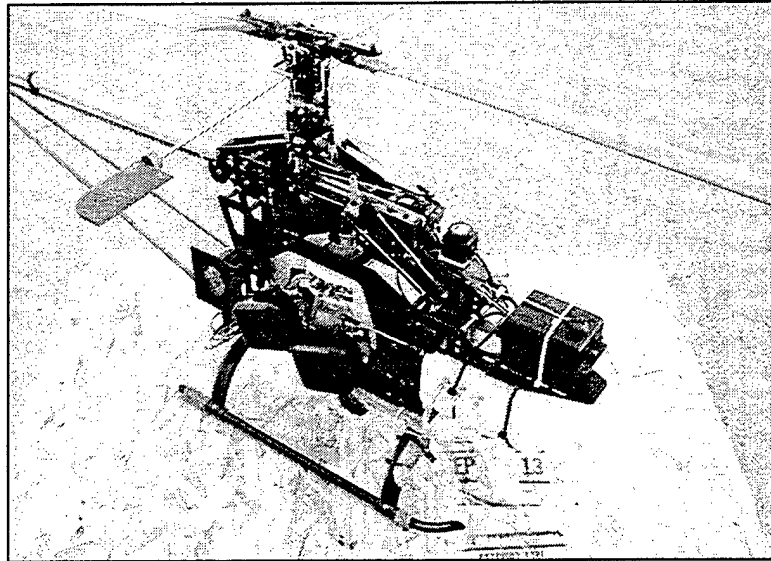


Figure 1.1. Bergen Industrial Twin Helicopter

## 1. General Arrangement

As the name “twin” implies, the helicopter has a two cylinder, two-cycle engine of special construction. Cylinders normally used in single cylinder helicopter engines were mounted by the manufacturer on a newly designed crankcase providing increased power. The crankshaft is mounted vertically, with the cylinders opposing each other, one forward and one aft. The resulting engine has about a 45 cubic centimeters displacement [Ref. 3]. An RC helicopter engine can be expected to produce enough lift from each 10 cubic centimeters of displacement to lift 10 kilograms. This general rule of thumb is influenced by many variables, such as main rotor disc area, fuselage area blocking rotor downwash, and reduction gear losses. [Ref. 1]

The manufacturer rates the payload capacity in excess of 20 pounds, which seems entirely plausible based on the rule of thumb cited above. This lifting capacity is remarkable, since the basic weight of the helicopter is only 16.45 pounds. The engine is provided with fuel through two carburetors on the starboard side of the vehicle with exhaust gases discharged through the port side of the engine to individual mufflers. The exhaust pipes from these two mufflers are fed straight down; this was an important factor in later design decisions. The factory-stock helicopter engine is started using a hand pull rope starter mounted under the helicopter at the lower end of the crankshaft. The engine is designed to idle at about 3000 RPM, and as RPM increases towards its nominal value of

about 10,000-11,000 RPM, a clutch at the top of the crankshaft engages and drives the main rotor through 90 to 14 reduction gearing. Fuel is fed to the carburetors from a translucent plastic tank mounted forward, which carries enough fuel for about 20 minutes of flight.

The chassis of the helicopter consists of two vertically mounted parallel plates made of a material called 'G-10,' which is an epoxy resin material impregnated with fiberglass, and is similar in appearance to that used in electronic printed circuit boards, but less brittle. The engine and associated reduction gearing is mounted between these two plates, with various accessories and control components attached where appropriate, as shown in Figure 1.2. The factory provided lightweight plastic landing skid is connected across the bottom of the two plates with the aid of two aluminum cross-members.

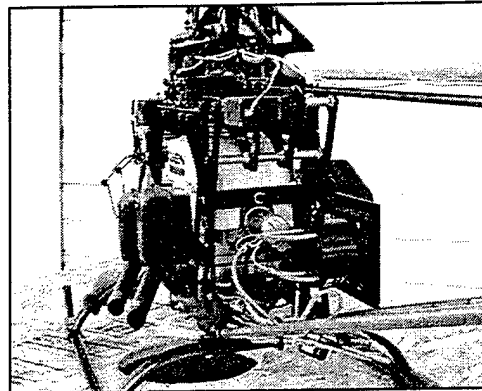


Figure 1.2. Engine Mounting in Chassis

## 2. Flight Control System

The Bergen Industrial Twin uses a Hiller control system to control main rotor blade angle. Hiller control systems are particularly useful when actuator torque is insufficient to position the main rotor blades to the desired blade angle. Unlike an aircraft propeller, a helicopter main rotor blade may have a changing blade angle as it moves around the rotor head each cycle. The blade angle may be at a maximum at one point in its cycle around the mast and fall to a minimum value 180 degrees later in the cycle. This cyclically changing blade angle creates an unsymmetric disc loading.

The main rotor blade angle is controlled through the action of the swashplate. The swashplate is a gimbaled collar surrounding the rotor shaft that can be tilted in any direction by the control actuators as shown in Figure 1.3. Tilting of the swashplate is accomplished by two cyclic actuators, the term 'cyclic' referring to the cyclically changing blade angle action discussed above. The swashplate is tilted fore and aft by the longitudinal cyclic actuator, while the swashplate is tilted left and right by the lateral cyclic actuator. If the swashplate is tilted forward, for example, the blade angle of the main rotor blades is manipulated so that more lift is produced aft of the rotor head and less lift is produced forward. This tends to tilt the vehicle forward creating a forward component of force from the main rotor lift vector, creating forward motion. Similarly, a tilt of the swashplate to the left causes more lift to be produced on the right side of the rotor disc and reduces the amount produced on the left side. This asymmetry tilts the vehicle and moves it to the left. A tilt in any intermediate direction creates motion in that particular direction.

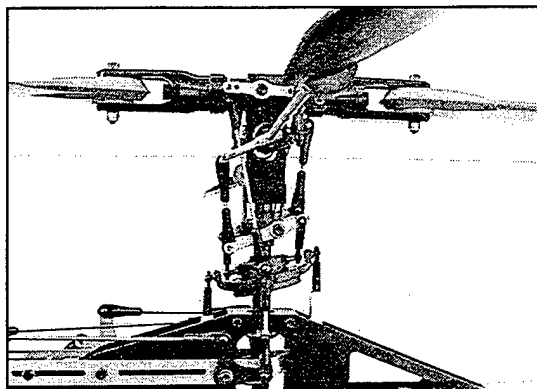


Figure 1.3. Swashplate Mechanism

The collective actuator moves the swashplate up and down the rotor shaft and does not induce any tilt to the swashplate. As the swashplate moves up, blade angle is increased by the same amount at all points through the cycle. This creates a uniform increase in lift across the disc with an overall increase in lifting force.

The process by which swashplate tilt creates an uneven lift distribution is a complicated one, as it involves the effects of gyroscopic precession. If a force is applied to a toy gyroscope for example, deflection occurs at a 90 degree angle from the direction from which force is applied. For a rotating airfoil, the effects of a change in an airfoil's angle-of-attack (AOA) appear as a change in airfoil lift 90 degrees later in the cycle.



In addition to the two large main rotor blades, two small airfoils called servo paddles are installed on the end of a flybar at right angles to the two main rotor blades. All four of these airfoils are subject to gyroscopic effects.

In the case of the main rotor blades, the linkage from the swashplate is such that blade angle is increased 90 degrees prior to the point in the cycle when it is needed. For example, if the swashplate were to be tilted forward, blade angle reaches a maximum on the starboard side of the cycle, and a minimum at the port side of the cycle. As the rotor turns clockwise when viewed from above, lift is increased aft and decreased forward, creating the desired asymmetry.

The servo paddles serve to assist in twisting the blades to their new positions, since the actuators lack sufficient torque on their own. The AOA of one paddle is increased by a linkage from the swashplate, while the AOA of the other paddle is decreased. Since the flybar between the paddles is free to rotate in the vertical plane at the head block, the flybar can move in a seesaw motion. This seesaw motion causes the main rotor blade angle to change through a connecting linkage. [Ref. 1]

The gyroscopic effect on the servo paddles must be considered. In our example of forward swashplate tilt, the linkage to the servo paddles increases AOA to a maximum as they pass the right side of the mast. The effect of the lift produced on the paddle is felt 90 degrees later, at which point the flybar seesaws. The seesaw motion increases blade angle of attack on the blade located on the starboard side. This increase in lift appears 90 degrees later when the blade is aft of the rotor, creating the desired asymmetry of lift.

A total of five electrically powered Futaba S-9202 actuators, or control servos, are provided to position throttle, collective, lateral cyclic, longitudinal cyclic, and tail rotor linkages. A small Futaba NR-4RB rechargeable battery located beneath the fuel tank provides 4.8 VDC power to the actuators through a Futaba RC receiver located just above the fuel tank. This crystal receiver is tuned to a frequency corresponding to RC channel 42. The receiver processes signals transmitted by a hand-held Futaba PCM1024ZH transmitter on the ground and produces Pulse Width Modulated (PWM) output signals to drive the actuators. The receiver may accommodate as many as nine different actuators, but, in the case of this application, only five actuators are used. The channel assignments are shown in Table 1.1.

Receiver Channel	Output
1	Lateral Cyclic
2	Longitudinal Cyclic
3	Throttle
4	Tail Rotor
5	Rate Gyro Sensitivity Switching
6	Collective Pitch
7	(Spare)
8	(Spare)
9	Channel 9 Switch

Table 1.1. Helicopter PWM Receiver Output Channels

These actuator or servo channels are not to be confused with the radio frequency channel assignments used on different RC vehicles. Fifty frequencies, from Channel 11 to 60 (72.010 to 72.990 MHz) are employed by RC enthusiasts to prevent cross-control interference when hobbyists fly in close proximity to one another. The FROG uses channel 26, while the helicopter came from the factory with a receiver and transmitter set to channel 42. As we will see in a later chapter, this difference must be accounted for in the ground control station.

In the case of the throttle, collective, lateral cyclic, and longitudinal cyclic, the receiver output is routed directly to the actuators as shown in Figure 1.4, commanding the actuator to rotate to a desired position.

For the tail rotor, however, the output voltage is routed to a Futaba G501 piezoelectric rate gyro which serves as a yaw damper, which can be seen on the helicopter as a small square box located immediately aft of the receiver. The yaw damper senses angular turn rate about the z-axis and uses this information to stabilize the helicopter in yaw. This feature allows the RC pilot better yaw control, as all helicopters experience considerable cross-coupling between control inputs. For example, as collective is increased and the main rotor produces more lift, it also produces more torque for the tail rotor to counteract. The yaw damper senses the yaw created and sends a countering signal to the actuator, even if no input is commanded by the RC pilot.

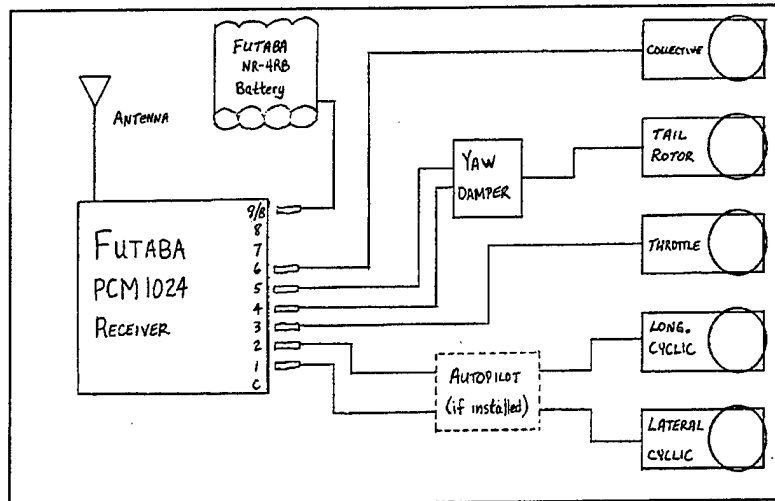


Figure 1.4. Futaba Receiver and Actuator Connections

The Futaba hand-held transmitter, shown in Figure 1.5, contains two primary levers for vehicle control. The right lever controls longitudinal and lateral cyclic. Left-right motion of the left lever of the transmitter controls the tail rotor, while up-down motion simultaneously controls the throttle, collective and tail rotor in a predetermined 'mixture.' This mixing feature of the transmitter increases throttle as collective is increased while adjusting the tail rotor to roughly compensate for the change in torque created.

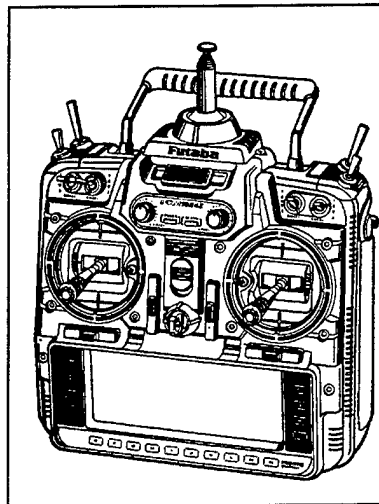


Figure 1.5. Futaba PCM 1024ZH Transmitter

The Futaba transmitter also has the capability to support a trainee. In this mode, one or more of the control channels is given over to another Futaba transmitter that has been connected to the instructor's transmitter by a training cable. The instructor pilot can regain control at any time.



## **II. AVIONCS SUITE DESIGN**

### **A. RAPID PROTOTYPING SYSTEM**

The RFTPS has been the subject of several previous theses and only a few aspects of this system which influence the design of the avionics suite will be presented. The following description is based on this earlier work where the reader may find more complete information on the RFTPS [Ref. 7,8]. Additionally, modifications to the RFTPS required to support helicopter operations will be discussed.

#### **1. Overview of RFTPS**

The RFTPS architecture includes both the airborne sensors, required power supply components and telemetry links, as well as a ground station. The ground station processes sensor data and generates commands to control the vehicle.

The avionics system on board the vehicle includes a Watson Inertial Measurement Unit (IMU), a Global Positioning System (GPS) receiver and air data sensors, such as an altimeter or airspeed sensor. The IMU and GPS produce data through serial interfaces that are connected to FreeWave™ wireless modems that transmit data to the ground station. Details of these components are reviewed in Sections C, D, and E below. The air data sensors in the FROG are connected to the IMU, and their signals are multiplexed into the digital data stream sent to the ground station.

The RFTPS ground station contains three major components; see Figure 2.1. First, a small "luggable" PC serves as the host for a Texas Instruments Digital Signal Processor (DSP) which is the primary processor for executing code controlling the vehicle. Additionally, the PC supports four hardware boards that handle input/output (I/O) functions to support the DSP, including two serial communications modules, one digital-to-analog module, and one Pulse Width Modulation module. [Ref. 7] The two serial boards receive downlink data from the IMU and GPS through the pair of FreeWave wireless modems. The Pulse Width Modulation module (IP\_68332) is connected to a Futaba receiver and allows PWM signals being transmitted to the vehicle to be captured. The fourth hardware board is the IP\_DAC module, which allows digital signals produced by the DSP to be converted to analog voltages to drive a Futaba transmitter set in the trainee mode.

The four I/O boards in the host PC are connected by ribbon cable to a communications unit, the second major component of the RFTPS ground station. The communications unit houses the two FreeWave wireless modems, the Differential Global Positioning System receiver, and a Futaba PWM receiver. Additionally, this communications unit provides a housing for these components and allows for connections to power supplies, antennas, and the modified Futaba transmitter. This Futaba transmitter, when placed in “trainee mode” and connected to another transmitter in the “instructor mode” as discussed in Chapter I, is capable of communicating control signals to the actuators on the vehicle for flight control.

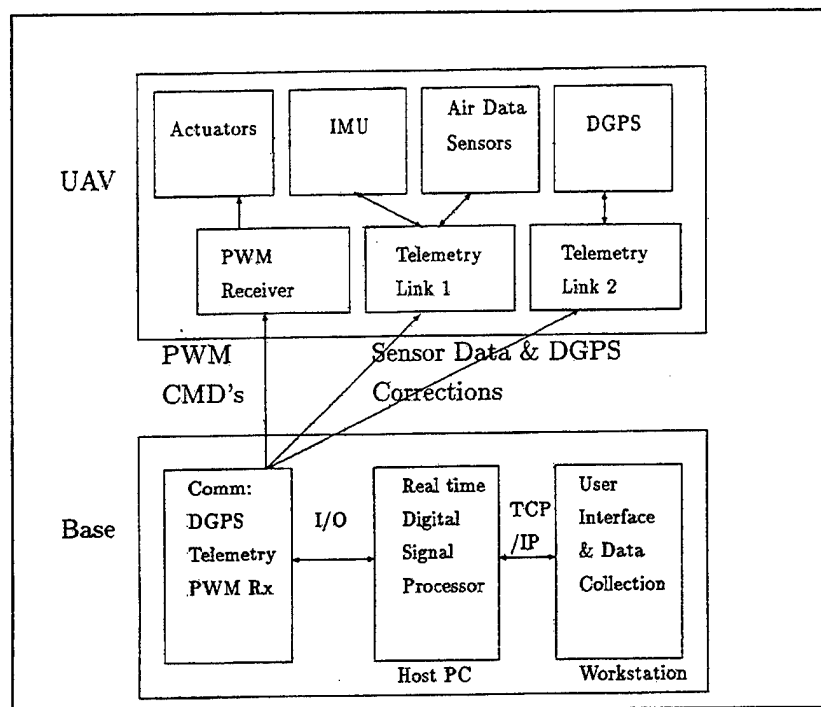


Figure 2.1. RFTPS Hardware Architecture From Ref. [8]

The third major component in the ground station is the User Interface and Data Collection Workstation. [Ref. 8] The workstation is a Sun workstation running the Xmath / SystemBuild graphical programming software. This software allows the user to develop control algorithms in a high-level block diagram environment and then generate real-time code for execution on the real time processor residing on the luggable PC. Additionally, the software supports a graphical user interface allowing the user to see displays of parameters of interest (navigation, PWM control signals, etc.). Input

commands, such as altitude or heading changes, can also be entered by the user through the graphical user interface, depending on software design. The workstation is connected to the PC via an Ethernet TCP/IP protocol connection.

## 2. Ground Station Hardware Modifications

Due to the open architecture employed in the design of the RFTPS, very few hardware modifications were required on the ground station. Since each RC vehicle, whether it be an airplane or a helicopter, comes from the factory with a preset RF operating channel, much as an automobile comes with a set of keys, the ground station Futaba transmitter and receiver must be capable of operating on the RF frequency channel of the helicopter. To allow interoperability between the FROG (channel 26) and the helicopter (channel 42), a multi-channel synthesized receiver manufactured by Futaba was installed in place of the crystal controlled, fixed channel receiver already in use for the reception of PWM signals in the ground station. Figure 2.2 depicts the new receiver. Behind the small plastic window in the lower left portion of the receiver are two small dials for setting the appropriate RF channel. Power to the receiver is supplied from a power supply within the ground station, and no external battery is required.

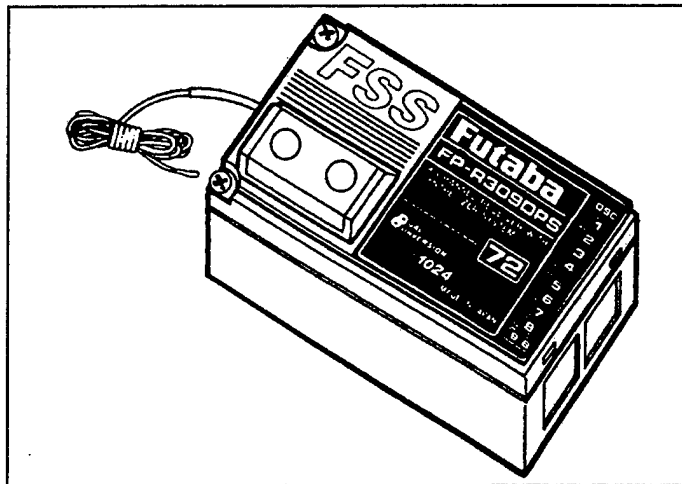


Figure 2.2. Futaba Multi-Channel Receiver

No further hardware modifications to the Futaba transmitter were necessary. The DB9 connector placed in the left side of the unit to allow it to be connected to the ground station visually identifies this previously modified transmitter. The transmitter has both



an airplane and a helicopter mode pre-programmed into internal software. It is necessary only to place the transmitter in this mode through the appropriate menus and to ensure that all necessary parameters are set identically to that in the UAV pilot's master controller when they operate in the instructor-trainee mode. The modified transmitter has no internal RF transmitter, as it has been removed for safety purposes, and can only be operated in the trainee mode with another Futaba transmitter.

A typical RC airplane flies with four actuators: elevator, aileron, rudder, and throttle. A typical RC helicopter flies with five actuators: longitudinal cyclic (corresponds to elevator), lateral cyclic (aileron), tail rotor (rudder), throttle, and collective. Fortunately, when in the helicopter mode, the throttle and collective are married together, as discussed in Chapter I, such that only four inputs must be made to the modified controller from software via the IP\_DAC module.

## **B. HELICOPTER AVIONIC SYSTEM DEFINITION**

To ensure maximum compatibility with the RFTPS ground station, the helicopter avionic system was assembled to make use of the same sensors as used on the FROG, in so far as possible. Although the Xmath / Realsim system is capable of supporting a wide variety of sensors, different software drivers must be written to support different sensors. For example, a software driver has previously been written to convert serial data received from the Inertial Measurement Unit at the serial board and process it for use by the system. This software expects the data arriving on this link to be in binary format with specific variables listed in a predetermined order. The software then parses this data and assigns each portion to a different variable, such as bank angle, acceleration in the x-axis and so forth. If a different sensor is used, new software must be written to account for the different information format. Since any modifications to this software would then make the system incompatible with the FROG, it was decided to use identical sensors, wherever possible. These sensors provide all the information necessary to control the helicopter, with the exception of an accurate low altitude data source. A later chapter details the development of a short-range, highly accurate altitude sensor to meet this requirement. The following sections discuss each of the other avionic components and their respective operational capabilities, power requirements, interface parameters and limitations.

### C. INERTIAL MEASUREMENT UNIT

The IMU employed on the FROG, and included in the present design, is the IMU-C604 produced by Watson Industries, Inc. The unit pictured in Figure 2.3 weighs only 2 pounds and measures 5.78" x 3.24" x 4.68" [Ref. 9]. Included in this compact package is a solid state gyro system and solid state vibrating element angular rate sensor, as well as two vertical reference pendulums, a triaxial fluxgate magnetometer and accelerometers. A microprocessor collects information from these sensors and is capable of producing output signals for bank angle, elevation angle, and magnetic heading, as well as accelerations (x,y,z axes), and tri-axial angular rates. Additionally, the unit contains a five channel integral analog-to-digital converter to allow the user to input analog data that can be output along with the other measured variables.

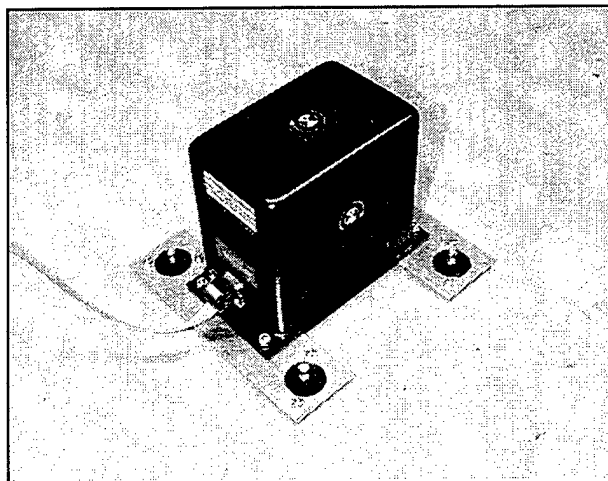


Figure 2.3. Watson IMU-C604

Interface with the IMU is accomplished through a 9-pin male DB-9 connector on the forward side of the unit. This is not, however, a standard serial connection as might be found on a PC. Table 2.1 details the pin-out for the Watson IMU, as well as the standard arrangement for a PC. In the Watson application, 28 VDC power to operate the unit is provided to the IMU through pin-2, while serial output is provided at pin-9. These details must be accommodated when developing onboard wiring for the IMU.

Pin	RS232	Watson IMU-C604
1	Carrier Detect	Power/Signal Ground
2	Transmit Data	+28 VDC Power
3	Receive Data	User A/D channel #1
4	DTR	User A/D channel #2
5	Ground	Receive
6	Data Set Ready	User A/D channel #3
7	Not Used	User A/D channel #4
8	Clear to Send	User A/D channel #5
9	Not Used	Transmit (User receives on this line)

Table 2.1. RS-232 and IMU Pin Assignments

For bench testing, or to set the various output modes of the IMU, the unit can be connected to a personal computer. Since the pin-outs of the IMU and computer differ, a direct connection is not possible with a standard cable. A special wiring harness must be developed to make the proper connections. The nine pins of the IMU can be connected to a terminal strip, allowing 28 VDC power, user analog inputs for A/D conversion, and serial communication to the PC to be connected appropriately. Most any terminal communications program such as ProComm®, HyperTerminal® (in Windows 95), or Crosstalk® can be employed to receive the serial output at 9600 baud (8-N-1). The IMU Owner's Manual details how to select output formats by typing various symbols and following prompts [Ref. 9]. The IMU can output data in ASCII decimal, hexadecimal, or binary. If the binary mode is selected, the data will be unrecognizable, because the terminal software interprets each byte as ASCII, and therefore prints various characters to the screen. In addition to selecting the transmission format, the user can select which variables are included in the output.

The choice of an output format is important because this choice effects the data rate of the IMU. The output data transfer rate is 9600 bits per second. Internal sampling of the analog sensor outputs occurs at 71.11 Hz. If an output format is selected which exceeds 135 bits per sample, including start bits, stop bit, and carriage returns, there will be insufficient bandwidth available to transfer the information. ( $135 * 71.11 = 9600$ ). In these situations, the microprocessor in the IMU selects every other internal sample for

transmission, or perhaps every third, fourth or fifth sample to reduce the bandwidth required. The user can expect the IMU to provide output information at an integer division of 71.11 Hz. For example, if ASCII format with 12 variables were selected for output, the information would appear on a PC terminal communications program screen as follows:

```
I +000.0 -01.3 304.0 -0.02 +0.00 -0.99 +00.0 +00.0 +00.0 +094 +119 +382
```

Notice in this case there are 71 characters in each data line plus a carriage return. The first character is a status character followed by the 12 selected data elements. Each ASCII character is transmitted by an 8 bit byte. However, when using the RS-232 asynchronous data communications protocol, these bits would be transmitted as part of a frame. In this case, a single leading 'start' bit is appended before the data, and a single 'stop' bit is appended to the end. (No parity bit is sent by the IMU in this application.) Therefore, each ASCII character requires 10 bits to be transmitted. Thus, each sample (line of data) requires the transmission of approximately 720 bits. The IMU must select only each sixth sample for transmission, reducing the sample rate to about 11.85 Hz. ( $71.11 \div 6 = 11.85$ ). At this sample rate, the bandwidth required is ( $720 * 11.85 = 8532 < 9600$  baud).

If, however, the binary mode is selected, each data element is a 14 bit, two's complement format number. The first seven bits are placed in an RS-232 asynchronous data frame (right justified), and the remaining seven bits are placed, right justified in the next data frame. Thus, 20 bits, when start and stop bits are included, are required to transmit each data element. Upon receipt, the user must strip off the left-most bit in each data byte before combining them to create the 14 bit data word.

As an example, the first data element in the example data line above is bank angle, measured  $\pm 180.0$  degrees. This requires seven ASCII characters (including the following space) which requires  $8 * 7 = 56$  bits to be transmitted in the ASCII mode. In binary mode, only 20 bits need be transmitted. This analysis demonstrates that the ASCII format, while convenient to the human observer, does not provide as efficient a transmission format.

An important consideration when determining how to mount the IMU on the helicopter is the orientation of the axes of the IMU. The IMU must be installed with the mounting base down, and the DB9 connector facing forward to align the IMU coordinate

system with the conventional aircraft coordinate system. Additionally, to ensure that the internal magnetometers are not influenced by disturbances, care should be given to using non-magnetic mounting materials and electrical connections.

As Table 2.1 describes, 28 VDC power should be provided across pins 1 and 2. However, the unit is equipped with an internal regulator allowing operation from as low as 24 VDC and as high as 32 VDC. Current demand is listed as about 350 mA, however, we found current draw to be nominally 250 mA at 24 volts.

The four 16-bit analog-to-digital converters in the IMU sample at 50 Hz, and therefore, following Nyquist, have a bandwidth of 0-25 Hz. They accept voltage inputs from -10 to +10 VDC. In shop testing, a DC bias of about -0.08 Volts existed in the A/D converter output. Watson reports that a single-pole anti-aliasing filter set at around 25 Hz is incorporated into the internal design of the A/D converter.

Accelerations can be integrated to obtain velocity, and again integrated to obtain displacement. However, this technique suffers from drift created by acceleration measurement error. To investigate this effect, the IMU was subjected to various accelerations and the data recorded. Specifically, the IMU was lifted from a resting position, moved through a series of random, somewhat cyclic motions, and then returned to its original position. This data was then introduced into MATLAB and processed through the SIMULINK diagram shown in Figure 2.4.

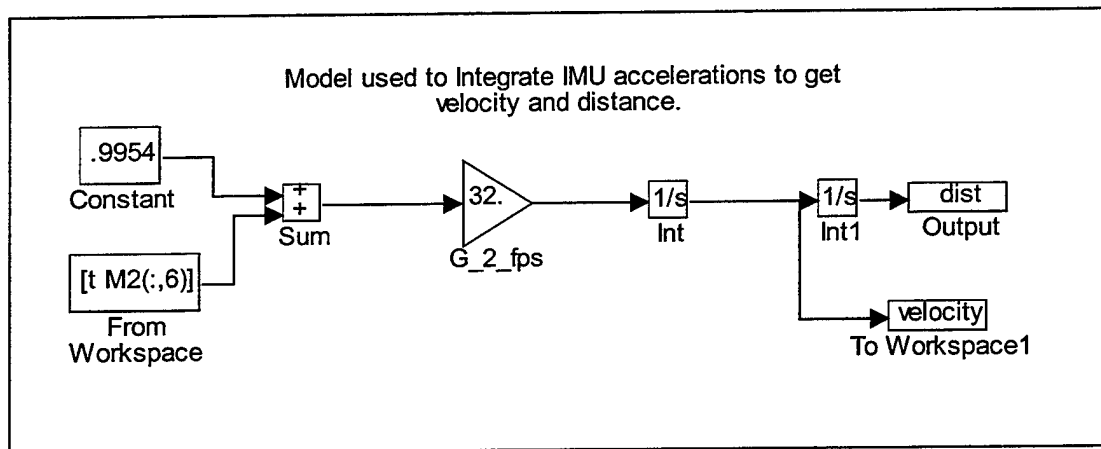


Figure 2.4. SIMULINK Model Used to Twice Integrate IMU Accelerations

The z-axis input accelerations, in g's, were corrected for the effects of gravity and installation bias by adding 0.9954, and then multiplied by 32.2 to obtain the proper units. The results are displayed in Figure 2.5. Notice that after only nine seconds, the error in

position is nearly 3 feet. Clearly, the quality of data produced by the IMU is such that it will be necessary to complementary filter the IMU output with an altitude source to control this drift.

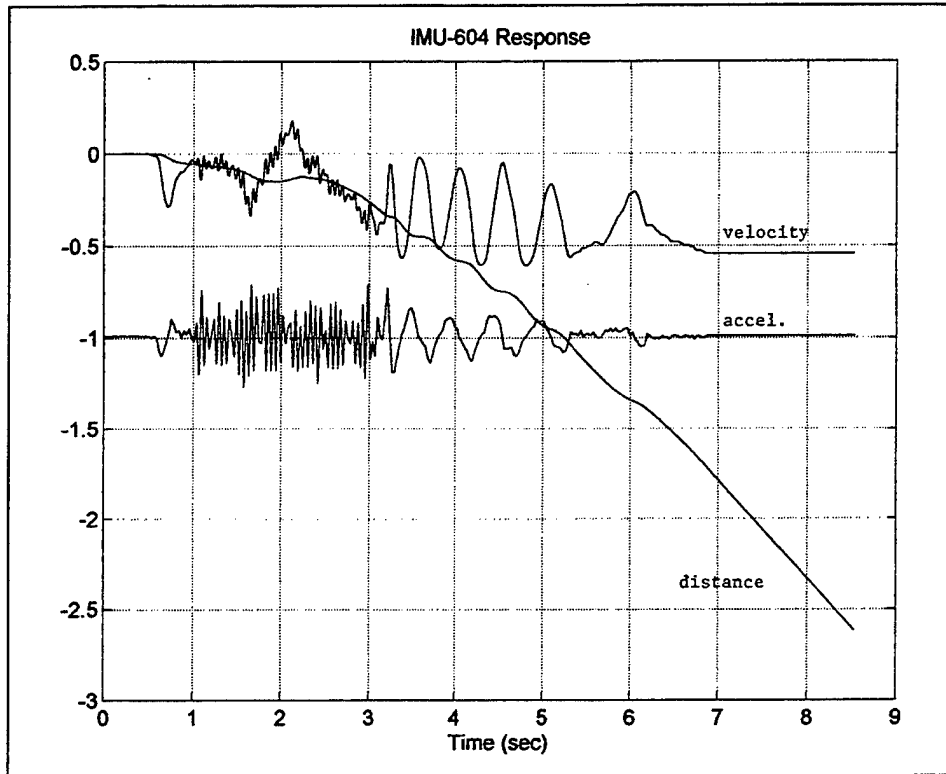


Figure 2.5. IMU-C604 Drift

#### D. DIFFERENTIAL GLOBAL POSITIONING SYSTEM RECEIVER

The Global Positioning System receiver incorporated in this avionics system is the Basic Oncore GPS Receiver manufactured by Motorola. The system provides data at one second intervals through an RS-232 interface. The GPS system consists of the receiver, an active antenna, and a power/data cable. These components are very compact and lightweight, with the receiver weighing only 3.8 ounces and measuring 4" x 3" x 1". The active antenna module is a cylindrical component 4 inches in diameter by 0.89 inches and weighs 4.8 ounces. These components are shown in Figure 2.6. [Ref. 12]

The serial output of the device provides latitude, longitude, height, velocity, heading, time, and satellite tracking status through a 10 pin connector that provides the

receiver with power as well as permitting RS-232 serial output. This output was intended by the manufacturer to be connected to a PC running controller software, but in this application the serial data has been used to support the software written to control the FROG. The system requires 12 VDC power and consumes about 1.8 watts.

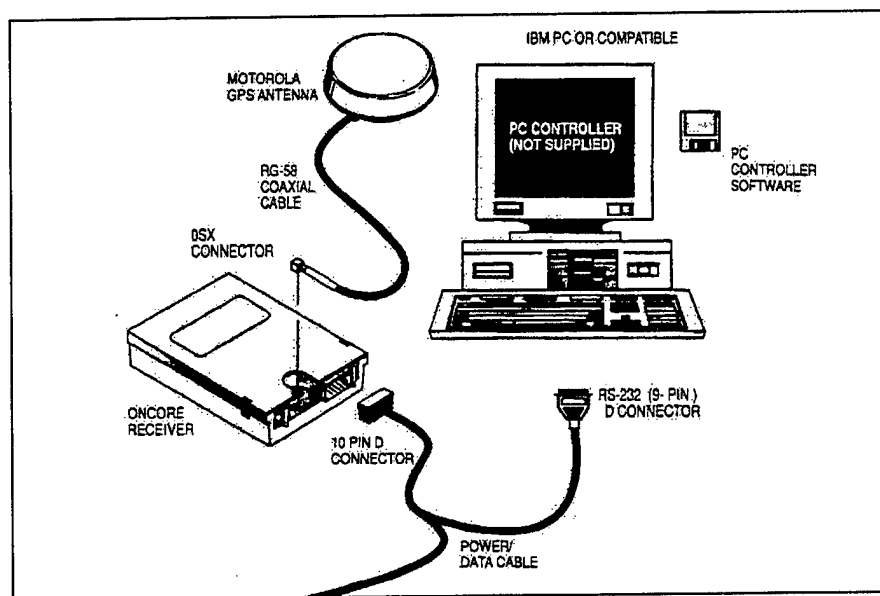


Figure 2.6. Motorola Oncore GPS Receiver From [Ref 12]

## E. TELEMETRY

The RFTPS uses FreeWave™ Wireless Data Transceivers to transmit data from the IMU and the GPS to the serial modules in the ground station. Both units operate at 9600 bps, and during flight, only the GPS requires two-way communication. The FreeWaves may be used in any situation where a standard 9-pin null modem is used, such as communication between two computers. The units are lightweight and easy to operate. Table 2.2 provides information pertinent to the present application.

An important feature associated with the FreeWave system is its Gaussian frequency shift keying (GFSK) modulation type. GFSK is a modified form of frequency shift keying (FSK) for transmitting binary data. With FSK, a pair of transmission frequencies are used, with one frequency representing a binary "1" and the other representing a binary "0." The transmitter keys the appropriate frequencies in turn to

represent a string of bits. Immediately adjacent to this pair of frequencies in the electromagnetic spectrum lie other possible pairs of frequencies.

Range	20 miles line-of-sight
Data Rate	1200 bps – 115.2 Kbps
Operating Frequency	902-928 MHz
Modulation Type	GFSK, spread spectrum, frequency hopping
Power	12 VDC, 120 mA
Dimensions	1.6in H x 3.9in W x 7.4in L
Weight	0.75 pounds
Antenna	Attached 3.5in whip or detached

Table 2.2. FreeWave Technical Specifications After [Ref. 10]

With Gaussian FSK, a Gaussian-shaped bandpass filter is placed around the pair of frequencies of interest to prevent interference from the adjacent pair of frequencies. Figure 2.7 depicts frequency shift keying.

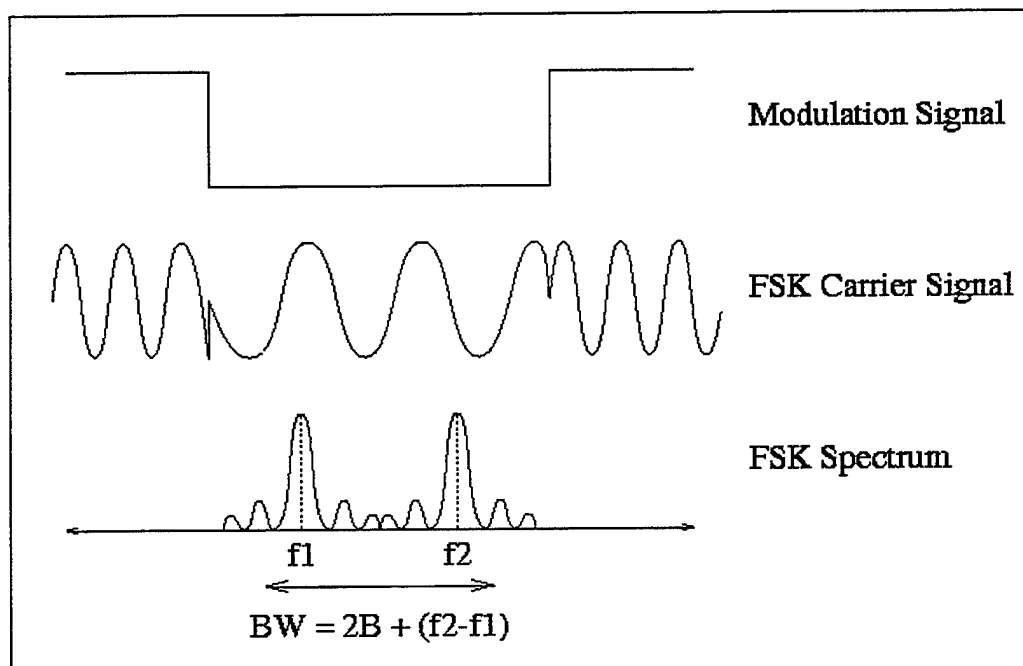


Figure 2.7. FSK Frequency Pair



Fifteen user-selectable hop patterns cause the transmitter to hop in a pseudorandom pattern from one pair of frequencies to another, thereby spreading the spectrum used. Frequencies of operation run from 902-928 MHz. FreeWaves are “slow hoppers,” meaning they transmit several bits before hopping on to another pair. Frequency hopping is one of several spread spectrum communications variants, allowing the simultaneous use of several transmitters in the same frequency band. Internal error detection and correction features with FreeWave prevent scrambled data in the statistically unlikely event that two separate FreeWave transmitters hop on to the same frequency pair together. When operating two FreeWaves pairs simultaneously, it is important to set each to a different user-selectable hop pattern to minimize interference. Most importantly, Spread Spectrum techniques meet the Federal Communications Commission (FCC) requirements for unlicensed operation. Spread spectrum technology, and GFSK modulation in particular, are in use in cellular telephones for this very reason. [Ref. 11]

Each FreeWave transceiver, see Figure 2.8 has a serial number, or “Unit Address” and must be programmed to operate with another serialized transceiver. This permits multiple FreeWaves to be used simultaneously. This is useful in this application, since two links are required.

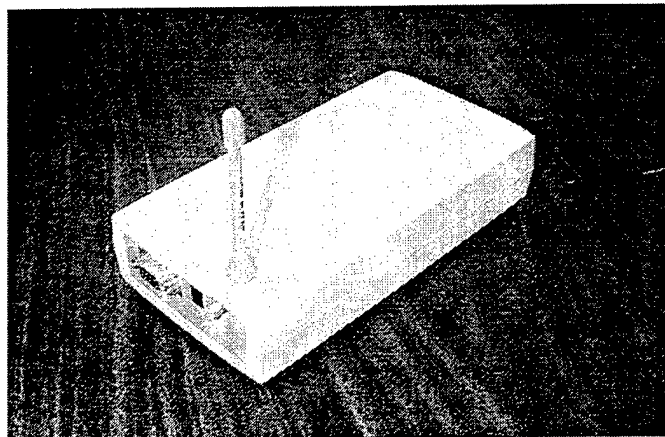


Figure 2.8. FreeWave Wireless Modem

### III. SONAR ALTIMETER DESIGN AND CONSTRUCTION

#### A. REQUIREMENTS

An aircraft traveling at 5,000 feet is adequately served with a barometric altimeter. Aircraft routinely operate with 1000 feet of altitude separation between aircraft. This translates to a static pressure differential of about 0.5 psi per thousand feet in the neighborhood of 5000 feet. Measurement errors are easily tolerated. However, in the region very close to the ground, altitude must be known much more precisely and a barometric sensor typically does not have sufficient accuracy. For example, the barometric altimeter on a Navy P-3C Orion aircraft can differ from field elevation by as much as 60 feet and still be considered safe-for-flight. In pilot-controlled applications, visual reference to the ground is used to judge altitude during the last few feet before landing. The helicopter for this project will almost always operate well below 60 feet, normally between the surface and 15 feet. A barometric sensor with sufficient sensitivity to measure fractions of feet would suffer from the changing pressure levels created by the beating rotors. These factors make a barometric altimeter such as that used in FROG unusable for automatic control in the helicopter. The following general requirements were developed for any altitude sensor to be used on board the helicopter:

- Usable range from the surface to 30 feet above ground level (AGL).
- Lightweight, preferably less than one pound.
- Operate on low voltage 0-24 volts DC.
- Low power, preferably in the tenths of amperes.
- Accurate within 2 inches when within a foot of the ground to allow for computer controlled landings, and accurate within 4 inches at higher altitudes.
- Sensor output must be analog DC voltage in the range of  $\pm 10$  volts to be compatible with the internal analog-to-digital converter in the IMU. In other words, there must be a known relationship between signal output voltage and vehicle altitude.
- Capable of operating in the helicopter flight environment.

## B. POLAROID 6500 SERIES RANGING MODULE

After reviewing possible alternatives, the Polaroid 6500 Series Ranging Module was selected to serve as the core of an ultrasonic ranging system. The Ranging Module drives an ultrasonic transducer, which serves as both a loudspeaker and a microphone for a very high frequency sound signal. A short emission of sound consisting of 16 pulses is transmitted which reflects off the ground and is reflected back to the transducer. By recording the time of travel of the sound pulse and knowing the speed of sound in air, the intervening distance can be determined. The ranging module is very light, weighing only a few ounces, and operates on 6V DC power, drawing only 0.1 amperes. Although limited to only about 35 feet maximum range, it can measure distances down to six inches (lower if external blanking is employed), with an accuracy of  $\pm 1\%$  of the reading over the entire range.

The transducer has a very narrow beamwidth, limiting the range of bank angles at which the transducer can receive a return signal from the ground. However, the helicopter is envisioned to operate primarily in a hover with minimal roll inputs. Turns will be accomplished by turning the helicopter around the main rotor using tail rotor control. In view of the anticipated operation of the helicopter, this limitation was not seen to be a serious problem.

The 6500 Series Ranging Module is not a ready-for-use component. As shown in Figure 3.1, the Ranging Module is a printed circuit board with attached components measuring less than 2 inches on a side driving a small transducer an inch and one-half in diameter. There is no power source, on/off switch, trigger mechanism, or output signal processing. The user must use the Ranging Module as the core in a larger system tailored to the user's intended application. A system for repeatedly triggering the Ranging Module and processing the output must be developed.

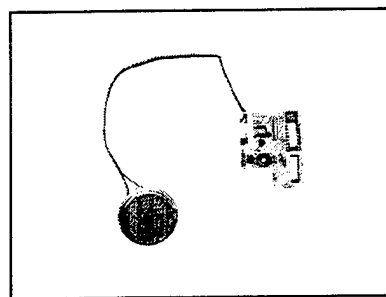


Figure 3.1. Polaroid 6500 Series Ranging Module and Transducer

Interface to the Ranging Module is through a Burndy 9-pin connector and ribbon cable provided by Polaroid. Only seven of the nine pins are used and their functions are indicated in Table 3.1. [Ref. 4]

Pin Number	Function
1	Ground
2	Multi-echo Blanking Reset – BLNK
3	Not Used
4	Initiation – INIT
5	Not Used
6	Internal Clock – OSC
7	Echo Return – ECHO
8	Internal Blanking Cancel – BINH
9	6 Volt DC Power Source

Table 3.1. Ranging Module Pin Interface

### 1. Transducer Selection

There are two transducers available for operation with the 6500 Series Ranging Module: an environmental grade electrostatic transducer, and a 7000 Series transducer. Both are very lightweight (the electrostatic transducer weighs only 8 grams) and are of rugged construction. The electrostatic transducer and the 7000 Series transducer require a 300 volt maximum combined voltage be applied to the transducer during transmission, including a 150 volt DC bias and a 150 volt AC spike when discharging. .

Polaroid also manufactures the 9000 Series transducer specifically intended to operate on the exterior of automobiles and heavy-duty trucks. However, it is not compatible with the Ranging Module and will not tolerate the bias voltage required by the other two transducers. Additionally, it has an asymmetrical beamform, with one of the axes presenting less than a 5 degree half-power beamwidth. Additionally, the 9000 Series transducer operates at a lower Sound Power Level (SPL) of only 110dB vs. 118 dB for the electrostatic transducer. [Ref. 4]

The electrostatic transducer provides greater than a 10 degree half-power beamwidth and a circular, rather than asymmetrical beamform. Although not as ruggedly

designed as the 9000 Series, the technical specifications for the environmental transducer show it is suitable for the expected conditions. Therefore, the electrostatic transducer shown connected to the Ranging Module in Figure 3.1 was selected.

## **2. Ranging Module Theory of Operation**

The 6500 Series Ranging Module can be operated in two different modes: a single-echo mode and a multiple-echo mode. The multiple-echo mode is of use in robotics when more than one object is to be detected, say one at 3 feet and one at 8 feet from the robot. The single-echo mode is more appropriate for the SONALT application, as only one return is expected. The single-echo mode is the default mode, as will be discussed in detail later.

6 VDC power is applied to pin 9 continuously during system operation, while a ground connection is provided at pin 1. Polaroid advises that the 6 VDC supply must be capable of providing 2.5 amperes for about 1 millisecond to support the load of the transducer during sound transmission.

A ranging cycle is initiated by applying a 6 VDC logic signal to pin 4 (INIT). The waveform for a typical ranging cycle is depicted in Figure 3.2. The INIT logic signal is taken high and maintained at this level awaiting an echo return, and then reset to the low logic level at maximum range. A period of the user's choosing can then pass before taking INIT high once again and initiating another ranging cycle. An echo returning after INIT has gone low will not be detected; INIT must be high to enable echo reception.

As depicted in Figure 3.2, when INIT goes high, a train of 16 pulses is emitted by the transducer, which lasts only 0.5 milliseconds. This chirp is of very high frequency and all that is heard by the human ear is a clicking sound. This chirp is produced at a nominal 118 dB Sound Pressure Level (SPL) measured at 1 meter, with a minimum of 110dB. The 16 pulses are transmitted at 49.4 KHz, while the range of human hearing is from 0-20kHz. To compare the SPL of the chirp with sounds in the human range of hearing, note that a hand-held circular saw used in carpentry emits 100 dB and that each increase of 3 dB in SPL is a doubling of sound pressure level [Ref. 5].

The train of pulses propagates away from the transducer and reflects off the target and returns to the transducer. Polaroid chose to use 16 pulses to improve detection of the return echo. If the circuitry were designed to transmit and detect a single pulse, a single spurious noise pulse would be considered an echo, causing an inaccurate reading.

Alternatively, at long ranges, a single weak returning pulse might be missed. Circuitry designed to identify an echo based on several pulses would optimize accuracy.

Upon detection, the circuitry takes the output of pin 7 (ECHO) high, and holds it high until INIT goes low as shown in Figure 3.2. The elapsed time between INIT going high and ECHO going high is directly related to the range to the target and may be computed using a simple time-distance relation based on the speed of sound (factoring in the round-trip distance traveled by the sound). The cycle can be repeated by returning the INIT to low and then bringing it high again to initiate the next cycle.

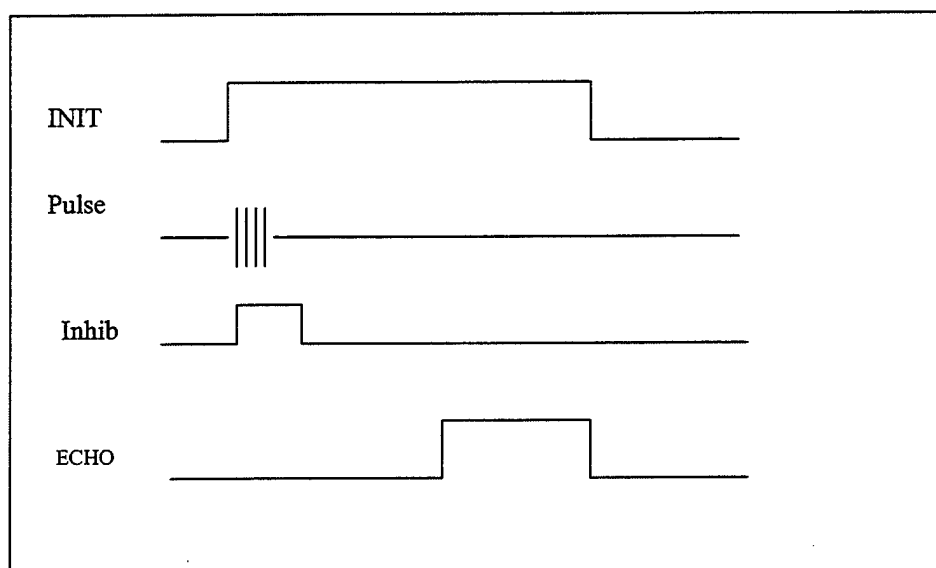


Figure 3.2. Waveform Logic Input and Outputs

Since the transducer serves as both a loudspeaker and a microphone, the receipt of return echoes must be inhibited during the time the 16 chirps are transmitted. Additionally, the transducer will continue to 'ring' after the voltage is removed, much as a bell rings after being struck. To prevent the outgoing chirps and subsequent ringing from being detected as a return signal, the 6500 Series Module inhibits returns during the first 2.38 milliseconds after INIT goes high. This 2.38 msec period determines the minimum range of the system, unless it is reset to a shorter period, as we shall see later. This minimum distance is a function of the speed of sound in air, which is determined by the following relation:

$$a^2 = \gamma RT$$

Where,

$a$  = speed of sound (ft/sec)

$\gamma$  = ratio of specific heats (1.4 for air)

$R$  = individual gas constant ( $1716.26 \text{ ft}^2/\text{s}^2\text{ }^\circ\text{R}$  for air)

$T$  = temperature (degrees Rankine)

Using the appropriate values for air and an ambient temperature of 70 degrees Fahrenheit,  $a = 1128 \text{ ft/sec}$ . During the 2.38 millisecond internal blanking period, the pulses travel 2.68 feet. Accounting for round trip travel we divide by two and find the minimum range is 1.34 feet. Temperature has an effect on the accuracy of this rangefinding system. Take for instance the effect of an increase from 70 degrees to 95 degrees Fahrenheit. The speed of sound now changes to 1154 ft/sec, an increase of about 2.5%. This increase in the speed of sound results in a slightly greater minimum range of 1.37 feet, only a small difference. But, of more interest, is the effect of this change in the speed of sound at a greater altitude. For an altimeter calibrated at 70 degrees, the SONALT would underestimate altitude by about 0.5 ft at 20 ft.

The user can modify the internal blanking setting of 2.38 milliseconds with an input at pin 8 (BINH). When BINH is taken high, internal blanking is discontinued. It is not wise to take BINH high any earlier than the departure of the 16<sup>th</sup> pulse that occurs in the first 0.5 milliseconds. However, blanking can be reduced below the default 2.38 milliseconds to provide for low altitude operations below 1.34 feet. This would be necessary if a control algorithm were to be developed to land the helicopter and altitude data was required down to a very few inches.

In the multiple-echo scheme of operations, it is necessary to reset the Ranging Module after receiving a return from an object; otherwise the ECHO signal at pin 7 would remain high for as long as INIT is held high. Reset is accomplished by taking pin 2 (BLNK) high and returning it low again. Since the return echo may have been detected early in the 16-pulse train, it is important to hold BLNK high for at least 44 milliseconds to let the entire train pass before returning it low.

Although the transducer creates a very highly directional beamform concentrating the vast majority of the transmitted energy into a narrow corridor, the sound power density of the departing signal suffers from spreading and attenuation losses. Additionally, only a small fraction of the transmitted energy is reflected off the target to return to the transducer, as much is reflected off in various other directions. This posed a

problem to the designers at Polaroid; the receiver circuitry can only be optimized to a small dynamic range. A very strong return produced by a nearby target would saturate the receiver and a weak signal from a distant target might be beneath threshold if a fixed gain amplifier was used. Since returning signal strength in this application will be directly related to distance to the target, which is also directly related to the time since INIT went high, a variable gain with time scheme was employed. An internal clock is provided within the Ranging Module that steps the receiver gain through 12 steps, from a gain of 0.25 up to a gain of 10. This allows the Ranging Module to have a much greater dynamic range and increases the maximum attainable distance. [Ref. 4]

As indicated, the Polaroid Ranging Module requires an external power supply, drive circuitry and output signal processing to be useful as an altimeter. A conceptual design for this circuitry was developed to meet the requirements of this application. The electronic expertise of Mr. Jerry Lentz, staff physicist for the Aeronautical Engineering Department was used to perform the detailed design and physical assembly of this circuitry. This development involved building a "breadboard" version of the circuitry, where components such as resistors, capacitors and circuit devices were temporarily assembled and interchanged to refine the design. Once a suitable circuit was assembled, it was permanently mounted and soldered on a circuit card for eventual installation on the vehicle. Mr. Lentz performed this assembly and with the aid of an oscilloscope and other tools produced circuitry based on the conceptual design. Necessarily, the hands-on portion of this development, including the sizing of various resistors, capacitors, and the like, was an iterative process. The fine details of the refinement of the initial design were the result of Mr. Lentz's work and credit is given for his considerable efforts. Figures 3.3 and 3.4 are schematics depicting the SONALT circuitry he developed based on the initial design. An overview of the operation of this circuitry, as developed in the initial general design, is given in the next several sections.

### **C. SONALT POWER SUPPLY**

The Polaroid 6500 Series Ranging Module operates on 6 VDC power. A high capacity 12 VDC power source used to provide power to other components was available to power the SONALT. A method for reducing the voltage without adding another large DC converter was needed. A small LM340K linear voltage regulator was utilized on the printed circuit card to develop approximately 5.2 VDC, which was sufficient to drive the



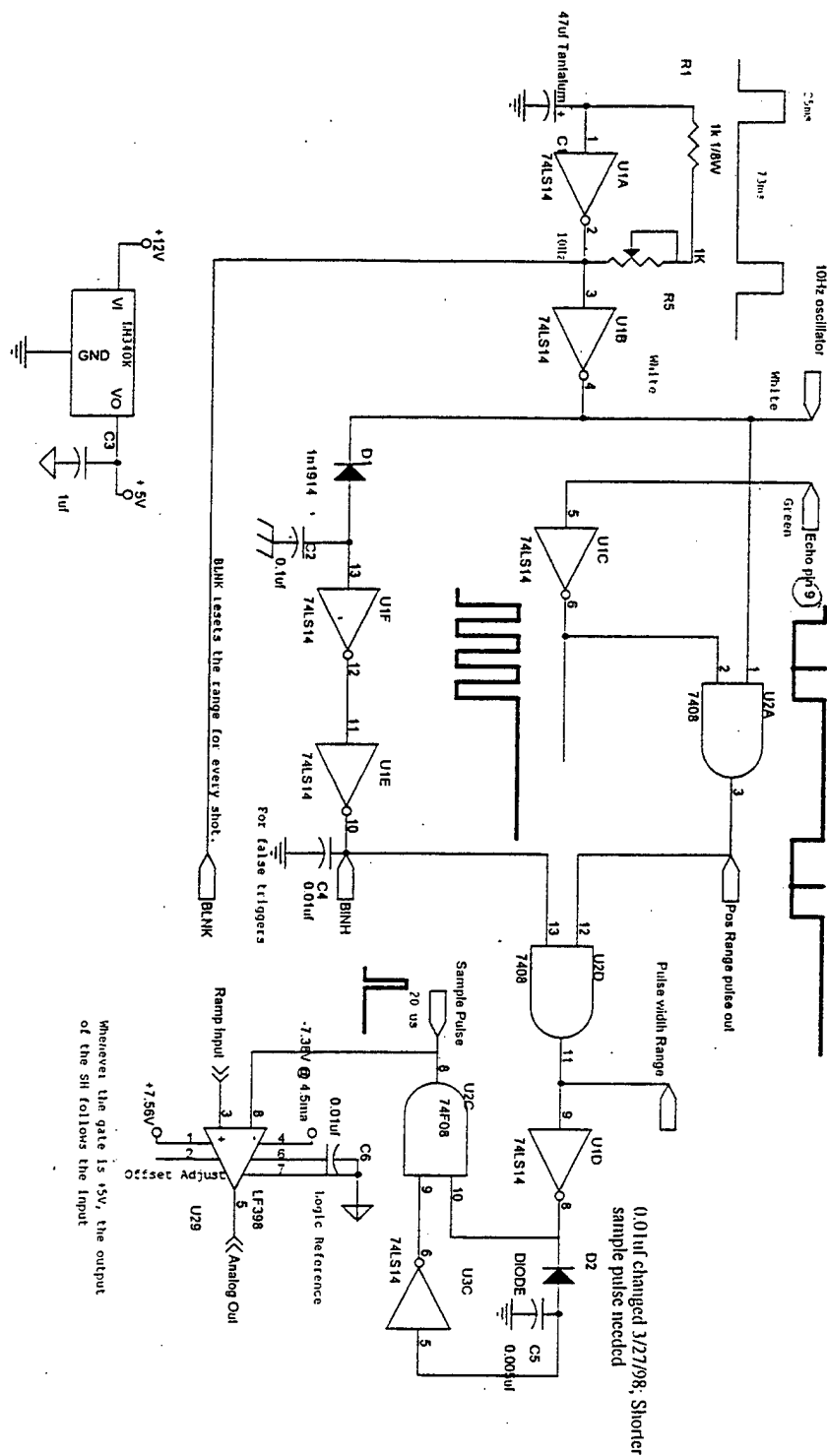


Figure 3.3. SONALT Schematic Part One



Polaroid Ranging Module, the oscillator and the output processing circuitry. This component may be found on Figure 3.4 connected to the 12 VDC input supply.

As we shall see in a subsequent section, the selection of the LF398 sample-and-hold device required both a +7V and -7V supply. A +7.56 VDC source was created by connecting a 270 ohm resistor to the 12 VDC supply, followed by a zener diode with voltage drop of 7.56 VDC. Thus, there was a voltage drop of 4.44 VDC across the 270 ohm resistor leaving the output of the resistor at a potential of +7.56 VDC. This voltage was applied to an ICL7660 CMOS voltage converter to develop the -7.56 VDC required. The ICL7660 delivers an open-circuit output equal to the negative of the input voltage to within 0.1%. It operates by charging a capacitor (C7) connected to the input supply voltage and also connected to the output supply, transferring the necessary charge to an open-circuit storage capacitor (C8). [Ref. 6]

#### **D. DRIVE OSCILLATOR**

An oscillator is needed to repeatedly trigger the Ranging Module to produce an acoustic pulse. Several different types of oscillators are available which produce specific types of waveforms: sinusoidal, sawtooth, and triangle waves are examples. A sinusoidal wave may be produced by a simple LC circuit. However, the Ranging Module requires the wave to consist of only two voltage levels, and not the continuously varying voltage of a sinusoidal wave. In addition to a DC power input, the Ranging Module requires the INIT logic input to be taken high (about 5-6 volts) and then low (about zero volts) for each cycle. This would be seen in the time domain as a rectangular waveform. Polaroid recommends using a simple oscillating circuit consisting of two Schmitt triggers, which accept standard Transistor to Transistor (TTL) logic inputs. The drive circuit developed is depicted in Figure 3.5.

The two Schmitt triggers are depicted as triangles with small circles on the right-hand vertex, which identify them as inverters. Inverters perform a basic logic function: given low logic input, the inverter outputs a high logic output. Figure 3.6 shows six inverters incorporated together into a single Dual In-line Package (DIP). A supply voltage must be provided at pin 14 and a ground at pin 7. It is standard practice to omit this supply voltage on diagrams such as Figure 3.5. This undepicted voltage is the source of the output voltage for low logic input.

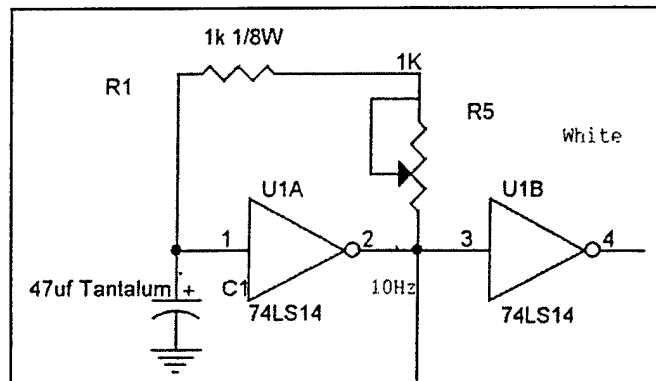


Figure 3.5. Rangefinder Oscillating Circuit

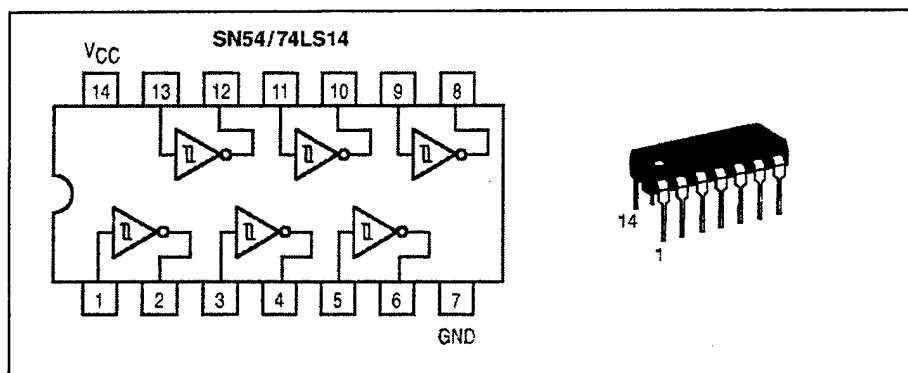


Figure 3.6. Motorola 74LS14 Schmitt Trigger DIP

Although an inverter is depicted by the symbology of a triangle and an appended circle, the internal circuitry in the Schmitt trigger is made up of several components providing the performance the manufacturer desires. Although the Schmitt trigger internal arrangement is not this elementary, its operation may be roughly understood by the following example. A simple inverter can be made of a NPN transistor and a resistor as shown in Figure 3.7. A transistor operates as a switch, and is controlled by applying a current to the base, labeled "A" in the figure. Whenever a voltage greater than an established value is present at the base, current flow is enabled (the "switch" is on) between the collector and the emitter (from the resistor to ground). This "pulls-down" the voltage at A-bar to close to ground potential. Thus an inversion has been created; A is high, and A-bar is low. When no current flow is present from base to emitter, the "switch" is off, and there is no flow of current through the transistor from collector to emitter. Therefore, the voltage at A-bar remains high, while A is low.

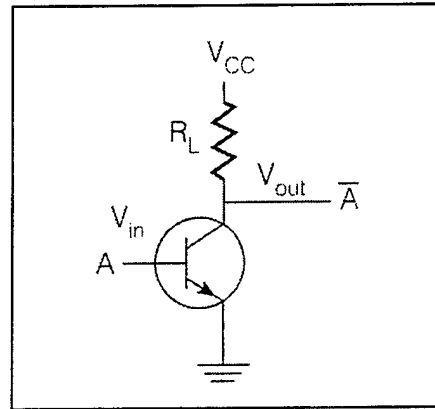


Figure 3.7. Simple Inverter

Referring again to Figure 3.5, we see that at start-up, the input to the left-hand inverter (U1A) would be low, since the capacitor is not charged and no other power source is available. This causes the inverter U1A to produce a high output. Current flows through the variable resistor R5 and through resistor R1 to begin charging the capacitor C1. The rate at which the capacitor charges may be controlled by setting the values of the two resistors and the capacitor. When the capacitor charges to the point where the voltage sensed at the input (pin 1) reaches about 0.6 V, the output is then switched low. The charge on the capacitor is then drawn down through pin 2, bringing the input to low logic again. This repeated switching from high to low creates an oscillating output which may be used to drive the Ranging Module at pin 4 (INIT) after being inverted by a second inverter (U1B). Due to the values of the resistors and capacitor chosen, an asymmetric pulse was created at pin 2 of U1A as shown in Figure 3.8. Also shown is the signal at the output of pin 4 of U1B, which is used to drive pin 4 (INIT).

A pulse repetition frequency (PRF) of 10 Hz was chosen for the oscillator based on several factors. First, the RFTPS control software operates at a discrete sampling rate of 25 Hz; a PRF of greater than 25 Hz would be wasted effort. Secondly, because INIT must be held high while the signal is propagating out and until it returns to the transducer, a minimum value for the INIT being high is related to the maximum range desired. Since the stated requirement was an altitude range from zero to 30 feet, the INIT must be high for a minimum of:

$$(2 \times 30 \text{ ft}) \div (1128 \text{ ft/sec}) = 53 \text{ milliseconds.}$$

An optimum solution might be to hold INIT high for 53 milliseconds and then bring it low for 2 milliseconds before going high again. This 55-millisecond pulse repetition interval (PRI) corresponds to about an 18 Hz PRF, close to the software sampling rate of 25 Hz. However, Polaroid recommends INIT be held low for as long as 100 ms for proper operation. This period was considered to be excessive and experimentation revealed that a shorter INIT low period was satisfactory. A 10 Hz PRF made a good compromise and good results were achieved during ground testing.

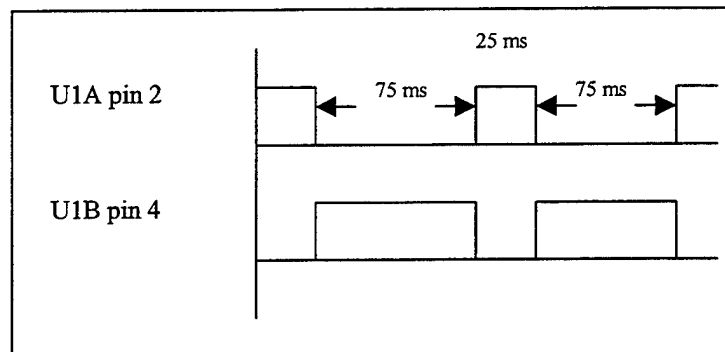


Figure 3.8. Oscillator Waveforms

A combination of the two resistors and one capacitor was chosen so the oscillating waveform created at pin 4 remained high for 75 ms and then went low for about 25 ms. The resulting PRI was 100 ms, which corresponds to a 10 Hz PRF. A variable resistor was employed to allow the user to fine tune the oscillator and adjust for variations caused by temperature.

## E. OUTPUT SIGNAL PROCESSING

Altitude is determined by measuring the time between INIT going high and ECHO going high. By applying the speed of sound and accounting for round trip travel, an accurate altitude may be computed. Since the IMU is being used to transmit the altitude information to the ground station through an analog-to-digital input channel, the SONALT output must be in a form compatible with that unit. The IMU analog-to-digital converter accepts analog voltage from 10V to -10V. Analog circuitry was developed to convert the information contained in the high/low logic waveform produced by the Ranging Module to an analog voltage proportional to altitude.

A two step process was envisioned. First, using logic gates on integrated circuits, AND the INIT signal with an inverted ECHO signal to produce a Pulse Width Modulated (PWM) signal. The resulting PWM waveform, as shown in Figure 3.9, will have the same PRI as the INIT signal (100 ms). The length of time the pulse is high (pulse width) is directly related to altitude. Note in Figure 3.9 the altitude is increasing, as shown by the pulse width of the PWM signal increasing with time.

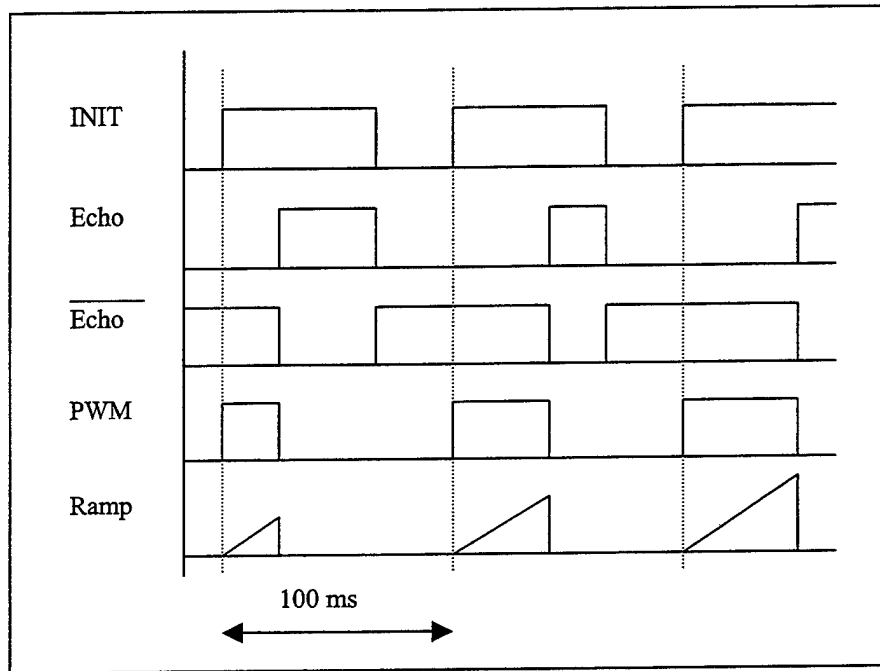


Figure 3.9. PWM Range and Ramp Waveforms

Secondly, the PWM waveform is processed to generate a voltage. This is accomplished by creating a ramp waveform where the voltage increases linearly with time until the PWM pulse goes low. This ramp waveform is sampled at its peak and the voltage measured is held until the next sample is taken during the next PRI. The details of these two steps will be discussed in the following subsections.

### 1. PWM Waveform Creation

The Schmitt trigger oscillator previously discussed is located in the upper left-hand corner of Figure 3.3. The output of pin 4 of U1B of the oscillator can be traced to its connection with the Polaroid Ranging Module, and also be traced to pin 1 of U2A, which is an AND gate on a 7408 TTL integrated circuit. The ECHO return from the

Ranging Module is inverted and then connected to pin 2 of U2A. The output at pin 3 is a PWM waveform. However, during the assembly of this circuit, it was noted that the 16 pulses of the echo appeared at the beginning of this PWM waveform. Additionally, there was a period of "dead-time" in the echo pulse due to the latency of the Ranging Module circuitry to produce and detect a pulse. In other words, even at zero range, the ECHO return from the Ranging Module does not appear for a short period. In order to trim the 16 pulse artifact and dead-time period from the beginning of this PWM waveform, the waveform is again AND'ed at U2D with a delayed version of the INIT signal. This delayed INIT signal is produced by a diode D1, the capacitor C2, and the two inverters, U1F and U1E. Capacitor C2 is charged by the leakage current coming out the input of the Schmitt trigger. Since the INIT signal was delayed by about 0.75 milliseconds, it may be used to reset internal blanking by inputting this signal to pin 8 (BINH) of the Polaroid Ranging Module allowing altitudes as small as 5 inches to be measured. Recall that all 16 pulses are transmitted in the first 0.5 milliseconds.

## **2. PWM Waveform to Voltage Conversion**

The design developed determines a voltage corresponding to altitude for each pulse of the altimeter, and continues to produce this voltage until another return is received. When plotted against time, the desired output voltage would appear as a staircase pattern, with each step lasting 100 milliseconds. The first step in creating this staircase involves creating a ramp waveform such as depicted in Figure 3.9. The ramp waveform is sampled at its peak, and that output held until the next sample is taken. See Figure 3.10.

The LM2917 Frequency to Voltage Converter is a fourteen-pin device intended for use in tachometer circuitry. In this application, however, individual components inside the device are used to create the ramp waveform. The components of the LM2917 are shown within the dotted lines in Figure 3.4. Incidentally, note that the zener diode used for +7.56 VDC voltage regulation is a component on this device. Most useful for creating a ramp waveform are the charge pumps. The Pulse Width Range is brought in to the LM2917 at pins 10 and 1 through diode D1. In tracing the connection through pin 1 of LM2917, we see the PWM Range signal is an input to a comparator, which drives two charge pumps.



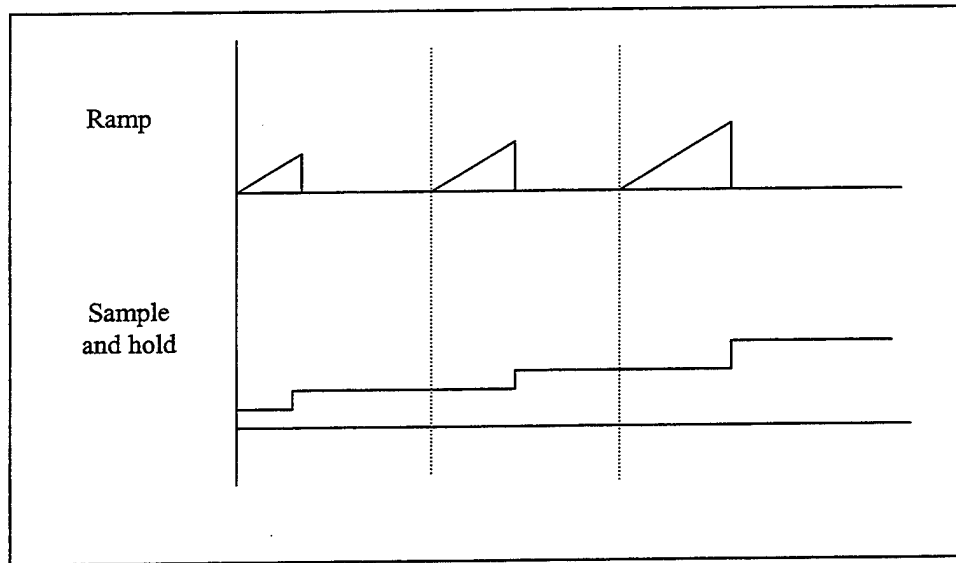


Figure 3.10 Sample and Hold

These charge pumps can be viewed as ideal current sources. They produce current at a constant rate regardless of voltage and thus can be used to charge a capacitor linearly with time, rather than exponentially. The comparator senses a constant reference voltage through pin 11. When the PWM range signal applied to pin 1 is high, the charge pumps provide a positive current to charge capacitors C2 and C1, which have been mounted on pins 14 and 13 of the LM2917 for convenience. Capacitor C1 has been sized so that at approximately 55 milliseconds (approx. 30-foot range) the capacitor is charged to five volts and because a charge pump drives it, the charge increases linearly with time. This produces the required ramp. Note the connection in Figure 3.4 between capacitor C1 and the sample-and-hold device, LF398.

The LF398 sample-and-hold circuit has been depicted in both Figures 3.3 and 4.4 for clarity. The device is supplied with  $\pm 7$  VDC supply voltage at pins 1 and 4, while the ramp input waveform is connected at pin 3. When a sample pulse is applied at pin 8, the device samples the ramp waveform voltage and outputs this voltage steadily until the next sample pulse, even if the input ramp waveform subsequently is reset. In this case, the sample pulse must be applied at the very peak of the ramp, just prior to the ramp being reset for the next cycle. A complication in this design is that the instant the sample pulse is needed is dependent on the altitude, which is precisely the unknown quantity to be measured.

Returning now to the PWM range output of pin 11 of U2D on Figure 3.3, we can follow the creation of this sample pulse. U1D produces an inverted form of the PWM waveform while diode D2, capacitor C5, and U3C produce a 20  $\mu$ sec delayed version of the PWM waveform. This delay is produced in a manner similar to the process used to create a delayed version of the oscillator by U1F and U1E. The AND gate U2C combines these two waveforms as shown in Figure 3.11 to create a 20  $\mu$ sec sample pulse which begins just after the PWM waveform falls. This sample pulse is input to the sample-and-hold device, LF398, at pin 8.

The sampling occurs just before the ramp input is pulled low by a NPN transistor at pin 8 of the LM2917 device. The base of this transistor is connected to a comparator, which compares the PWM waveform to a reference voltage. When the PWM waveform at pin 10 goes low, the comparator applies a voltage to the base of the transistor pulling pin 8, and the ramp input down in preparation for the next cycle.

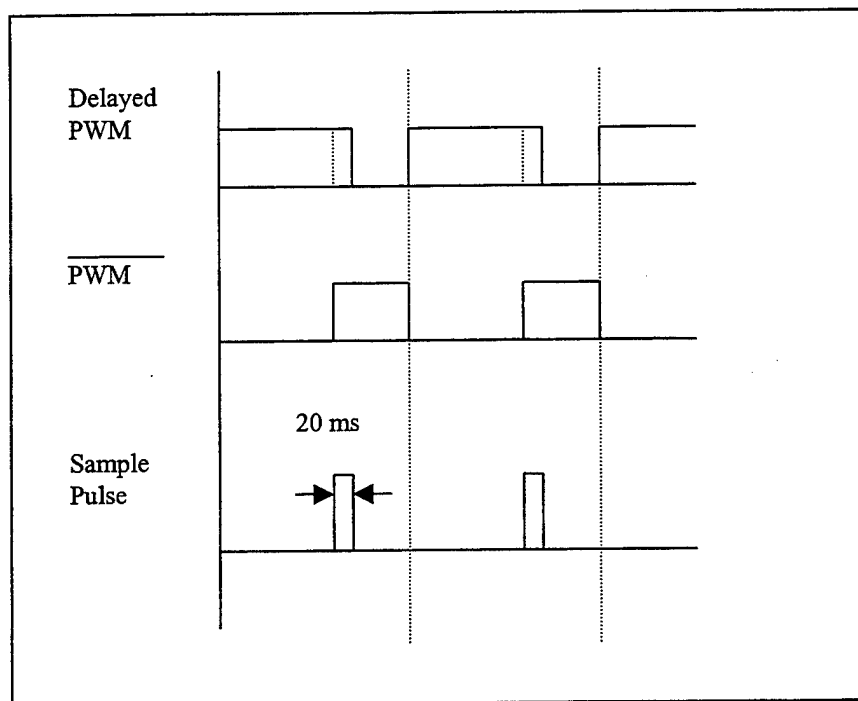


Figure 3.11. Sample Pulse Waveforms

Expansion capability was provided in that a spare AND gate and three inverters are still available to allow an additional Ranging Module to be added.

## F. TRANSDUCER MOUNTING

Several factors influenced the design of the mounting for the transducer. The transducer is essentially a thin piece of foil stretched across a grooved backplate to form the moving element that creates sound from an input voltage, and then converts returning sound into electrical energy [Ref. 4]. This foil has been reported to be very sensitive to vibrations. Additionally, as noted earlier, a very high voltage is placed across the transducer during each transmission, which would likely induce noise into other electrical components and wiring on the vehicle. Furthermore, the transducer must be mounted with a clear path to the ground.

A lightweight aluminum frame was developed, across which a sheet of rubber could be stretched, and pressure plates attached to hold the rubber sheet securely to the frame, as shown in Figure 3.12. The transducer is fitted in an undersized hole cut in this rubber sheet, allowing the transducer to be firmly attached. This aluminum frame, or mount, is attached below the aluminum deckplate on the underside of the helicopter to prevent electrical noise from penetrating up to avionics installed on the deckplate.

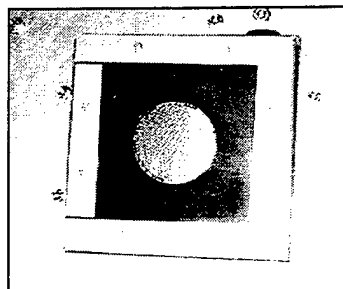


Figure 3.12. Transducer Mount

## G. SONALT TESTING

Testing involved mounting the transducer on the side of a box to allow sound signals to be emitted horizontally towards a flat wall. The SONALT circuitry was driven by the same 12 VDC converter used on the vehicle to ensure conditions close to those in flight could be duplicated. The analog output voltage from the SONALT circuitry was connected to the "IMU Word 4" input channel to the IMU. The serial output was then connected to a laptop computer to record and display the voltages measured by the A/D converter. This equipment was placed on a cart and rolled from a position very close to the wall out to maximum range, stopping at intervals to record data. The minimum range

proved to be about 5 inches where voltage reached a minimum. Further decrease of range resulted in the same voltage value. Data was recorded at 1-inch intervals for the first foot, and then measurements were made at one-foot intervals to 25 feet. Additional measurements were made at 30 feet and greater. The maximum range was measured at about 32 feet, beyond which a constant voltage was produced.

Detailed data are provided in Appendix A. The results appear to be quite linear, however a linear fit through the data produces an error of nearly four inches at ranges less than a foot. A fifth order curve-fit produced very small coefficients for all but the linear terms, but was able to reduce error to less than an inch. The following relationship was developed:

$$alt = -0.0026x^5 + 0.0475x^4 - 0.315x^3 + 0.9524x^2 + 5.0434x + 0.6764$$

Where x is the input voltage and altitude is measured in feet. This equation can be implemented easily in the RFTPS software to obtain altitude in feet. Figure 3.13 plots the data recorded with a polynomial curve fit.

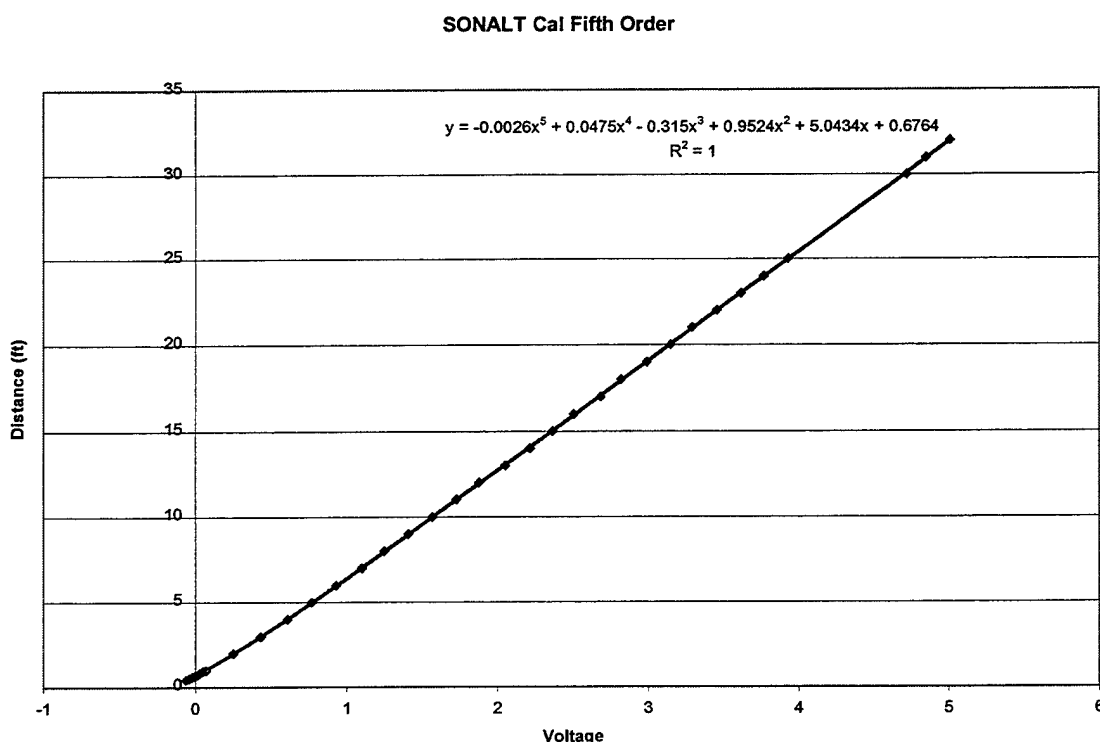


Figure 3.13. SONALT Calibration

Additionally, the SONALT's tolerance to angle-of-bank deviations was tested by positioning the transducer 10 feet from a wall and progressively tilting the transducer until the return was no longer detected. At this close range, the maximum deviation was measured as 16 degrees. This wall was very smooth and hard and tended to reflect all signals such that the angle of incidence equaled the angle of reflection. An uneven ground surface might improve this limitation, although soft ground might not reflect energy as well as the hard wall.

The results provided in Figure 3.14 were recorded during a test run where the cart was moved across the floor towards the wall while continuously recording data. The run began at nearly 30 feet from the wall and continued for approximately 23 seconds. During this time period the data appeared smooth and was uninterrupted by any bad data points or outliers. When inspected in a short time scale, the jagged appearance of the data can be seen to be stairsteps of about 100 milliseconds, just as expected.

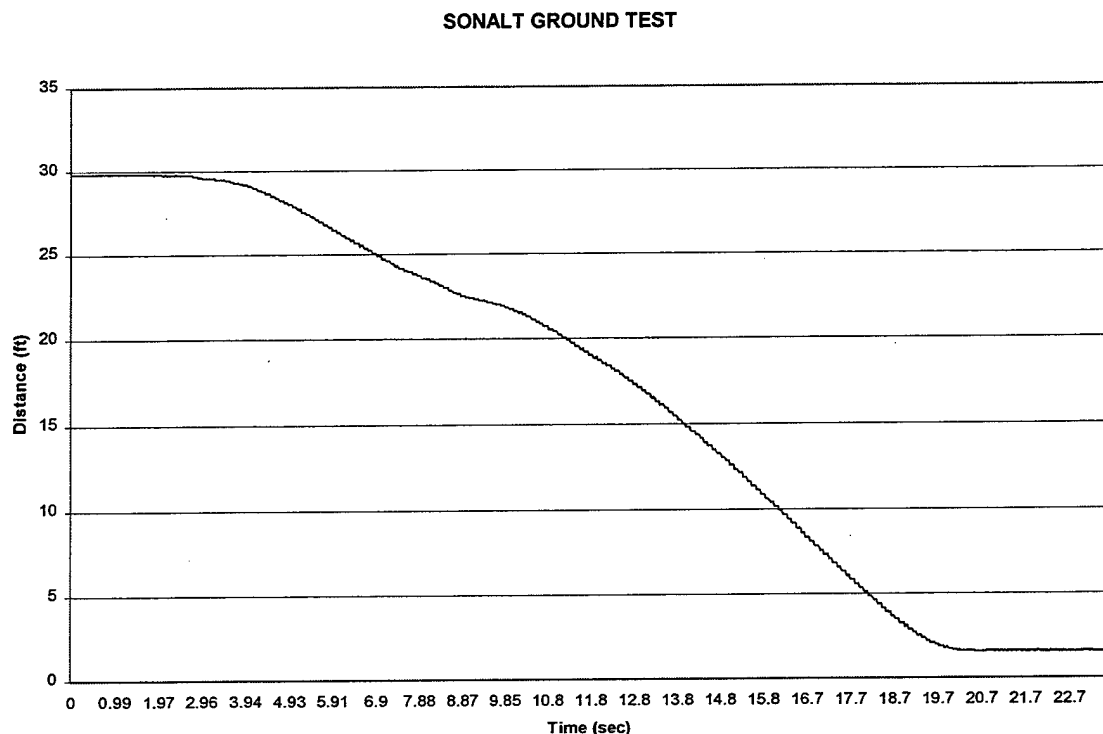


Figure 3.14. SONALT Ground Test

## **IV. AVIONICS RACK AND POWER SUPPLY DESIGN**

### **A. REQUIREMENTS**

The basic helicopter, while possessing a lift capability in excess of 20 pounds (as discussed in Chapter I), does not provide for any cargo area or suitable enclosure to house the avionics suite. A platform of sufficient size to carry the necessary components with a large margin for future growth was needed. A test flight with 15 pounds of steel plate attached to the landing skid was performed to confirm the advertised lifting capacity. Test flight results revealed that the 15 pound payload required a very small increase in collective at trim and the UAV pilot felt confident that 20 pounds could easily be lifted.

Several factors influenced the ultimate design of the avionics platform:

- The physical volume needed to mount the equipment.
- The presence of the pull-starter on the underside of the helicopter.
- The need to place the IMU on centerline as near to the CG as possible.
- Weight and structural strength.
- Ease of construction and availability of materials.

A method of mounting the components and sensors on the helicopter and providing power was developed. The location of each component was determined and its effect on the vehicle center of gravity was assessed. Additionally, to ensure adequate protection from vibration, methods for isolating sensitive equipment were examined.

### **B. SKID DESIGN**

Two options to mount components were available. First, a framework or platform could extend laterally from the helicopter. With a support structure loaded with equipment covering the flanks of the helicopter, access to the pull-starter would be severely restricted, since only 4 inches clearance would be available to reach under the laterally mounted rack and grasp the pull-starter handle. Additionally, the IMU would be mounted off-center, although the effects of this displacement could be accommodated with a software transformation. With components loaded outboard, the carburetors on the starboard side would be obscured, and heat shielding would be necessary on the port side adjacent to the exhaust. The existing plastic landing skid could be retained.

The second option, and the option selected, was to build a framework below the helicopter to serve as both an avionics rack and landing skid. The IMU could be mounted on centerline, and a large flat surface would be available to mount electronic components. Ample room would be available under the nose of the helicopter for the future installation of a camera. The pull-starter could easily be reached, and access for an electrically powered starter shaft could be provided through the bottom of the rack to replace the hand starter.

Available materials were inventoried and a large stock of ½ inch aluminum channel was located. Engineering drawings were produced and the landing skid shown in Figure 4.1 was constructed with 308 square inches of surface area. All joints were welded except where the skid rails attach to the legs below the avionics platform, which were attached with screws for easy removal. Connection between the helicopter frame and the avionics rack was accomplished through the use of attachment plates on the upper rack cross-members. These mounting plates formed a sandwich which mated with the composite chassis at the same holes provided for the original plastic landing gear. 0.050" aluminum sheeting was used for the platform deck and was attached to the aluminum frame with screws. The total weight of the rack and skid assembly was 5.65 pounds, including an access tube provided for the starter. This left a useful payload of more than fourteen pounds available for avionics equipment.

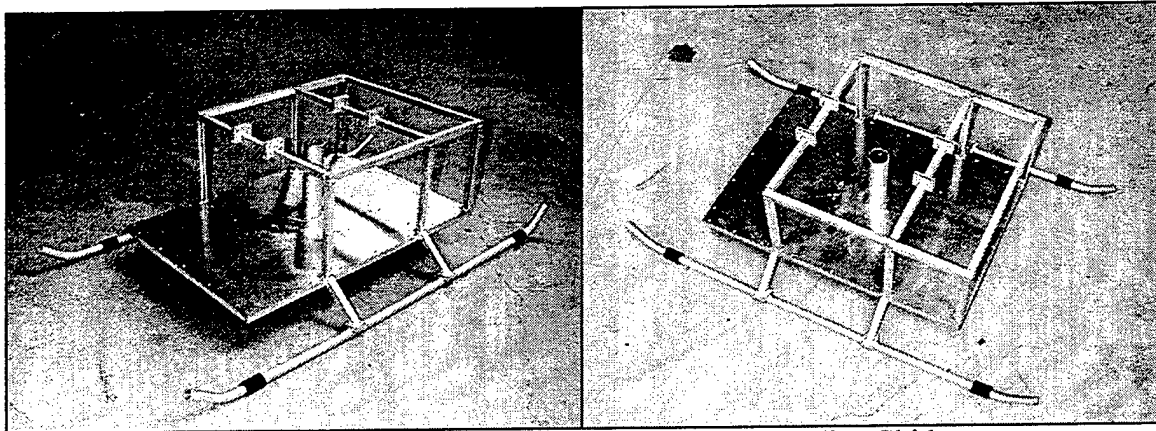


Figure 4.1. Aluminum Avionics Rack and Landing Skid

### C. COMPONENT PLACEMENT

Placement of components on the avionics rack was primarily influenced by weight and balance considerations. An overhead view of the placement of components

on the rack is shown in Figure 4.2. The circular tubing in the center of the rack provides access for an external starter shaft. The position of this access is predicated on the location of the bottom of the engine crankshaft. The IMU (black box) was positioned immediately aft of the starter access with the electrical connections facing forward, as required to properly orient the IMU coordinate system. This located the IMU as close as possible to the predicted center of gravity.

A power panel interconnection panel and two switching power supplies were attached to the frame in the starboard quarter, while a battery was placed on the port side to provide lateral balance. The FreeWave wireless modems were placed in the center area along with the GPS and SONALT circuitry (not shown). The SONALT transducer was mounted on the bottom of the rack. The entire forward portion of the platform was left vacant for future use.

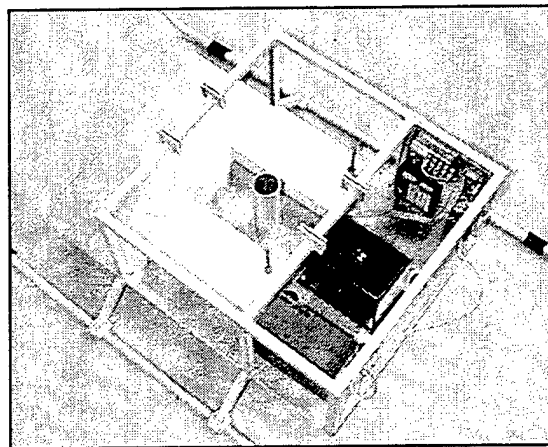


Figure 4.2. Component Placement on Avionics Rack

The center of gravity was tracked using a spreadsheet program, which recorded component position and weight. The system used for recording positions is similar to that used on full-size aircraft. The leading edge of the avionics rack was used as a datum from which fuselage stations were measured aft in inches. The deck of the avionics rack served as the waterline for vertical measurements, positive up. Lateral measurements were taken from centerline, positive to starboard.

The center of gravity for the basic helicopter was obtained by suspending the helicopter on a horizontal metal rod inserted through open spaces in the chassis. The vehicle was then allowed to rotate such that the center of gravity swung below the suspension rod. The angle of inclination was then measured with a precision level with a



built-in protractor. Several different suspension points were used, and the intersection of the lines-of-position was plotted to determine the center of gravity. As shown in Appendix B, the center of gravity was located directly below the rotor mast, as expected, at a point located 14.25 inches aft of the leading edge and 12.4 inches above the avionics deck. A similar procedure was followed to obtain the center of gravity for the avionics skid alone. This information, along with component weights and positions was recorded in the spreadsheet and the final position of the center of gravity determined.

The spreadsheet program allowed several different component arrangements to be considered and the effect on the movement of the center of gravity quickly determined.

The top of the horizontal stabilizer on the tail of the helicopter was chosen as the location for the GPS antenna for two reasons. The device weighs only 4.8 ounces, but a position this far aft is helpful in maintaining the center of gravity near the rotor mast. Additionally, this location provides a more unobstructed horizon for the antenna and is somewhat removed from the electrical noise generated by other avionics and the spark plugs of the engine.

#### **D. POWER SUPPLY SYSTEM**

The components incorporated into the design of the avionics suite must be steadily supplied with a power. Pertinent data is listed in Table 4.1.

<b>Component</b>	<b>VDC</b>	<b>Amperage (mA)</b>	<b>Watts</b>
IMU	24	250	6.00
FreeWaves (2)	12	240	2.88
GPS	12	150	1.80
SONALT	12	150	1.80
<b>Total</b>			<b>12.48</b>

Table 4.1. Avionics Power Budget

A MILSPEC battery (BA-5590/U NSN 6135-01-036-3495) of the same type used in the FROG was selected due to its ability to produce 24 VDC power, as well as its availability. The battery consists of two 12 volt cells enclosed in a single casing. Linking these two cells in series can create a 24 volt source. Batteries are typically rated in milliamp-hours (mAh). This battery is rated 14,400 mAh when wired in series [Ref.

15]. The 12.48 watt load described above requires 520 milliamps at 24 volts. Even when accounting for the converter efficiency (probably around 80 %), the battery is clearly capable of supporting the intended application. Two batteries of this type are used by the Marine Corps in its AN/PSC-3 man-pack mobile satellite communications package, which is capable of transmitting 35 watts of power [Ref. 13].

Battery voltage decreases over time as components continue to draw power. Additionally, the voltage in a system is drawn down temporarily when one component draws peak power. Household plumbing systems are a useful analogy. Water pressure is everywhere influenced by the demands of one faucet or shower. Two voltage converters were selected, identical to those used on FROG: one producing a constant output of 24 VDC with an input voltage anywhere within the range of 18-36 VDC to support the IMU. A second converter creating 12 VDC with input voltage 18-36 VDC supports the remaining avionics. The converters are rated at 2 amps and 2.5 amps respectively, fully adequate for the demand. These converters aren't simple transformers. A transformer uses a ratio of windings around a magnetic core to step voltage up or down by the ratio of the windings. These converters are switching regulators capable of maintaining a constant output voltage throughout a range of input voltages.

A power supply panel was assembled upon which the converters, associated switches, test points, and connectors were mounted. The supply panel is shown in Figure 4.3.

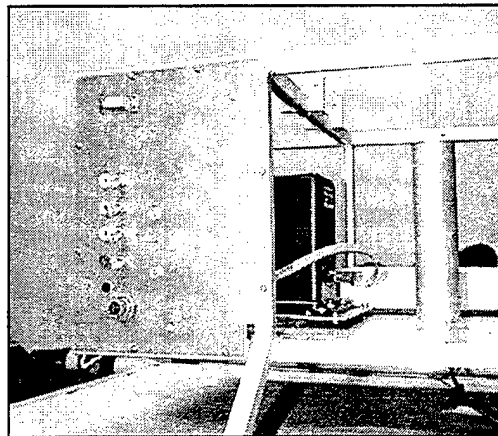


Figure 4.3. Power Supply Panel

A single-pull, double-throw switch allows selection of either an external 24 VDC power source for ground testing and maintenance, or the internal 24 volt battery. 24

VDC and 12 VDC switches control the output of the two converters, and an extra switch for future use was provided. 24 VDC external power may be attached through a MILSPEC three pin female connector. Additionally, a female DB9 connector was provided on the panel face to allow access to the IMU to adjust the unit's parameters stored in EEPROM (Electrically Erasable Programmable Read Only Memory). The panel mounted serial connector can also be used to sample data directly from the IMU to a laptop computer as described in Chapter II, without unplugging the connector from the IMU. On the interior side of the power panel, a terminal strip was provided for easy connection to the IMU's A/D converters. Wiring diagrams for the power supply system and for signal connections are contained in Appendix C.

## **E. VIBRATION ISOLATION**

Although vibration caused by the main and tail rotors, as well as vibration produced by the engine and reduction gearing was anticipated, it proved to be a much greater problem than anticipated. Sensitive electronics, such as the IMU, and later, a camera, need to be protected from the harsh vibrations produced by the helicopter. The reduction gearing between the engine and the main rotor provides a ratio of 90:14, while the tail rotor turns at roughly 4.5 times faster than the main rotor. Since the helicopter has a two-blade main rotor, it was expected that there be a predominant vibration frequency at the main rotor RPM, called "1P" for "once per" revolution of the main rotor, and also a strong artifact at double that frequency, called "2P." The vibration frequency spectrum was determined with three different test procedures.

First, a small, hand-held RPM reader produced for the RC enthusiast was used to measure the RPM of the main rotor blade while in flight. The device has a small window, similar to the viewfinder on a camera, through which the operator is able to view the blades of the helicopter in flight. The device operates much like the timing strobe on an automobile used by mechanics. The operator of the RPM reader adjusts the frequency of the strobe to make the main rotor appear to stop when viewed through the rangefinder. When this condition is reached, the rotor RPM can be read off an LCD display. This measurement produced a reading of 1570 RPM (26.2 Hz). A single blade passes a fixed point with a frequency of 26.2 Hz, however, with two blades on the main rotor, spectral components will also be seen at 52.4 Hz.

A second test was conducted using a three-axis accelerometer mounted on the helicopter and connected via an umbilical to a spectrum analyzer. The spectrum analyzer revealed high energy around 28 Hz and 56 Hz. 28 Hz equates to a main rotor RPM of 1680 RPM. A later test revealed a main rotor frequency of about 27 Hz. Note that the RPM will vary with the lift and collective required to hover, which in turn vary with air density and current weight of the helicopter. Therefore, the variation in readings can be traced to variations in weather conditions, fuel weight, avionics weight, collective/throttle settings, and engine performance. The vibration spectrum for the later test is plotted in Figure 4.4.

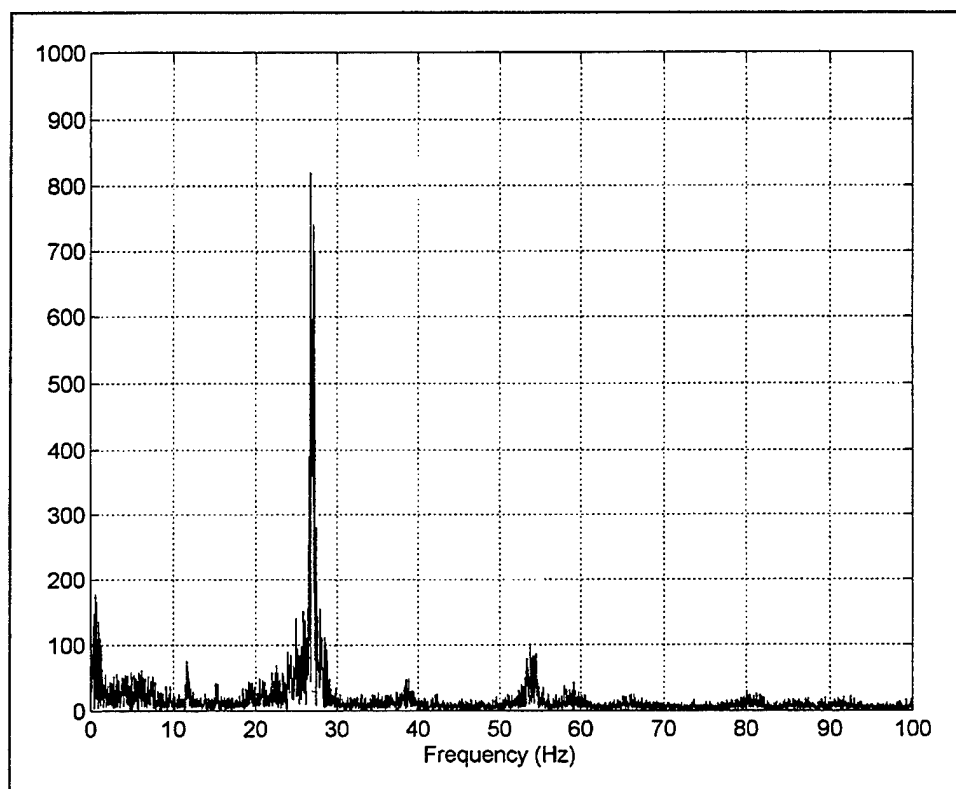


Figure 4.4. Vibration Spectrum

The 27 Hz main rotor frequency was selected as a design point for the purposes of vibration isolation. The power transmitted at this frequency and at the higher 2P frequency of 54 Hz is far greater than the other vibration frequencies measured. Rubber mounts are available to isolate equipment from vibrations. To achieve proper isolation, however, the proper mount must be selected for the application. In addition to providing

protection from the periodic vibrations caused by the main rotor blades, these mounts provide protection against damage to equipment caused by shock, such as a hard landing.

Initially, consideration was given to isolating the entire platform, such that all components mounted on the platform would be protected. This approach is complicated by the need to evenly distribute weight across the several mounting points to achieve proper vibration isolation. If components are not flown on a particular flight, for example, the loading would become uneven, and the expected isolation would not be achieved. Therefore, since not all components require shock mounting, it was decided that only the most sensitive equipment would be shock/vibration mounted.

To determine the proper mount for a particular application, it is useful to consider the avionics component and the associated mounts as a simple spring-mass-dashpot system as shown in Figure 4.5.

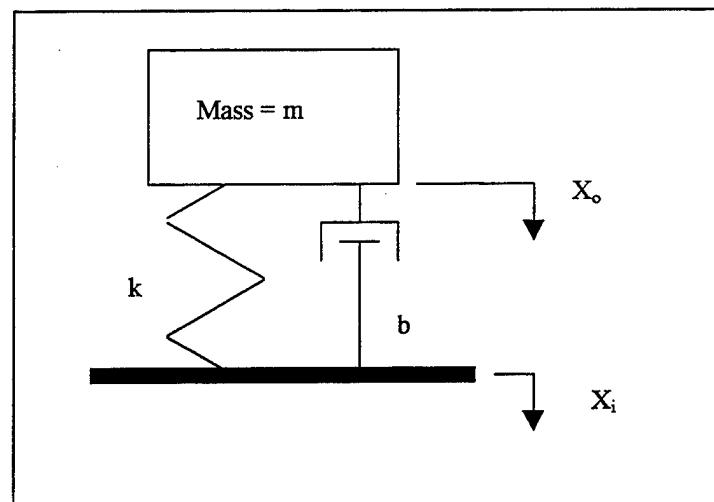


Figure 4.5. Simple Spring-Mass-Dashpot System

In this system, the vibrating structure causes a deflection across the spring that transmits a force to the supported mass. The nature of the motion produced is a function of the mass of the component, the spring constant ( $k$ ) of the mount, and the damping ( $b$ ) afforded by the mounting material. The platform vibration is considered an input to this system, and is represented as  $x_i$ . The response of the component is represented by  $x_o$ . The transfer function from input to output is:

$$H(s) = \frac{X_o(s)}{X_i(s)} = \frac{bs + k}{ms^2 + bs + k}$$

Where  $s = j\omega$ , where  $\omega$  is the periodic frequency of the vibration in question in radians per second. Notice that for a very small excitation frequency,  $H(s)$  is very nearly one. This means the mass would follow the motion of the base. If however, the input vibration frequency were to be very high,  $H(s)$  would be very small, indicating that the motion of the mass would be very small.

In this case, a mount with a certain  $k$  and  $b$  must be selected such that 1P and 2P frequencies are greatly attenuated. Lord Mechanical Products produces a series of lightweight mounts such as shown in Figure 4.6. A mounting arrangement of four 100PDL-A mounts was selected, with one mount at each corner of the IMU. Each mount is rated at 0.5 pounds capacity with a spring constant  $k = 8$  pounds per inch = 96 pounds per foot. No value for the damping constant ( $b$ ) is published. Lord Mechanical Products advises that these mounts are manufactured from an elastomeric material, which differs from the common steel spring in that its stiffness changes with the rate of deflection, not simply with distance. This gives the elastomeric mount the properties of a spring and also a damper. Damping is thought to be rather light, and is assumed to be about  $\xi = 0.1$ , lacking more detailed specifications.

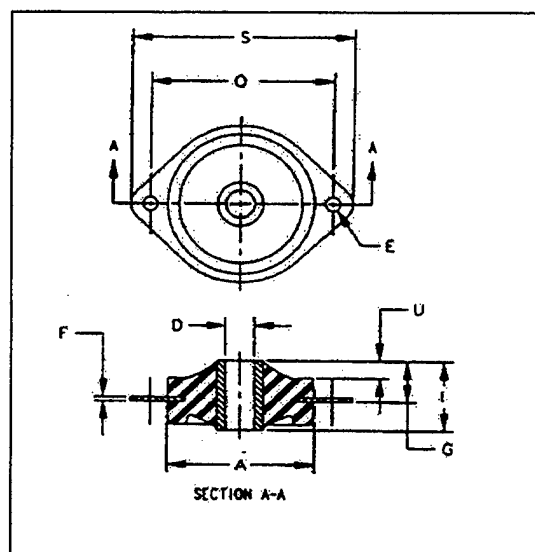


Figure 4.6. Elastomeric Platform Mount for IMU

Inserting the values for the variables and dividing the numerator and denominator of the transfer function above by the value of the mass, we find the characteristic equation in the denominator. The IMU weighs just 2 pounds (0.0622 slugs) and the spring constant

constant  $k$  must represent all four mounts and is expressed in pounds per foot. ( $k = 8 * 12 * 4 = 384$  pounds/ft) The resulting characteristic equation is:

$$s^2 + \frac{b}{.0622}s + \frac{384}{.0622} = 0$$

Therefore, the natural frequency,  $\omega_n$  is:

$$\omega_n = \sqrt{\frac{384}{.0622}} = 78.57 \quad (\text{Radians/sec})$$

Assuming damping  $\xi = 0.1$ , the second term of the characteristic equation must become:

$$2\xi\omega_n s = 2(.1)(78.57)s = 15.71s$$

The transfer function then becomes:

$$H(s) = \frac{s + 6173}{s^2 + 15.71s + 6173}$$

A bode diagram for this transfer function is given in Figure 4.7. Notice that at lower frequencies the gain from input to output is slightly greater than one, or 0 dB. The gain increases, reaching a peak at about 78 rad/s, the natural frequency of the system. The computed natural frequency of the mounts was confirmed by testing. The height of this peak is a function of the amount of damping in the system -- the more damping, the lower the peak. From the peak, the gain decreases, crossing the 0 dB point at a value of 1.414 times the natural frequency. The region from DC to the axis crossing point is known as the region of amplification. As frequency continues to increase, the gain steadily decreases. This region is known as the region of isolation. The computed natural frequency was confirmed through laboratory testing. The elastomeric mounts were placed on the IMU and the IMU was displaced from its neutral resting position and then released. The response was measured. A spectral analysis of the accelerations revealed a peak around 13 Hz (81 rad/s).

The 100PDL-A mount was chosen because 1P and 2P, at 27 Hz (170 rad/s) and 56 Hz (339 rad/s) respectively fall in the region of isolation. This was the lowest cutoff

frequency available using off-the-shelf mounts. The gain at 1P and 2P can be computed by substituting  $j\omega$  for each frequency into the transfer function. 1P (27 Hz) has a gain of about -11.34 dB and 2P (54 Hz) has a gain of -24.91 dB.

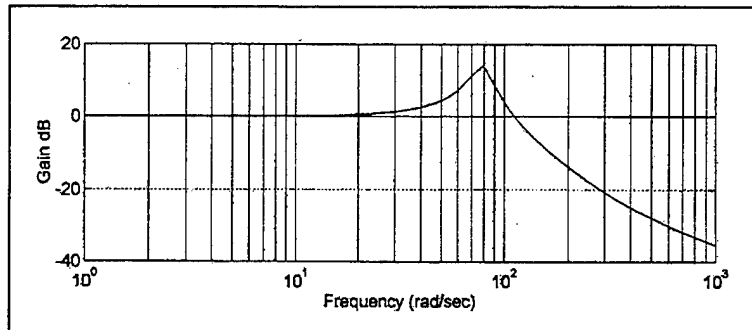


Figure 4.7. Bode Diagram of Elastomeric Mounts on IMU

The region of amplification makes the choice of mount in an avionics application a compromise. If the disturbing frequencies are known, then a lightly damped system with the natural frequency located well below the disturbing frequencies would be a best choice. In this application, however, there will be a time as the rotor RPM is increased for takeoff, that the predominant vibration frequencies passes through the natural frequency of this lightly damped system. During this period prior to takeoff, IMU data may be unusable for flight control.





## V. INITIAL FLIGHT TESTING AND SYSTEM MODIFICATION

### A. INITIAL FLIGHT TESTING

Due to delays in fabrication of the aluminum avionics frame, the development of the SONALT and assembly of the power panel were completed in parallel with the construction of the frame. The avionics rack was first flown without any components attached. See Figure 5.1. Recall that earlier lift-capacity testing involved strapping thick metal plating to the stock plastic landing skids without noticeable vibration or adverse effect on handling qualities. However, upon lift-off with the avionics rack installed, a severe vibration developed in the newly created helo-avionics rack system. The attachment plates at the top of the avionics rack were connected to the bottom of the composite material used in the chassis of the basic helicopter. In this area, the composite material proved to be quite flexible and allowed the avionics rack to vibrate laterally with such violence the helicopter was immediately landed. As it hovered, the engine and rotor appeared fairly steady, while the rack vibrated below.

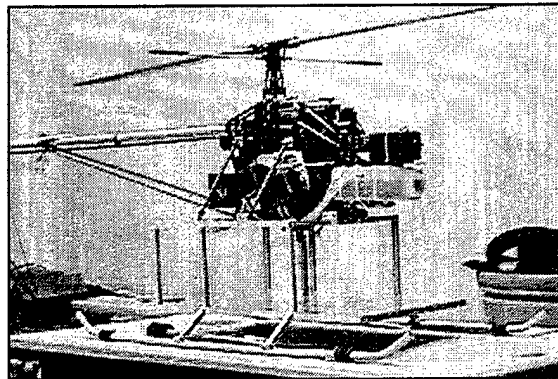


Figure 5.1. Helicopter with Vacant Avionics Rack

The new overall vehicle structure created by the addition of the avionics rack contained vibration modes that were excited by the main rotor frequency and/or associated harmonics. The flexibility of the chassis composite material allowed motion and no practical method was available at this late stage to “soften” the structure, to isolate the rack from rotor and engine vibration. It was thought that by stiffening the structure with supports, the natural frequency of the structure could be increased to a frequency well above the main rotor frequency. Therefore, four lateral supports made of thin

aluminum tubing were attached, two to a side, to stiffen the structure as shown in Figure 5.2.

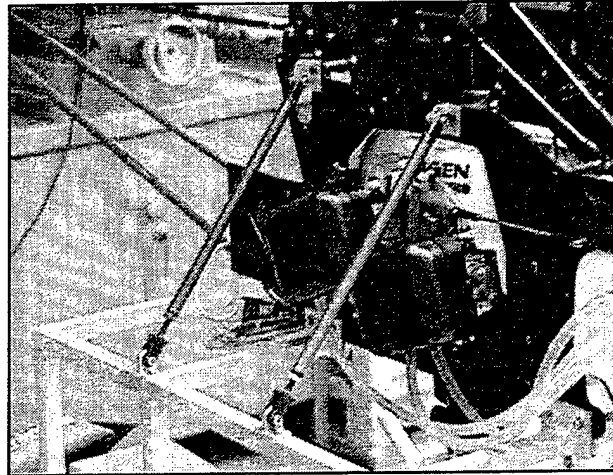


Figure 5.2. Avionics Rack Lateral Supports

The helicopter was then flown to assess the effect of the structural changes. Instead of reducing the vibrations, the lateral supports served only to change the nature of the vibration, and caused much of the vibration energy to propagate out the tail boom. A videotape of the flight revealed extensive shaking of the entire frame and twisting of the tailboom and reduction gearing. Again the helicopter was quickly returned to the deck.

It became evident the solution to the vibration problem would not be an easy one. Blade tracking and blade balance were checked and were found within limits. A subsequent flight of the helicopter in its original configuration showed no excessive vibrations. Awaiting an acceptable solution to the problem of how to mount the avionics components, a modification of the avionics system was conceived.

## **B. SYSTEM MODIFICATION**

To prove the operation of the SONALT inflight, and collect limited acceleration data, a small avionics package was developed consisting of the SONALT circuitry and transducer, a three-axis accelerometer, and associated power supply. The analog outputs of these sensors would be transmitted to the deck via an umbilical or tether, and there connected to the avionics rack. The rack would be located in the vicinity of the hovering

helicopter. Figure 5.3 shows the arrangement with the modified avionics package mounted just below the fuel tank on the nose of the helicopter.

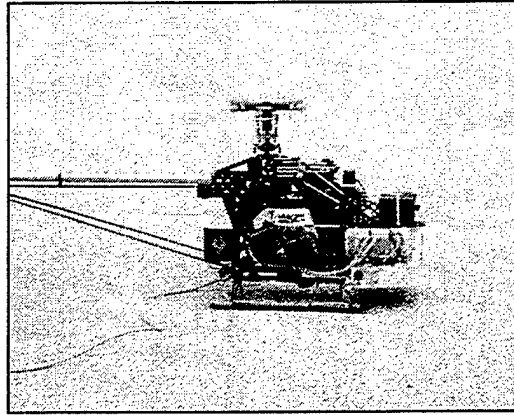


Figure 5.3. Helicopter with Modified Avionics Package

The three-axis accelerometer used was built by Crossbow Industries and has a bandwidth of 100 Hz for accelerations from  $-4$  to  $+4$  g's. It requires 5 VDC power and produces a DC signal output from 0 to 5 VDC. A 2.5 VDC output represents zero g's, with roughly a 0.5 VDC per g calibration. For example, a 3 VDC output voltage would represent roughly 1 g.

An aluminum box was constructed to contain the SONALT and the accelerometer, along with the required 12 VDC power source for the SONALT. Since 5 VDC power is needed for the accelerometer, a simple linear regulator was used to convert the necessary 5 VDC power. The SONALT circuit board was placed inside the box along with a power supply box and a terminal strip, as shown in Figure 5.4. Eight AA-cell batteries were used to supply 12 VDC power. Each cell is rated at 2800 mAh, providing ample power and lifetime.

Batteries produce the 12 VDC required for flight operations, however, a three position switch was provided to allow the selection of external power for ground operations and testing, as well as battery power. The center switch position removes power from both sensors. 12 VDC external power is provided through a 5mm audio style jack. The terminal strip was installed to allow easy disassembly of the unit, when necessary. Analog output voltages are routed out of the box through a multipin connector to a five conductor, shielded cable used as an umbilical. A wiring diagram of this avionics package is included in Appendix D. Table 5.1 gives color coding for the umbilical wiring.

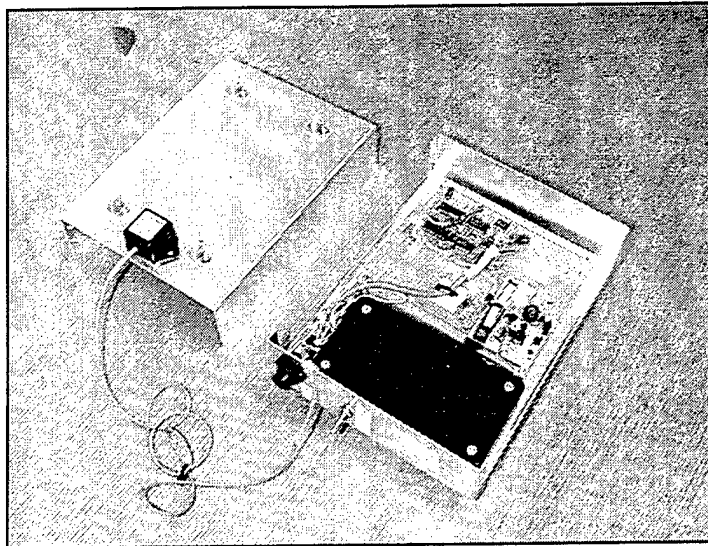


Figure 5.4. Internal View of Modified Avionics Package

Color	Signal	IMU Channel
Red	X acceleration	Channel 1
Black	Y acceleration	Channel 2
White	Z acceleration	Channel 3
Green	Altitude	Channel 4
Bare wire	Ground	N/A

Table 5.1. Umbilical Wire Connections

The transducer mounting originally designed to be attached to the bottom of the avionics rack was attached to the bottom of this aluminum box, with wiring routed through a 0.5 inch hole with protective grommet.

This, lightweight (1.86 pounds) package was then mounted below the fuel tank on the helicopter with layers of foam rubber providing vibration insulation on the top and rear of the aluminum box. The umbilical cable was routed alongside the starboard skid rail and then inboard to a centerline position very nearly below the center-of-gravity. A thirty-foot length of umbilical connected the helicopter to the remaining components on the avionics rack on the deck as shown in Figure 5.5.

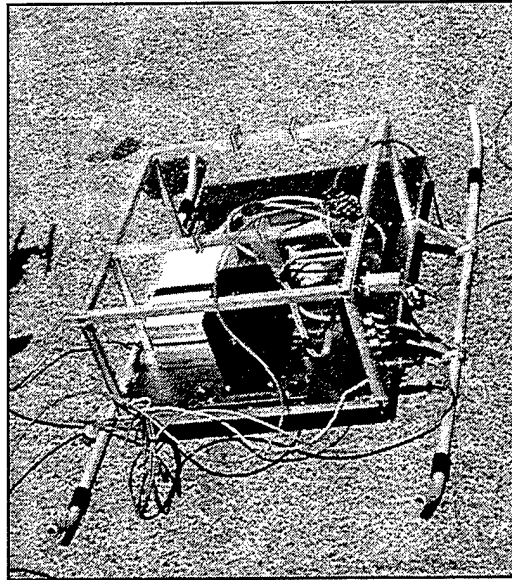


Figure 5.5. Avionics Rack Supporting Umbilical Flight

Under this arrangement, the components on the avionics rack performed just as they would in flight, with the four analog voltages being fed into the IMU through the terminal block to the IMU's internal A/D converters. This information was then transmitted by the FreeWave wireless modem to the ground station, where it was recorded along with PWM signals sent to the aircraft during flight.

Due to the vibration problems encountered during early test flights with the skid, more detailed acceleration information was desired. Data is recorded by RFTPS software at 25 Hz, and by Nyquist, is unable to preserve information greater than 12.5 Hertz. Although a single pole anti-aliasing filter with a 20 Hz cutoff frequency is provided in the IMU prior to A/D converter sampling, the roll off on this filter is such that 27 Hz main rotor vibrations are attenuated only slightly before sampling and create strong aliasing in the resulting accelerometer data. Therefore, a method of recording digital data with a higher sampling rate was required to accurately reconstruct the spectrum of vibration. This information will be helpful to further investigate vehicle vibration.

A Tattletale® Data Logger was attached to the analog signal outputs available on the avionics skid. The Data Logger was programmed to sample the four channels at 200 Hz and output data through a serial interface to a laptop computer. Single pole lowpass filters were installed prior to sampling. The cutoff frequencies of the filters were set at 23 Hz for channels 1-3, and 160 Hz for channel 4.

### C. PWM TO BLADE ANGLE CORRESPONDENCE

As discussed in Chapter II, the RFTPS ground station has the capability to capture transmitted signals from the Futaba transmitter and record this information contemporaneously with flight data received through the FreeWaves. Futaba receivers produce PWM waveforms for use by the actuators. PWM signals may be reduced to a numerical value by measuring the length of the pulse in microseconds. This data, however, is useless, unless it is known what position the various flight controls on the vehicle correspond to a given PWM value.

In conjunction with Matt McEwen, whose thesis work involved the development of a linear model of this helicopter, relationships were developed between pulse duration and blade position for collective, lateral cyclic, longitudinal cyclic, and tail rotor through a series of measurements [Ref. 14]. Due to a broken wire in the ground station, collective PWM measurement was not possible. However, since the relationship between throttle and collective due to mixing by the Futaba transmitter was known, it was possible to relate collective blade angle with throttle PWM. It is important to note, that due to presence of the yaw damper between the PWM receiver on the helicopter and the tail rotor actuator, actual tail rotor blade angle may differ in flight from that called for by PWM. Moreover, due to mixing in the transmitter, tail rotor blade angle also varies with the position of the collective control to a small degree.

Measurement of blade angle for a given PWM signal was accomplished using a set of levels specifically designed for the task. The helicopter was first leveled fore and aft with a small level placed along the tail boom, and the flybar was secured in a level attitude with the use of a brace. The main rotor blades were thereby positioned athwartships. Recall that flybar position has an effect on blade angle, and by fixing the flybar at a level attitude, consistent measurements can be produced. Figure 5.6 shows the leveling process.

Next, a commercially produced level was placed on a main rotor blade as shown in Figure 5.7. This level measures the angle of the blade chord line with respect to the earth. It was then possible to use the Futaba transmitter to advance the rotor blade through the range of operation one-degree at a time while recording the associated PWM with the RFTPS ground station. Appendix E includes detailed results obtained from these measurements.

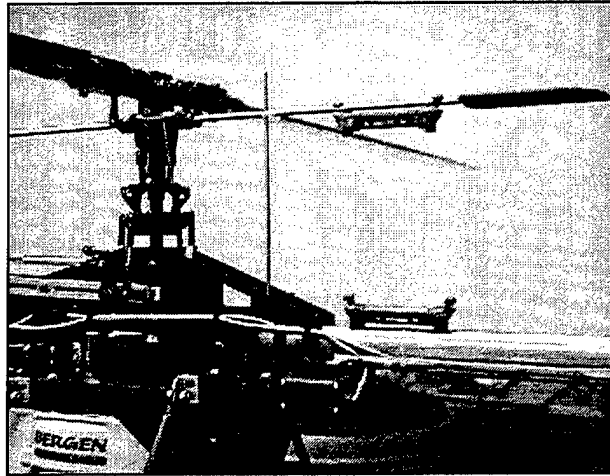


Figure 5.6. Leveling in Preparation for Blade Angle Measurements

The plots of PWM versus blade angle were linear in all cases and a simple linear regression analysis produced the following relationships. For collective blade angle in degrees versus throttle PWM:

$$\text{AOA} = -.0208 * \text{PWM} + 33.31$$

For Longitudinal Cyclic:

$$\text{AOA} = .0263 * \text{PWM} - 40.274$$

For Lateral Cyclic:

$$\text{AOA} = .01184 * \text{PWM} - 18.26$$

For Tail Rotor:

$$\text{AOA} = -0.0981 * \text{PWM} + 151.324$$



Figure 5.7. Blade Angle Measuring Level



During later test flights (see Chapter VI), PWM was measured and averaged during a stable hover. Table 5.2 contains trim values for the basic helicopter and 1.8 pounds of payload.

Control Actuator	Trim PWM
Longitudinal Cyclic	1594
Lateral Cyclic	1558
Tail Rotor	1491
Throttle	1504

Table 5.2. Flight Control Trim PWM Values

#### D. REALSIM SOFTWARE MODIFICATIONS

Thus far, activities have revolved around developing hardware for use on the aircraft compatible with the ground station hardware and software. Next, software modifications will be discussed. The RFTPS uses the MATRIX<sub>x</sub> Product Family of software. The Graphical User Interface (GUI) that ties the various components of this software product together is called RealSim. Zanino [Ref. 7] and others have written extensively about the architecture of this software.

A copy of the most current version of the software written for FROG was obtained and stored in a separate directory on the ground station SPARC so that changes could be made without effecting the FROG. The RealSim software provides an Interactive Animation Editor, allowing the user to build custom pages for display on the monitor during flight testing. These pages are constructed using a library of dials, gauges, and digital readouts that can be attached to variables in the software. In this way, current output parameters can be displayed to the screen and user inputs may be commanded through the use of the mouse and keyboard.

Using the Animation Editor, a new page specifically designed to support testing of the SONALT and accelerometer sensor package was developed and is shown in Figure 5.8. Data displayed are: altitude measured by the SONALT, PWM commanded by the Futaba transmitter, and accelerations measured by the three-axis accelerometer. Both raw data in volts (microseconds in the case of PWM) and the computed values are displayed.

Raw IMU A/D converter data are assigned variable names, "word1\_imu" through "word4\_imu," corresponding to the channel assignments shown previously in Table 5.1.

Using the intuitive block format used to build a system in Xmath, these variables can be tracked to the A\_D\_IMU Superblock, where equation blocks convert these voltage values to g's (for accelerometer data) and feet (for the SONALT).

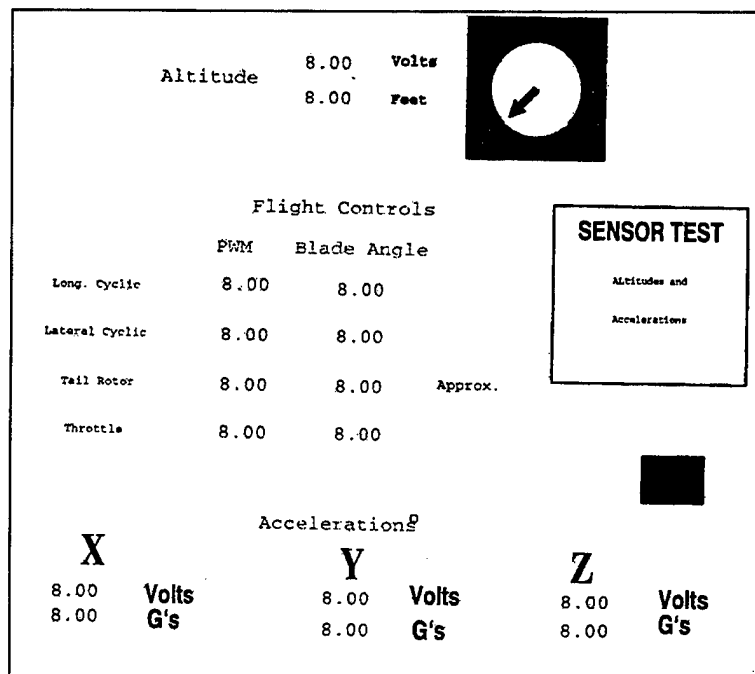


Figure 5.8. RealSim Sensor Test Animation Page

In a similar manner, the PWM data is assigned variable names TP7 through TP15. Table 5.3 shows the assignment of these variables. These variables may be tracked through the block diagrams to the Command\_Tx Superblock, where the equations developed above convert the PWM data into the associated blade angle. In the case of PWM and IMU data, the newly created variables can be accessed by the Animation Editor for display during flight test. Appendix F contains the modified Superblock diagrams performing these conversions and creating the new variables.

Additionally, variables of interest for flight test, such as IMU data, altitude data, accelerations, and PWM may be selected using the Data Acquisition editor collection to file for use in post-flight analysis. This information may be converted to an ASCII text file from Xmath through the use of the "save" command with appropriate keywords at the Xmath command line for use in other software packages for analysis.

With the modified avionics box now mounted on the helicopter and the data retrieval equipment ready to record data via the tether, the helicopter was flown and the quality of data was assessed.

Variable Name	Actuator
TP7	Longitudinal Cyclic
TP8	Lateral Cyclic
TP9	Not Used
TP10	Trainer Light
TP11	Tail Rotor
TP12	Not Used
TP13	Throttle
TP14	Collective (Not functional)
TP15	Not Used

Table 5.3. PWM Variable Assignments

## VI. AVIONIC SYSTEM TESTING

### A. FLIGHT TESTING

Flight testing was conducted for two purposes. First, data was collected to assess the performance of the SONALT and three-axis accelerometer. Additionally, flight test data was used to validate a linear model of the helicopter produced by Matt McEwen [Ref. 14]. The modified avionics package was mounted below the helicopter fuel tank and tethered to the avionics rack on deck. Data was fed to the ground station by a FreeWave modem where it was captured by the RealSim Data Acquisition Editor. The ground station was capable of capturing the three-axis accelerometer signal voltages, and the SONALT signal voltages through the IMU A/D converter, along with the PWM signals being sent to the helicopter by the pilot. These data are recorded at 25 Hz. Additionally, the Tattletale data logger was connected to the terminal strip on the avionics rack to collect data, which was subsequently transferred to a laptop computer via serial link. The data was collected at 200 Hz, and was limited to 38.46 seconds due to available memory. Once the data buffer was filled, a short period was required to transfer this information to the laptop for hard disk storage.

Due to the data limit on the data logger and to synchronize the recordings of the two systems, a series of separate data collection sessions was devised, each session focusing on a specific maneuver. Both data collection systems were started together and data recorded until the Tattletale buffer was full. During the collection session, prebriefed maneuvers were performed by the UAV pilot as shown in Figure 6.1. Each data collection session is reviewed in the following section.

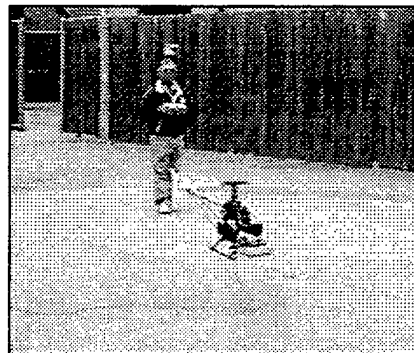


Figure 6.1. Avionics Package Test Flight

## B. DATA QUALITY

To facilitate post-flight analysis, PWM data recorded by the ground station was exported in ASCII from Xmath and imported to MATLAB along with Tattletale data. The data was analyzed and differences in starting time between the two data collection systems was determined, and corrections applied.

Vibration proved again to impact avionics performance. During initial flight testing, data similar to that during ground testing (see Chapter III) was observed for only short periods. Noise was present in the data and became worse as time progressed until the data became useless. Postflight inspection of the SONALT revealed that vibrations had caused soldered connections on the 12 VDC battery assembly to fail. As the power connection deteriorated during the flight, the data became steadily worse until the connection failed completely.

Two subsequent test flights continued to reveal only short periods of good data, typically at lower altitudes. Postflight inspections continued to reveal components shaken to failure. Partial failure of a lead on the capacitor charged by the charge pump on the LM2917 integrated circuit caused intermittent results during flight. During a later inspection, the variable potentiometer on the Polaroid 6500 Ranging Module which allows the sensitivity of the module to be adjusted, was found to be intermittent. Intermittent operation of the potentiometer could allow the system to go to maximum sensitivity and possibly cause false triggers due to detection of the ringing transducer immediately after blanking is turned off. Figure 6.2 contains unfiltered data recorded during one of these flights.

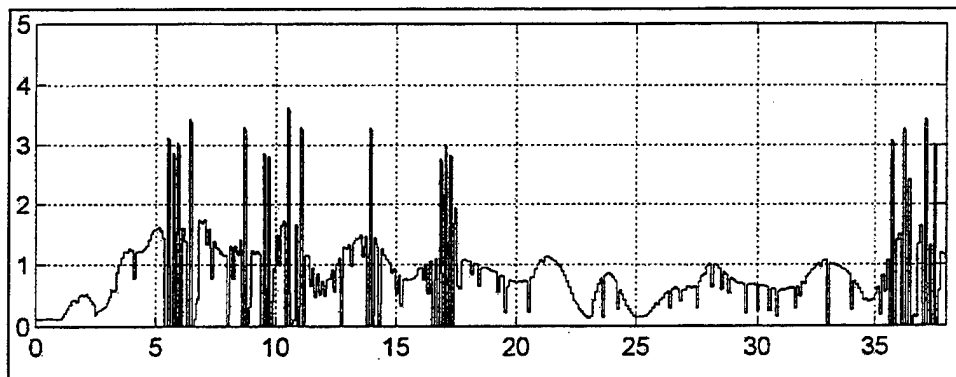


Figure 6.2. SONALT Data Containing Noise Spikes

The general path of flight can be discerned by “eyeball integration” of the data, but large transients are present when the altitude is greater than one foot. The altitude drops to zero on this graph during these transients. The graph is produced from Tattletale data which does not record negative voltage values, but the ground station does. Where the Tattletale shows zero, the ground station showed negative voltage.

Faulty components were replaced and the remaining components were checked and where possible reinforced with silicone sealant to prevent vibration failure. Data quality improved significantly and an analysis of the results is provided below. Detailed data is provided in Appendix G.

### 1. Vertical Doublets

Figure 6.3 contains test data taken with the UAV pilot commanding collective control doublets after a period of generally level flight. The data appears much improved with fewer noise spikes. Occasional drops in data last for 100 ms each, indicating that the drops are the result of a single PRI. Examination of the slope of the doublets reveals a high rate of climb and subsequent descent, through which the altimeter tracks well. Most of the data drops occur in the vicinity of these maneuvers, however.

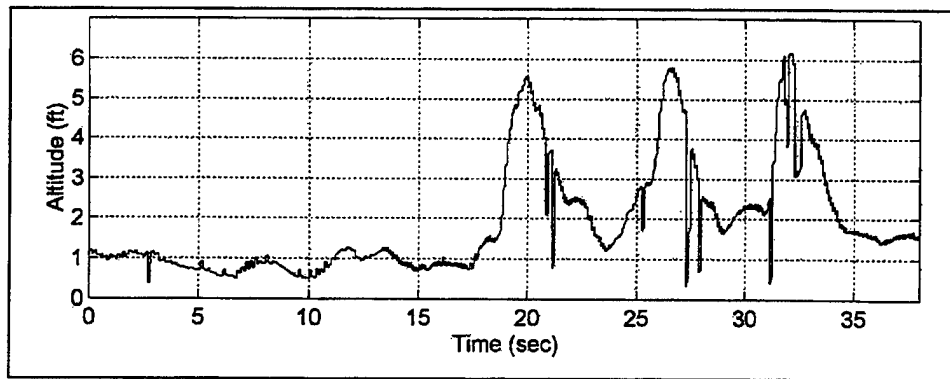


Figure 6.3. Unfiltered Altitude During Vertical Doublet Maneuvers

An analysis of this data reveals that most of the sharp transients are drops in altitude from an altitude of several feet down to an altitude below one foot. Furthermore, these drops very frequently last for one altimeter cycle, or 100 ms, before returning back to near the previous altitude. Analog techniques such as low-pass filtering can also help smooth high frequency transients, but the cutoff frequency required to adequately suppress these transients begins to effect the good data as well. The graph in Figure 6.4 contains a

spectral analysis of the altitude data from an early flight where electrical component failures created many transients. A large spike can be seen in the area of 5 Hz. This is because the data often dropped to zero for 100 ms, jumped to a high value for 100 ms and so forth. This created oscillations with a period of 200 ms (5 Hz). A filter with a cutoff frequency of only 2 or 3 Hz would be necessary to smooth the data. This filtering would cause the peaks on the doublets in Figure 6.3 to be reduced in height and delayed in time.

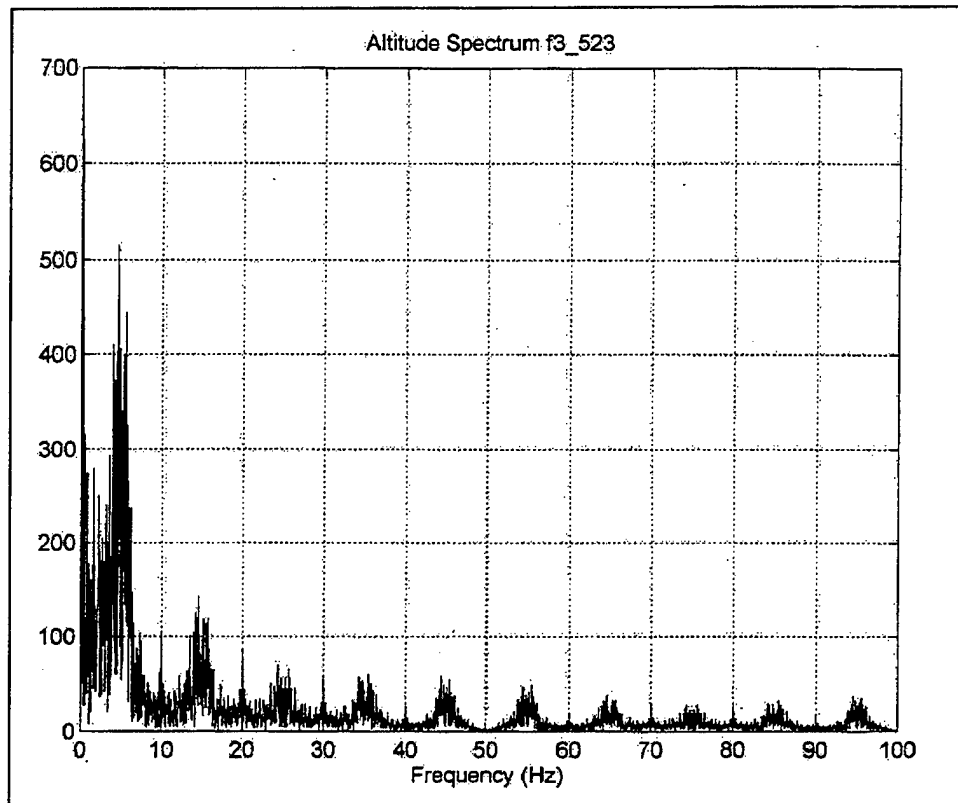


Figure 6.4. Altitude Data Spectral Analysis

An advantage to digital signal processing is that non-frequency based filter techniques can be employed easily. For example, computer code was written to analyze each data element and compare it with the previous data point. If the data drops from an altitude greater than one foot to an altitude below one foot, that point, along with all points during the next 100 ms cycle can be ignored, using the previous value instead. Additionally, each data point can be averaged with the previous seven points (previous .035 seconds) to smooth transients. Figure 6.5. presents the results of such a filter.

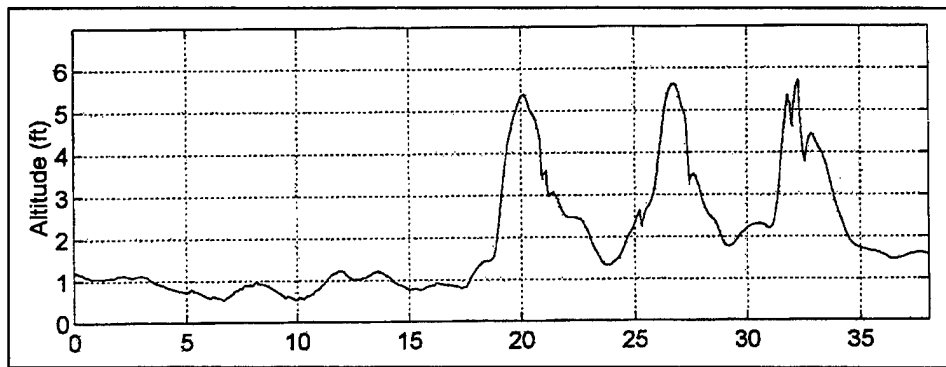


Figure 6.5. Filtered Altitude During Vertical Doublet Maneuvers

Acceleration and PWM actuator control signals were also analyzed. Figure 6.6 depicts z-axis (vertical) accelerometer data.

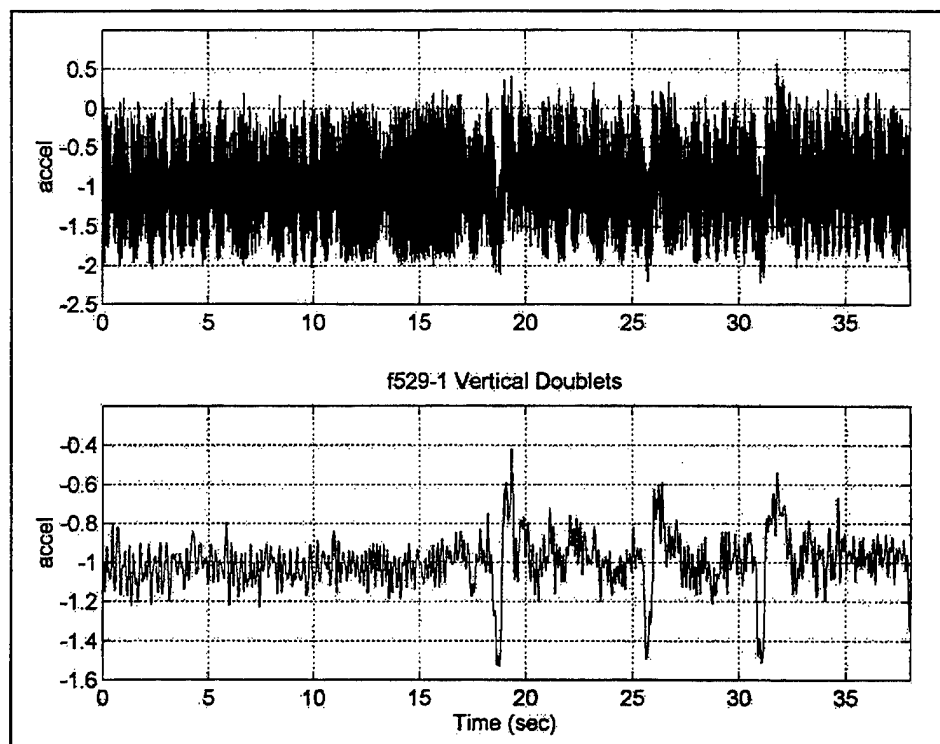


Figure 6.6. Z-Axis Accelerometer Data During Vertical Doublet Maneuvers  
Top: raw data, Bottom: filtered data

Note that the z-axis is defined as positive down. The raw data in the top graph contains high frequency noise generated by the helicopter engine and rotor system and the overall acceleration of the vehicle is not apparent. A fourth order Butterworth low-pass



filter was employed with a cutoff frequency of 40 radians/sec (6.4 Hz) to remove the 27 Hz (1P) and 54 Hz (2P) spectral components. The accelerations corresponding to each of the three doublet maneuvers can be clearly seen. The results are provided in the bottom graph in Figure 6.6.

As described in Chapter V, the PWM varies inversely with collective blade angle on this helicopter. An increase in PWM causes a decreased blade angle. Figure 6.7 depicts altitude and PWM information for the vertical doublet maneuvers. This information can be used to develop or validate a mathematical model of the helicopter.

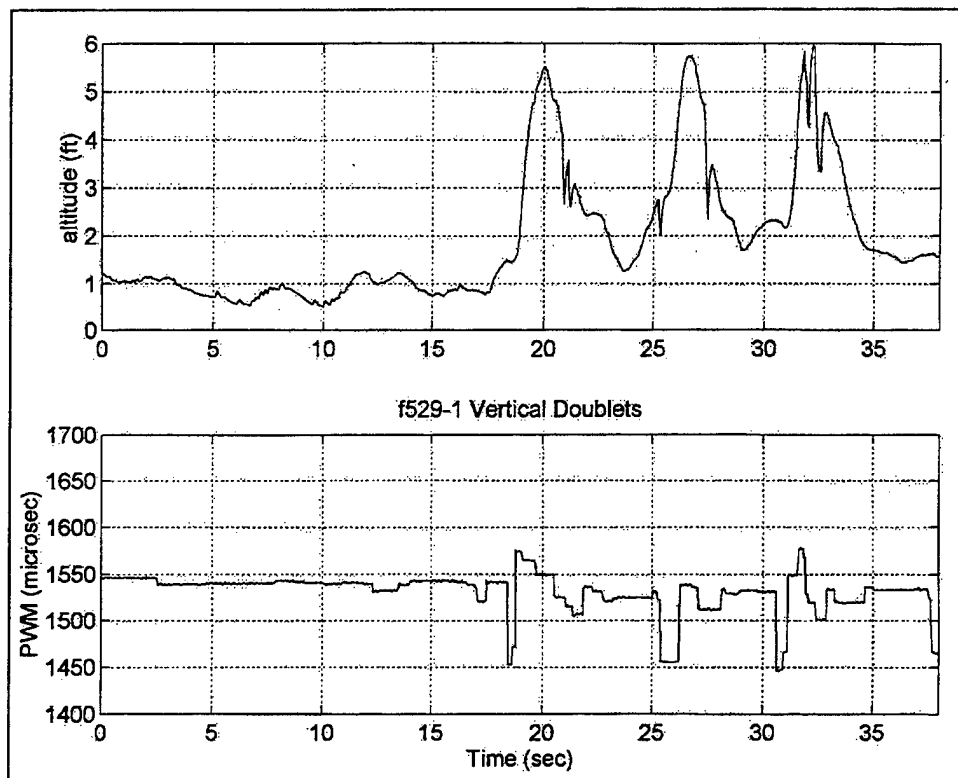


Figure 6.7. PWM Measurements During Vertical Doublet Maneuvers

## 2. Lateral and Longitudinal Doublets

Lateral and Longitudinal Doublets were performed to gather accelerometer information to support Major McEwen's model identification work, but the altitude data collected is also useful in assessing SONALT performance. Filtered and unfiltered data for the lateral doublet maneuver is provided below in Figure 6.8.

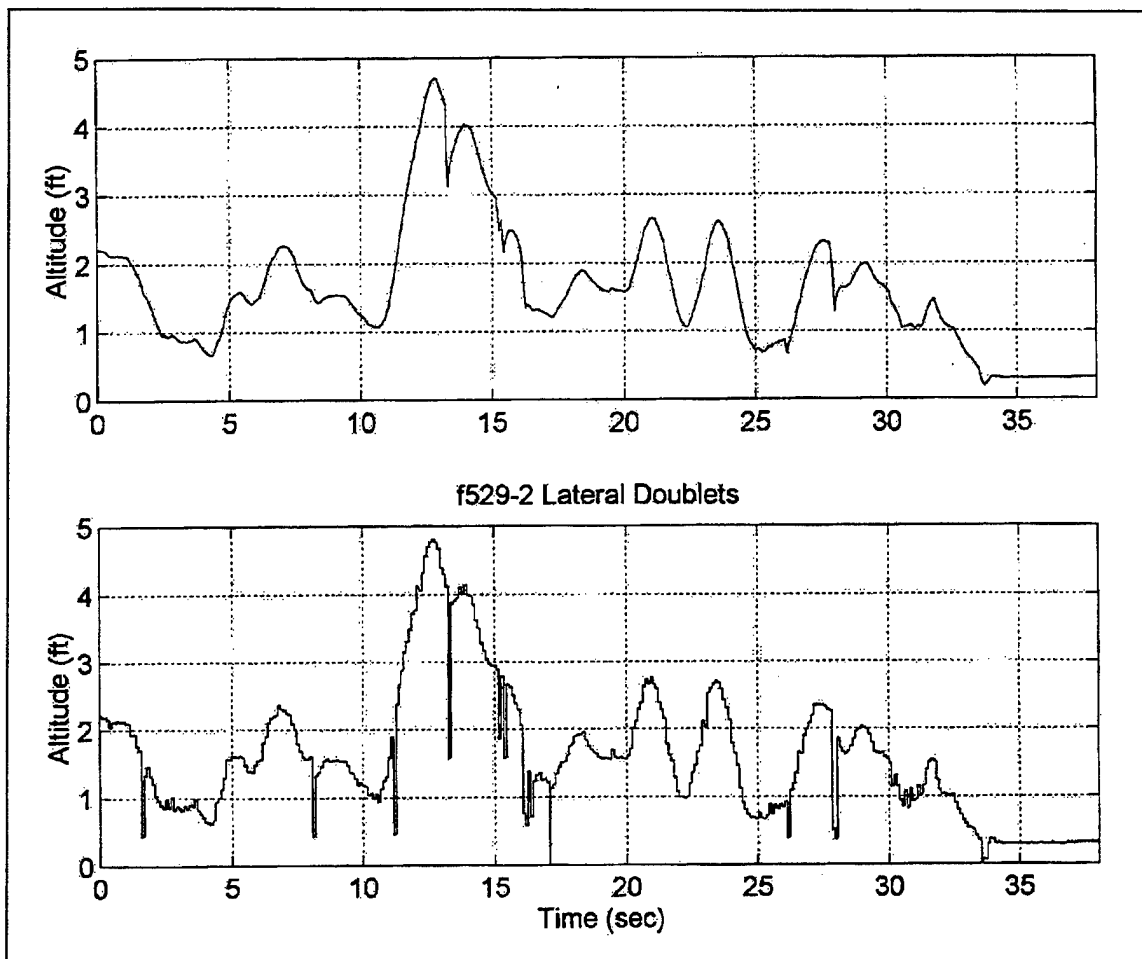


Figure 6.8. Unfiltered Altitude During Lateral Doublet Maneuvers

As the UAV pilot performed these maneuvers, the altitude information was recorded. While performing these maneuvers, the pilot's primary attention was placed on creating the lateral and longitudinal inputs required, and naturally, altitude varied through these maneuvers. This data reveals a potential cause of bad data points. Although not evident from the altitude data in the vicinity of 12 seconds in Figure 6.8, the helicopter was completing a lateral motion to the left and had rolled to the right when the drop in data occurred. Longitudinal data (see Appendix F) also revealed dropped data during maneuvers, probably associated with vehicle pitch. Recall that the SONALT transducer produces sound energy in a narrow beam of only 10 degrees, as discussed in Chapter III. Due to the narrow beamwidth, as the vehicle pitches or rolls, the gain of the transducer and the amount of energy reflected to the vehicle from the ground is decreased, reducing

the signal to noise ratio, making drops in data more likely. The SONALT will be more reliable at a steady level attitude.

### C. COMPLEMENTARY DATA FILTERING TO PRODUCE VELOCITY AND ALTITUDE ESTIMATES

Access to all states is desirable when designing a controller for an air vehicle. In designing an altitude controller using techniques such as Linear Quadratic Regulator (LQR) theory, access to velocity information allows both the derivative of altitude ( $-w$ ) and altitude to be used for state feedback. In this application, no direct velocity sensor is available to sample this state. However, by complementary filtering  $z$ -axis acceleration data with altitude, estimates of altitude and velocity can be produced. Figure 6.9 depicts such a complementary filter arrangement.

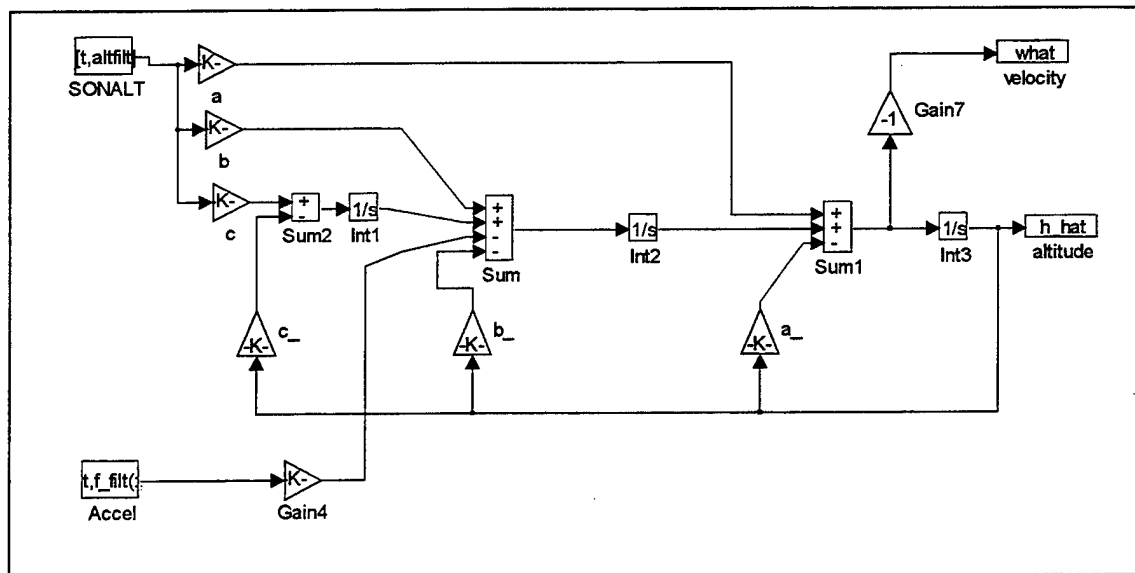


Figure 6.9. Complementary Filter

SONALT data previously processed element-by-element to remove data drops is brought into the filter at the top left of the block diagram, and  $z$ -axis accelerometer data is brought in at the bottom left. The accelerometer data is fed through block "Gain4" to change the units of measure from  $g$ 's to  $\text{ft}/\text{sec}^2$ . The filter consists of three integrators, with SONALT information fed forward through three gains and an estimate of altitude fed back through the same three gains. Accelerometer data is introduced prior to the center

integrator. An estimate for altitude is produced at the output of the third integrator, and an estimate for velocity can be produced from the input to the third integrator.

Installation bias is accounted for in this filtering scheme. In other words, if the three-axis accelerometer is not perfectly aligned to the aircraft body axis, an error in z-axis acceleration would be present. Instead of reading a value of  $-1.0$  g (gravity only, measured with respect to the downward-pointing z axis) with the helicopter at rest on a level surface, for example, the reading might be  $-0.99$  g. If a simple integration of acceleration were conducted to obtain a velocity estimate, this difference would compound over time causing a large velocity error. With the use of three integrators in this filter, the left-most integrator "learns" this bias error and outputs a value to compensate for it.

Consider the steady-state condition where the vehicle is at constant altitude and zero vertical velocity ( $w = 0$ ). An examination of Figure 6.9 reveals that feedback values would equal feed-forward values at each of the summers. Due to the opposite signs provided on the summers for these inputs, their effects neutralize one another. Also at steady-state, the left-most integrator produces a value of equal magnitude to the acceleration being input. Therefore the input to the right-most integrator would be zero and the altitude estimate unchanged.

The values for each of the feed-forward and feedback gains is related to the bandwidth of the SONALT and three-axis accelerometer. The values for  $a$ ,  $b$ , and  $c$  are computed through the following relation, where  $\tau$  is the bandwidth of the SONALT.

$$(s^3 + as^2 + bs + c) = \left(s + \frac{1}{\tau}\right)^3$$

Since the SONALT operates at a PRF of 10 Hz, it may have a bandwidth no greater than 5 Hz by application of the Nyquist theorem. Several values for  $\tau$  were evaluated and  $\tau = 2$  Hz produced acceptable results. By inserting a value of  $\tau$  in the equation above and expanding the right-hand side, the gains may be computed by term-by-term comparison. Gains computed were  $a = 37.7$ ,  $b = 473.8$ , and  $c = 1985$ .

Flight data from the longitudinal doublet maneuvers was filtered and the results are provided in Figure 6.10. Note that the velocity,  $w$ , is positive when the vehicle is descending, which is proper in the aircraft coordinate system used. The velocity information produced tracks well with altitude and is usable for controlling the helicopter with a LQR controller.

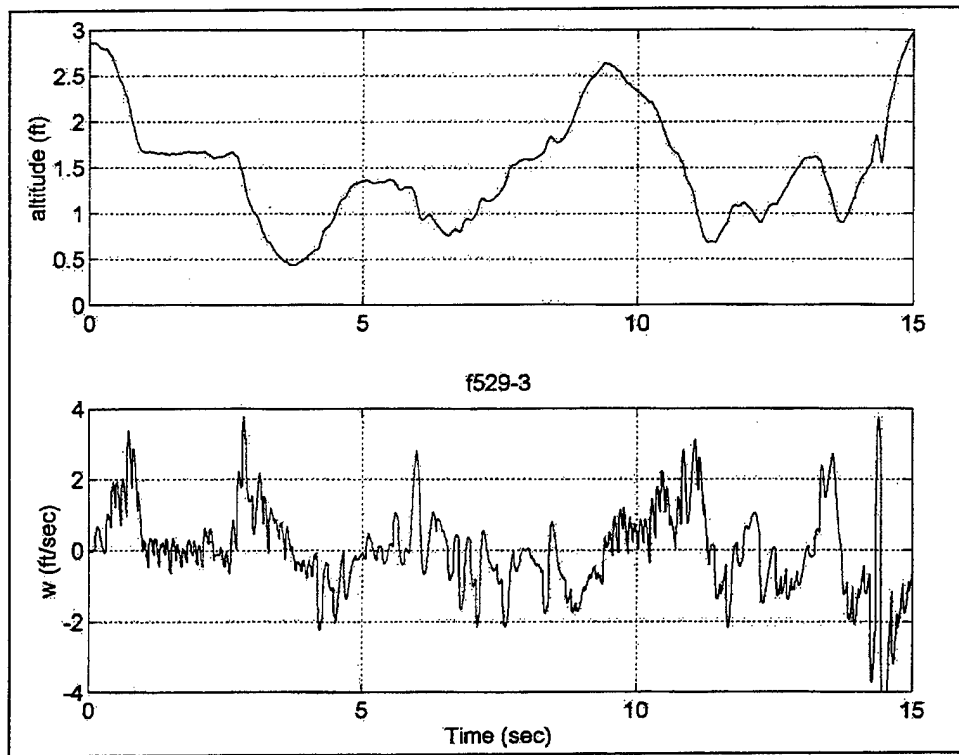


Figure 6.10. Altitude and Velocity Estimates Produced by Complementary Filter

## **VII. CONCLUSIONS AND RECOMMENDATIONS**

### **A. OVERVIEW**

This thesis has touched on broad areas fundamental to avionics development: avionics sensor selection, power requirements, mounting and vibration protection, telemetry and communications, digital and analog interfaces, data acquisition, and circuit design and testing. Much remains to be accomplished beyond the initial steps taken.

### **B. SPECIFIC COMMENTS**

#### **1. Sonic Altimeter**

The precision altitude measuring system designed for compatibility with the RFTPS was proven to be a successful approach for this application. Much more testing remains to be accomplished, however. The doublets performed during flight testing provided data for modeling, but were not the sort of maneuvers that would typically be performed under computer control. Hovering operations without abrupt maneuvers should be performed to obtain a better measure of SONALT performance. Once telemetry is installed and altitude is no longer restricted, maximum range should be determined. The effects on performance of different surfaces (ground, pavement, etc.) should be investigated. The narrow beamwidth of the altimeter limits vehicle pitch and roll, yet these limits have not been precisely determined. Future flight test could determine these limits and perhaps test different approaches, such as the use of multiple transducers set at different angles to accommodate pitch or roll. Polaroid provided a variable potentiometer on the 6500 Series Module to allow the user to adjust the sensitivity of the transducer. Test flights should determine what sensitivity setting is appropriate for optimum performance. In summary, the sonic altimeter is usable as a precision data source for control of the vehicle in a hover at low altitude. With the use of the three-axis accelerometer and complementary filtering, vertical velocity can be estimated.

#### **2. Avionics Mounting and Vibration Control**

The most challenging aspect of this project was not an avionics issue, per se, but rather the task of mounting the components on the helicopter and providing the

appropriate protection from vibration. The avionics rack developed compounds the vibration problem and provides no cushion on landing. A more sophisticated approach should be investigated, perhaps involving disassembly of the current helicopter and replacing the composite chassis with a new structure capable of supporting avionics. The use of a shaker table and advanced finite element computer modeling might aid the development of a more suitable mounting scheme. Alternatively, following the lead of some commercial vendors, a mounting system which connects to the bottom of the plastic landing skid might permit the vibrations to be dampened by the plastic skid. This work might involve more detailed flight testing and analysis of the vibrations present and subsequent design by a student with aircraft structure and vibration experience.

### **3. Avionics Package Weight Reduction**

Mr. Kelly Johnson, the lead aircraft designer at Lockheed Skunk Works and developer of the F-104, U-2, and SR-71 aircraft was fanatical about reducing aircraft weight. He concerned himself with design changes resulting in only a few pounds on an aircraft of several thousand pounds gross weight. Weight also plays an important factor in the performance of this helicopter. Although this helicopter has considerable weight lifting capability, the reduction of weight in the avionics system will greatly aid vibration isolation.

Several areas for weight reduction are available. The DC switching converters, power distribution panel and the battery weigh four pounds. The converters are electrically oversized for the load drawn, and any further reductions in power requirements due to the choice of different sensors could allow lighter converters to be used. The MILSPEC lithium battery is not rechargeable. Due to the short flight endurance of the helicopter (about 20 minutes), smaller rechargeable batteries could be incorporated in any design.

Considerable telemetry bandwidth is currently wasted. The FreeWave wireless modem may be set to as high as 115 KBPS; only 8.3% of capacity is being used to support the IMU. A multiplexing scheme could be employed to take the two parallel transmission paths of the FreeWaves, and combine them into one serial stream.

#### **4. Data Quality First Priority**

Quality data is essential to the proper performance of an automatic controller. Sensors other than those used on the RFTPS should be investigated to determine if better, more lightweight, more energy efficient sensors are available that are more suitable for the present application. Before making any attempt to control the vehicle with software, emphasis should be placed on developing a complete sensor system capable of providing the data of sufficient quality. Lightweight miniature sensors and electronics such as the Tattletale data logger should be examined for airborne use, since the low power consumption and capability of such hardware can greatly enhance data collection.

#### **5. Controller Design**

It is recommended that further flight testing be done to provide altimeter and vertical acceleration data to develop a model of the helicopter altitude dynamics. Once a quality model is obtained, altitude control can be attempted using the existing modified avionics package. Further modeling of the autopilot (not yet installed) could lead to development of heading, speed, and position controllers.

#### **6. RFTPS Ground Station**

A separate ground station should be constructed to support the helicopter. A new ground station designed to receive information from the sensor suite on the helicopter could be devised, and with modification of the various drivers, still allow use of the existing software.

### **C. SUMMARY**

Much was learned about the performance characteristics of the helicopter and its basic vibration and aerodynamic qualities. This information should serve as a firm foundation for follow-on research with the helicopter. A successful SONALT has been developed which can be used to control the helicopter.





## LIST OF REFERENCES

1. Schluter, Dieter., *Schulter's Radio Controlled Helicopter Manual*, p. 26,60. Argus Books Limited, 1981.
2. *Futaba PCM1024ZA Instruction and Operation Manual*, Futaba Corporation of America, Irvine, California, 1993.
3. *Helicopter Owner's Manual*, Bergen Machine & Tool, Inc., Wisconsin, March 15, 1997.
4. Biber, C., *The Polaroid Ultrasonic Ranging System: Operations Manual*, p. 5. Polaroid Corporation, Ultrasonic Components Group, Cambridge MA.
5. Sound. *The World Book Encyclopedia*, 1985; 18:490.
6. *Principles and Applications of the ICL7600 CMOS Voltage Converter*, p. 11-11, Harris Semiconductor Corporation, April 1994.
7. Zanino, James A., *Uniform System for the Rapid Prototyping and Testing of Controllers for Unmanned Aerial Vehicles* Master's Thesis, Naval Postgraduate School, Monterey, CA, 1996.
8. Hallberg, Eric N., *On Integrated Plant, Control and Guidance Design* Doctoral Dissertation, Naval Postgraduate School, Monterey, CA, 1997.
9. *IMU-C604 Owner's Manual*, Watson Industries, Inc., Eau Claire, Wisconsin, August 1995.
10. *FreeWave User Manual, V3.4*, FreeWave Technologies, Inc., Boulder, Colorado, 1996.
11. Chayat, Naftali, *Frequency Hopping Spread Spectrum PHY of the 802.11 Wireless LAN Standard*, p.2, Presentation to IEEE 802, <http://grouper.ieee.org/groups/802/11/main.html>, 11 March 1996.
12. *Oncore GPS Receiver Quick Start Kit Manual*, p. 5, Motorola, Inc., 1995.
13. *Marine Corps Order 2100.3A*, Commandant of the Marine Corps, 26 June 1989.
14. McEwen, Matt, *Dynamic System Identification and Modeling of a Rotary Wing Unmanned Aerial Vehicle for Stability and Control Analysis* Master's Thesis, Naval Postgraduate School, Monterey, CA, 1998.

15. *Military Battery Specifications*, Eternacell Power Conversions Inc., May 1998,  
[http://www.eternacell.com/spec\\_mil.htm](http://www.eternacell.com/spec_mil.htm)

## APPENDIX A. SONALT CALIBRATION DATA

<u>Voltage</u>	<u>Distance (ft)</u>	<u>Polyfit (ft)</u>	<u>Close-up (ft)</u>	<u>Overall (ft)</u>	<u>Polyfit 4th (ft)</u>
0.028	0.41666	0.2990026	0.4105984	0.1137464	0.395182911
0.044	0.5	0.3943747	0.4952832	0.2146872	0.480374015
0.061	0.58333333	0.4957523	0.5852608	0.3219368	0.571248968
0.078	0.666666	0.5971761	0.6752384	0.4291864	0.662489539
0.093	0.75	0.6867061	0.7546304	0.5238184	0.743295774
0.109	0.833333	0.7822443	0.8393152	0.6247592	0.829795127
0.125	0.916666	0.8778234	0.924	0.7257	0.916606567
0.136	1	0.9435578	0.9822208	0.7950968	0.976468449
0.326	2	2.0820215	1.9878528	1.9937688	2.03218479
0.508	3	3.1779593	2.9511424	3.1419704	3.078135274
0.68	4	4.2185458	3.861504	4.227084	4.093161748
0.838	5	5.1785993	4.6977664	5.2238744	5.044835081
0.992	6	6.1181867	5.5128576	6.1954296	5.987379708
1.153	7	7.1045348	6.3649984	7.2111464	6.985915779
1.296	8	7.9840813	7.1218688	8.1133048	7.882071169
1.464	9	9.0215694	8.0110592	9.1731832	8.943758462
1.625	10	10.020061	8.8632	10.1889	9.968132739
1.793	11	11.066381	9.7523904	11.248778	11.04226888
1.926	12	11.897917	10.4563328	12.087849	11.89523653
2.1	13	12.990059	11.37728	13.18558	13.01326179
2.26	14	13.998597	12.224128	14.194988	14.04233343
2.42	15	15.011226	13.070976	15.204396	15.07147566
2.56	16	15.900633	13.811968	16.087628	15.97153585
2.73	17	16.984837	14.711744	17.160124	17.06351
2.89	18	18.009483	15.558592	18.169532	18.09011977
3.02	19	18.84502	16.246656	18.989676	18.92346727
3.19	20	19.94172	17.146432	20.062172	20.01245045
3.35	21	20.978128	17.99328	21.07158	21.03706981
3.5	22	21.953475	18.7872	22.0179	21.99804375
3.65	23	22.932418	19.58112	22.96422	22.96020728
3.82	24	24.046233	20.480896	24.036716	24.05333659
3.96	25	24.96696	21.221888	24.919948	24.95684573
4.72	30	30.019844	25.244416	29.714636	29.96881153
4.88	31	31.095371	26.091264	30.724044	31.06170925
5.02	32	32.039812	26.832256	31.607276	32.03374863

Figure A.1. SONALT Calibration and Curve Fit Data

### SONALT Calibration

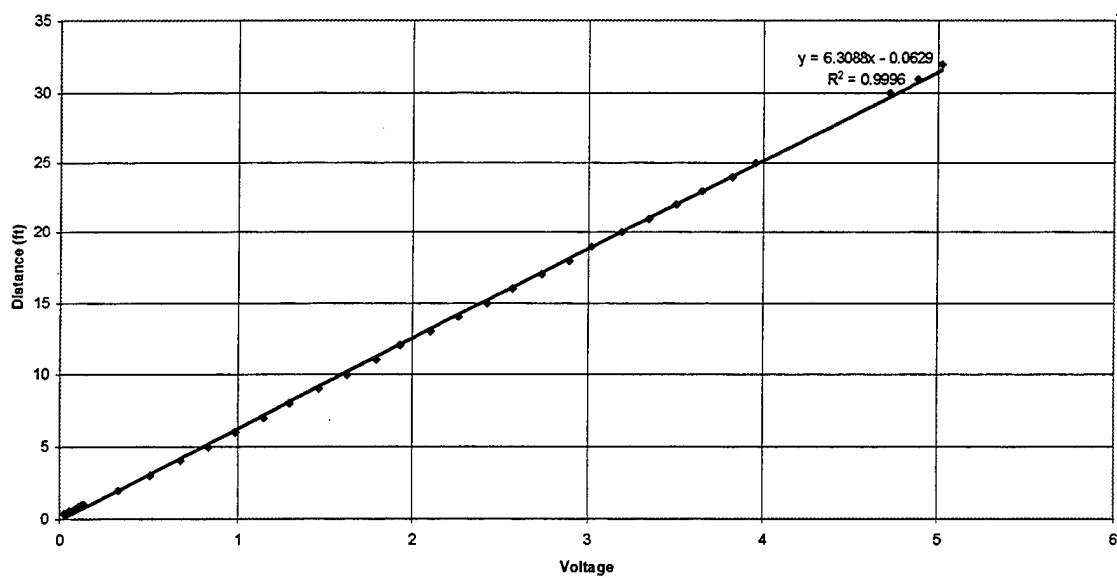


Figure A.2. SONALT Linear Curve Fit

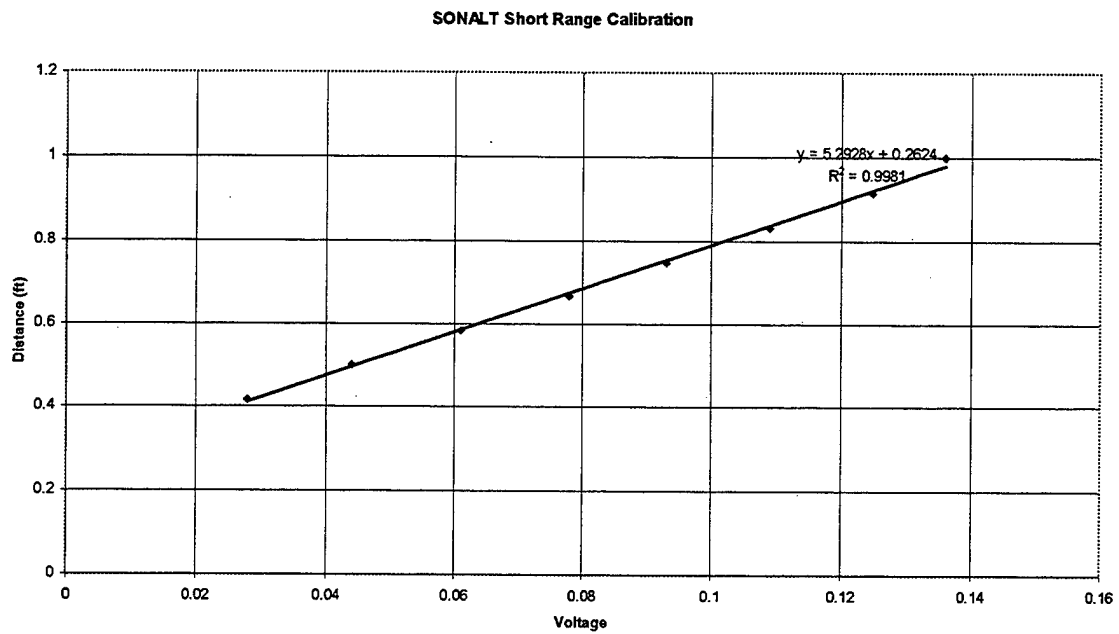


Figure A.3. SONALT Short Range Curve Fit

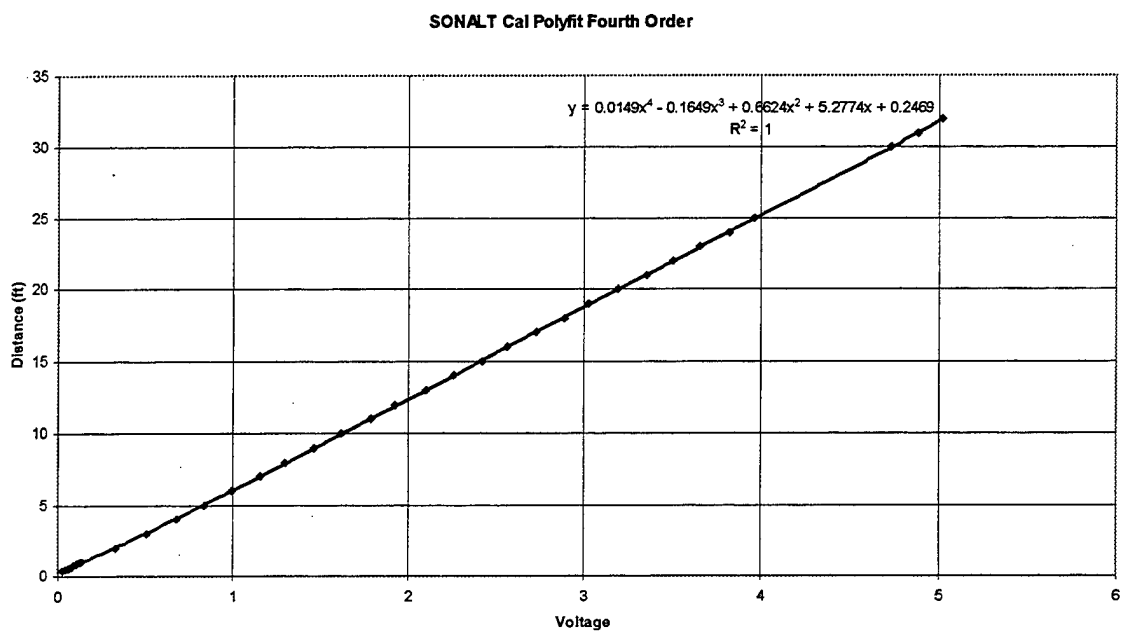


Figure A.4. SONALT Fourth Order Curve Fit

## APPENDIX B. WEIGHT AND BALANCE LOG

Component	Wt. (lbs)	X (in)	Mom. (in-lbs)	Y (in)	Mom. (in-lbs)	Z (in)	Mom. (in-lbs)
Base Helo dry	16.44	14.25	234.27	0	0	12.4	203.445
removed skid	-0.62	11	-6.82	0	0	6.5	-4.03
Skid/rack	5.65	12.2	68.93	0	0	2.1	11.865
Battery	2.32	18	41.76	-4	-9.28	4	9.28
IMU	2	18	36	0	0	2.59	5.18
Freewave	0.75	12	9	4.5	3.375	0.33	0.2475
SONALT Circuit	0.42	19	7.98	-7	-2.94	3.5	1.47
SONALT TXDCR	0.19	10.5	1.995	-5	-0.95	-0.5	-0.095
Power Panel	1.66	18	29.88	6.5	10.79	3.5	5.81
Camera	3	3	9	0	0		0
DGPS Rec.			0		0		0
DGPS Ant.	0	41	0		0		0
Autopilot	0.485	0	0		0		0
Fuel	0.855	3.5	2.9925	0	0	7	5.985
<b>Total</b>	<b>33.15</b>		<b>434.9875</b>		<b>0.995</b>		<b>239.1575</b>

	<b>CG X</b>	<b>CG Y</b>	<b>CG Z</b>
<b>CG is at</b>	<b>13.12179487</b>	<b>0.030015083</b>	<b>7.214404223</b>

**Moment at the mast is                      37.4 in-lbs nose down**

### Notes:

- 1) Locations are referenced in inches from the front edge, center of avionics platform  
x is positive towards tail, y positive to starboard, z positive up from deck
- 2) Moment at the mast refers to moment that must be generated by rotor to maintain longitudinal stability.

Original CG wet = 13.72	Original wet moment at mast = 9.62 in-lbs nose down
Original CG dry = 14.25	Original dry moment at mast = 0
Rotor Mast is at 14.25	

### Fuel Weight

Full	1.71
Half Full	0.855

<b>Max Gross Limit</b>	38.15	(20# payload)
Current Payload	16.71	

Figure B.1. Weight and Balance Log





## APPENDIX C. AVIONICS SYSTEM WIRING DIAGRAMS

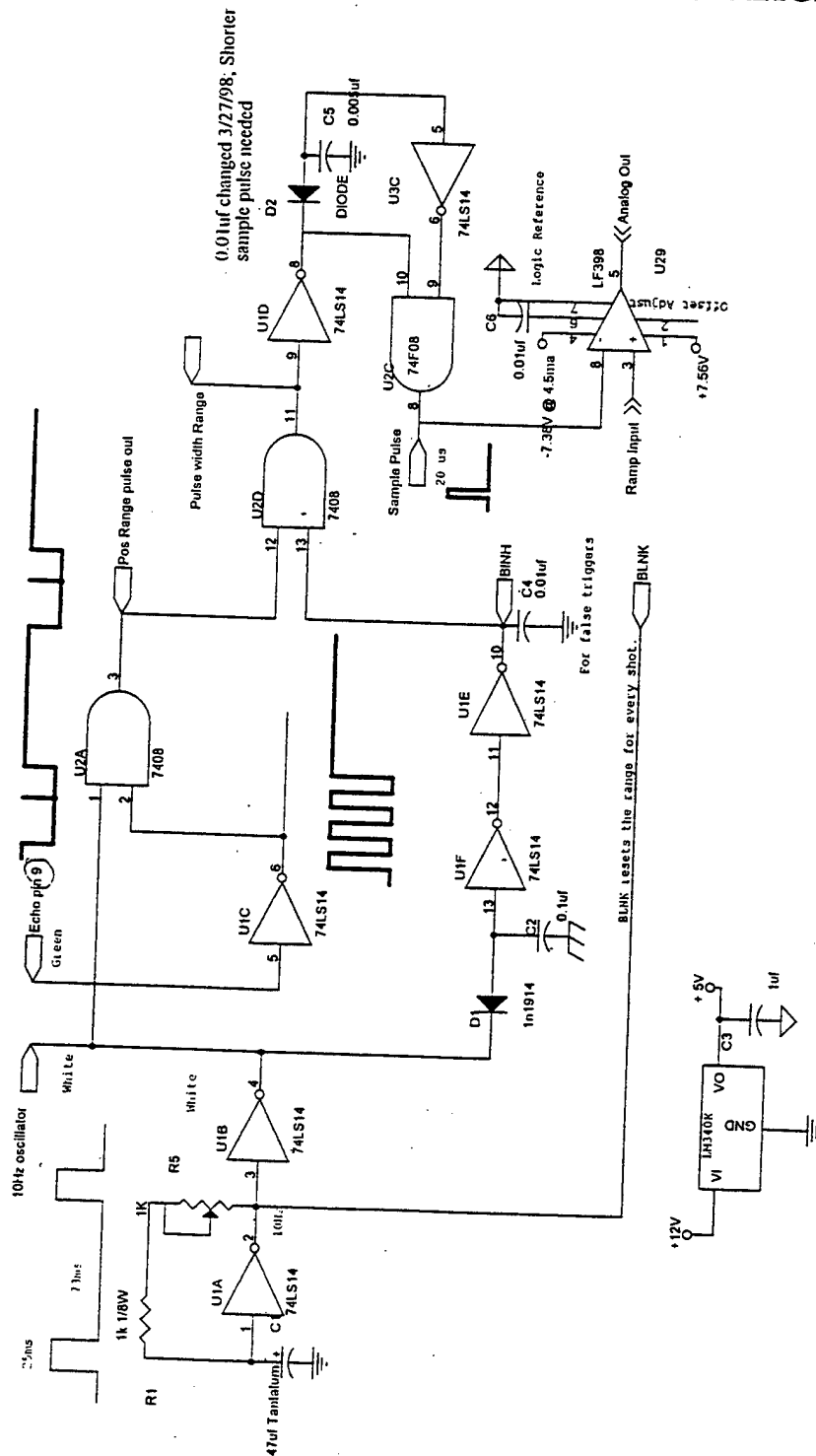


Figure C.1. SONALT Wiring Diagram Part One



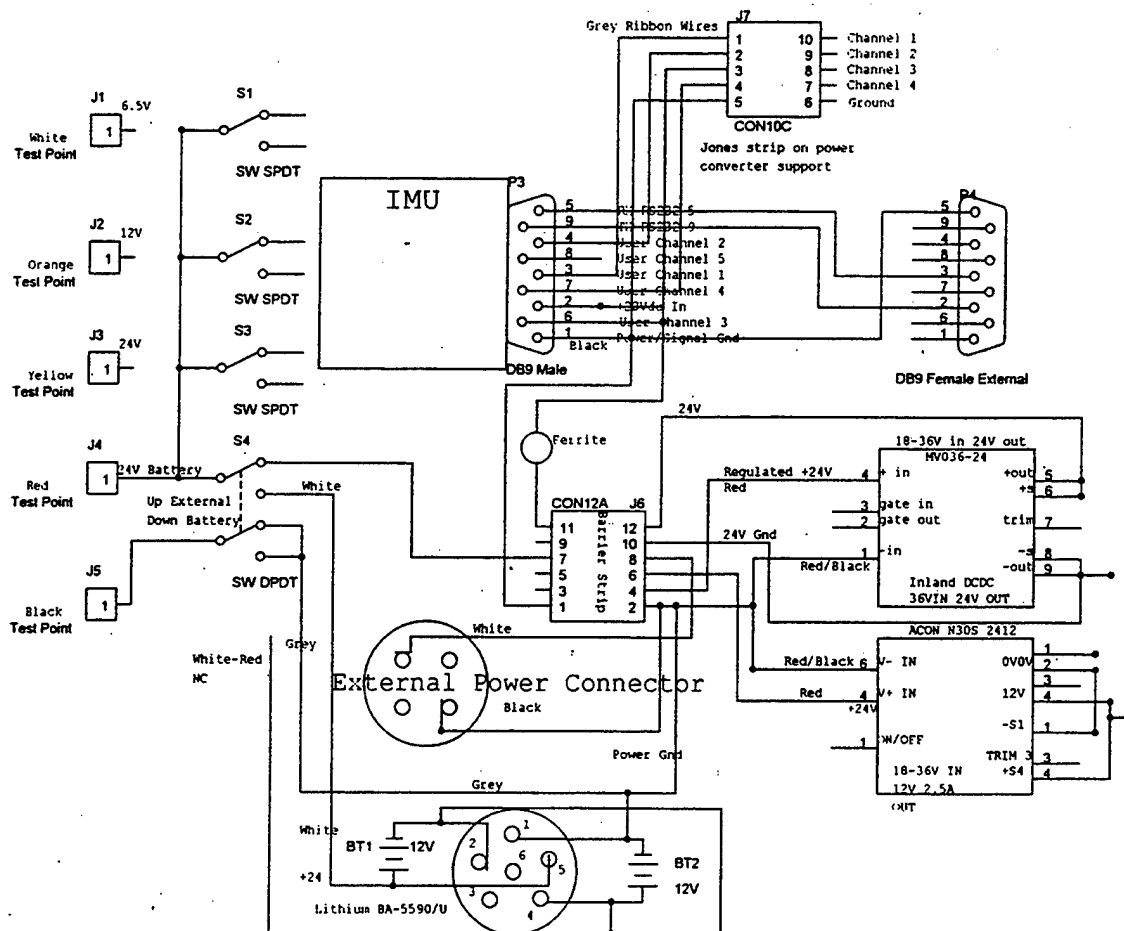


Figure C.3. Avionics Power and Signal Distribution



## APPENDIX D. MODIFIED AVIONICS PACKAGE WIRING

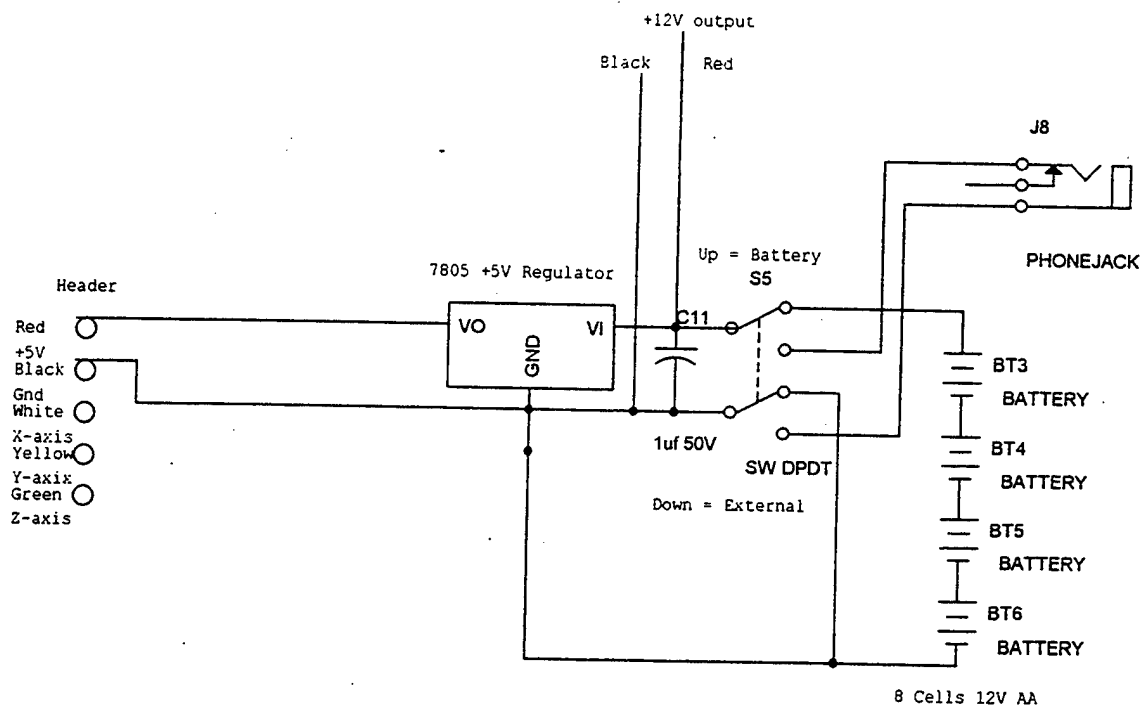


Figure D.1. Modified Avionics Package Wiring Diagram



## APPENDIX E. BLADE ANGLE VS. PULSE WIDTH DATA

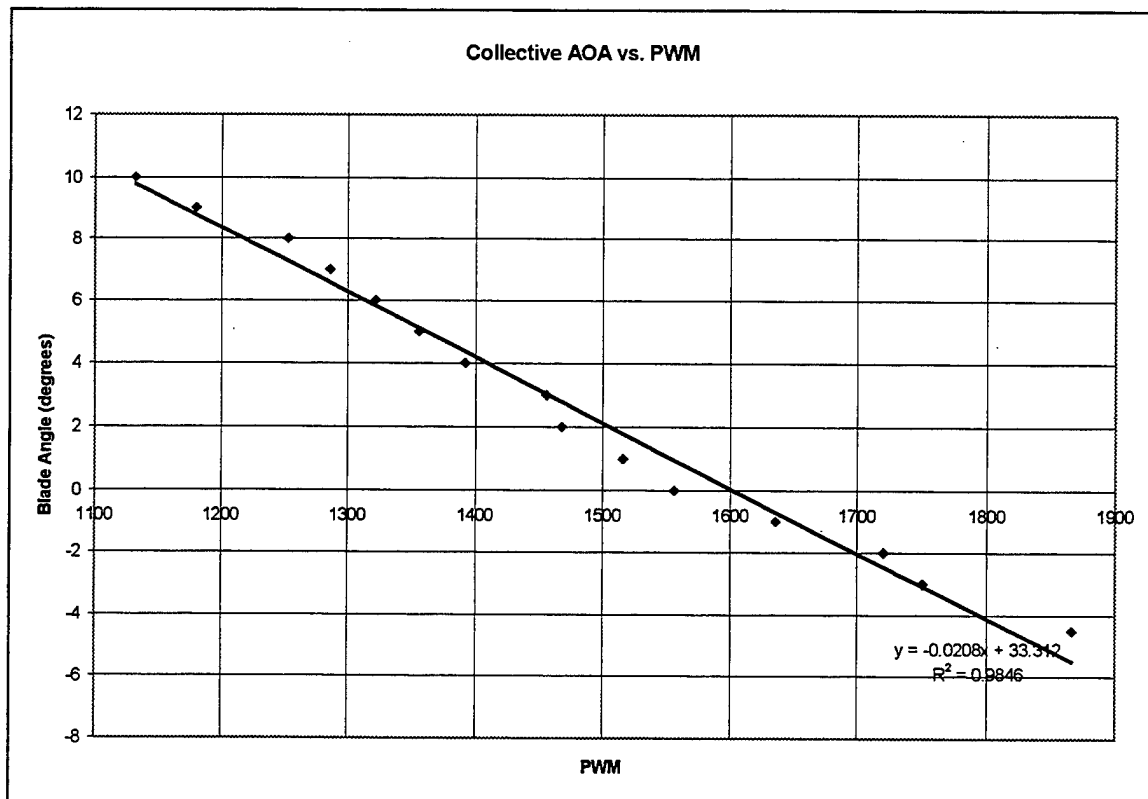


Figure E.1 Collective Blade Angle vs. Throttle PWM



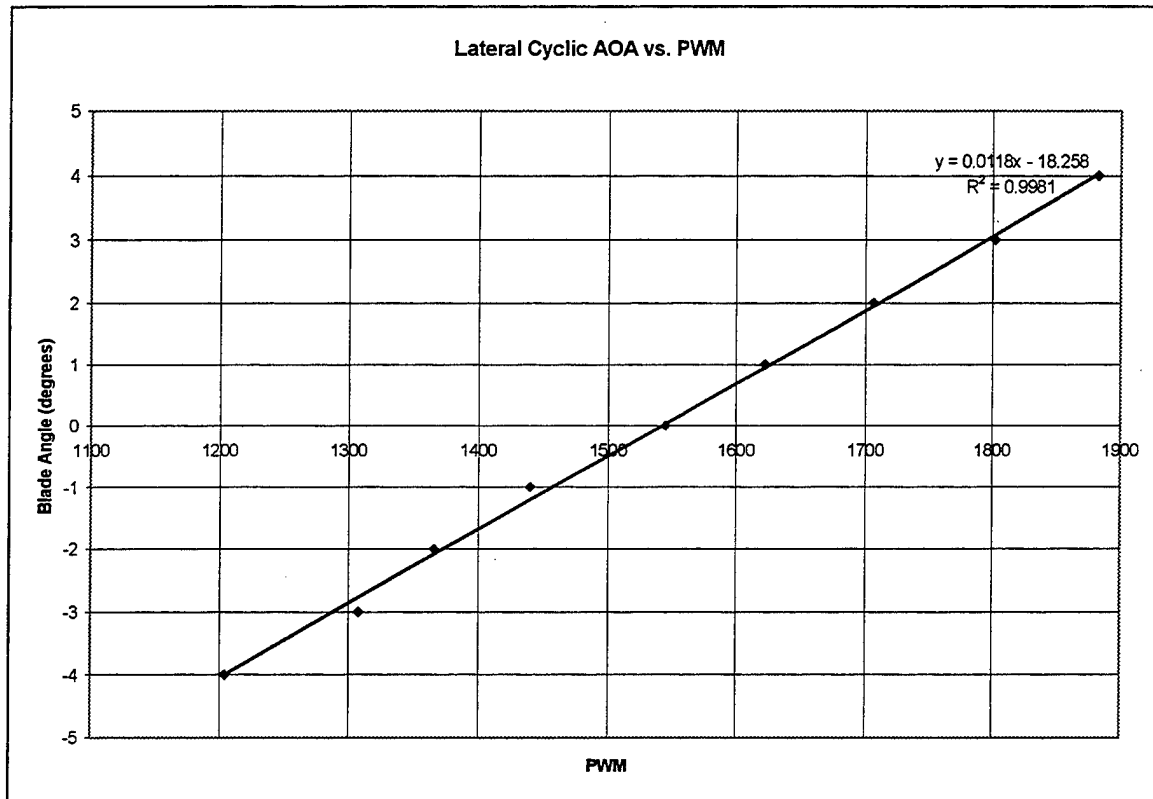


Figure E.2. Lateral Cyclic Blade Angle vs. Lateral Cyclic PWM

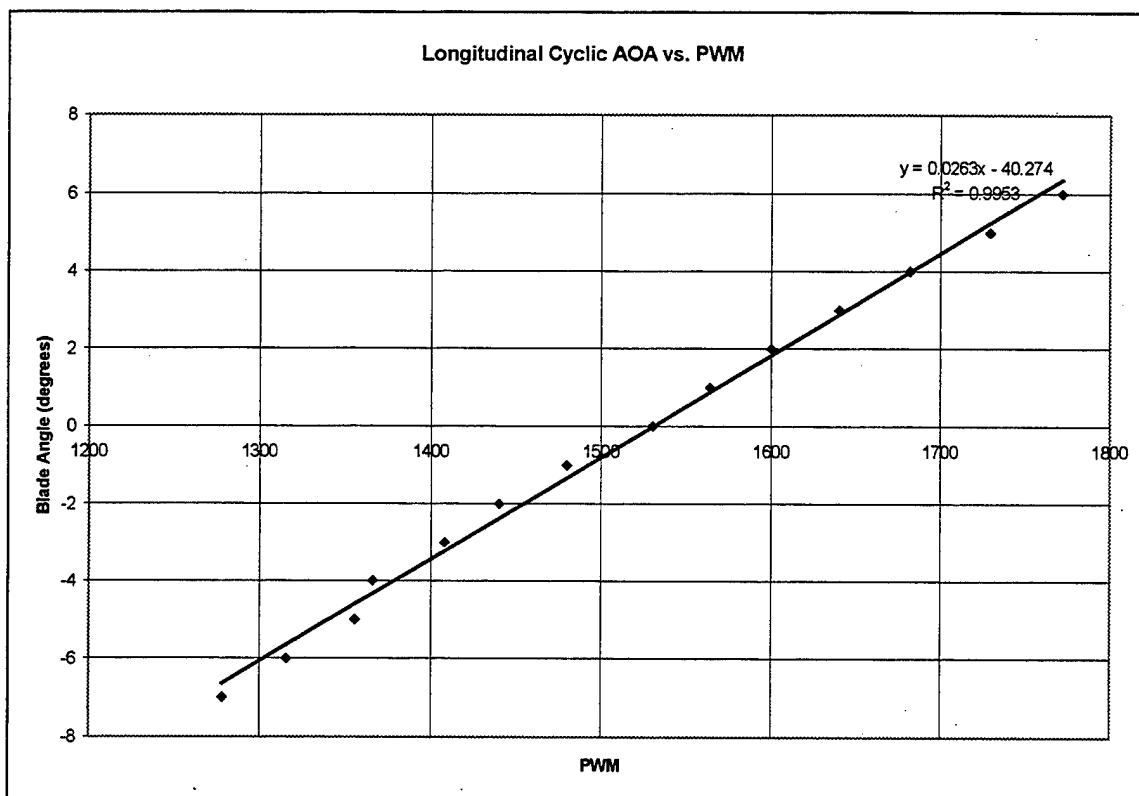


Figure E.3. Longitudinal Cyclic AOA vs. PWM

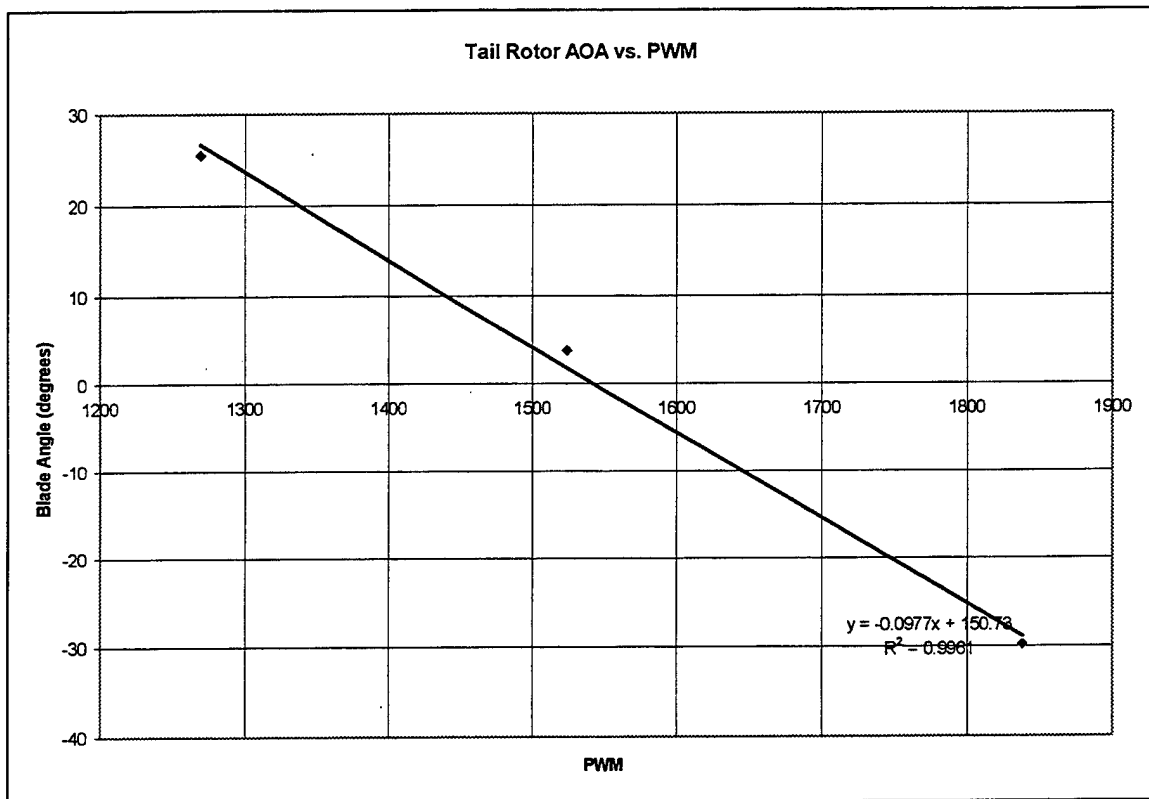


Figure E.4. Tail Rotor AOA vs. PWM

## APPENDIX F. REALSIM SUPERBLOCK DIAGRAMS

1-JUN-98

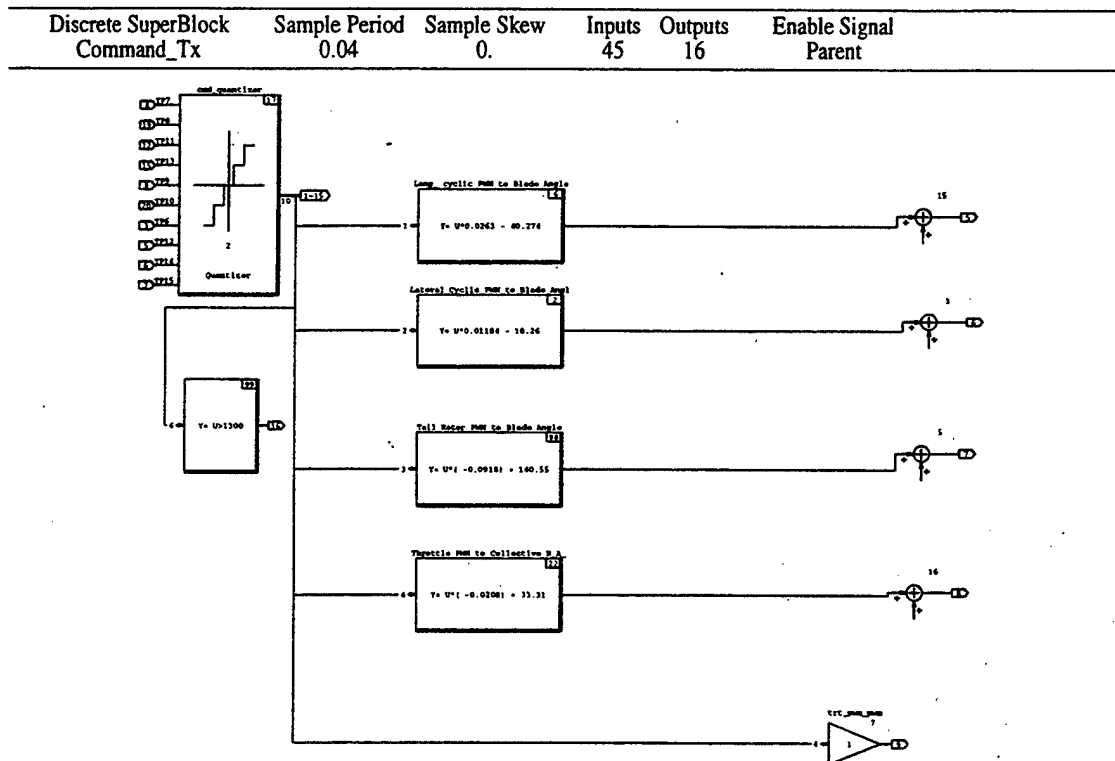


Figure F.1. PWM to Blade Angle Conversion Blocks

1-JUN-98

Discrete SuperBlock	Sample Period	Sample Skew	Inputs	Outputs	Enable Signal
A_D_IMU	0.04	0.	20	4	Parent

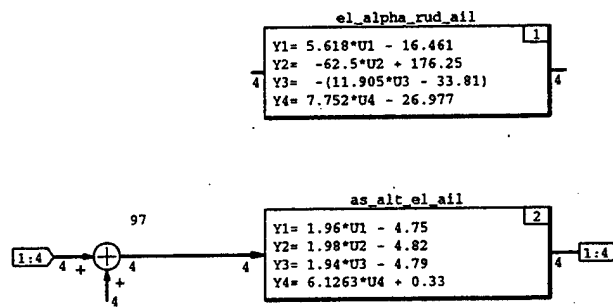


Figure F.2. Acceleration and Altitude Voltage Conversion Superblocks

## APPENDIX G. FLIGHT TEST DATA

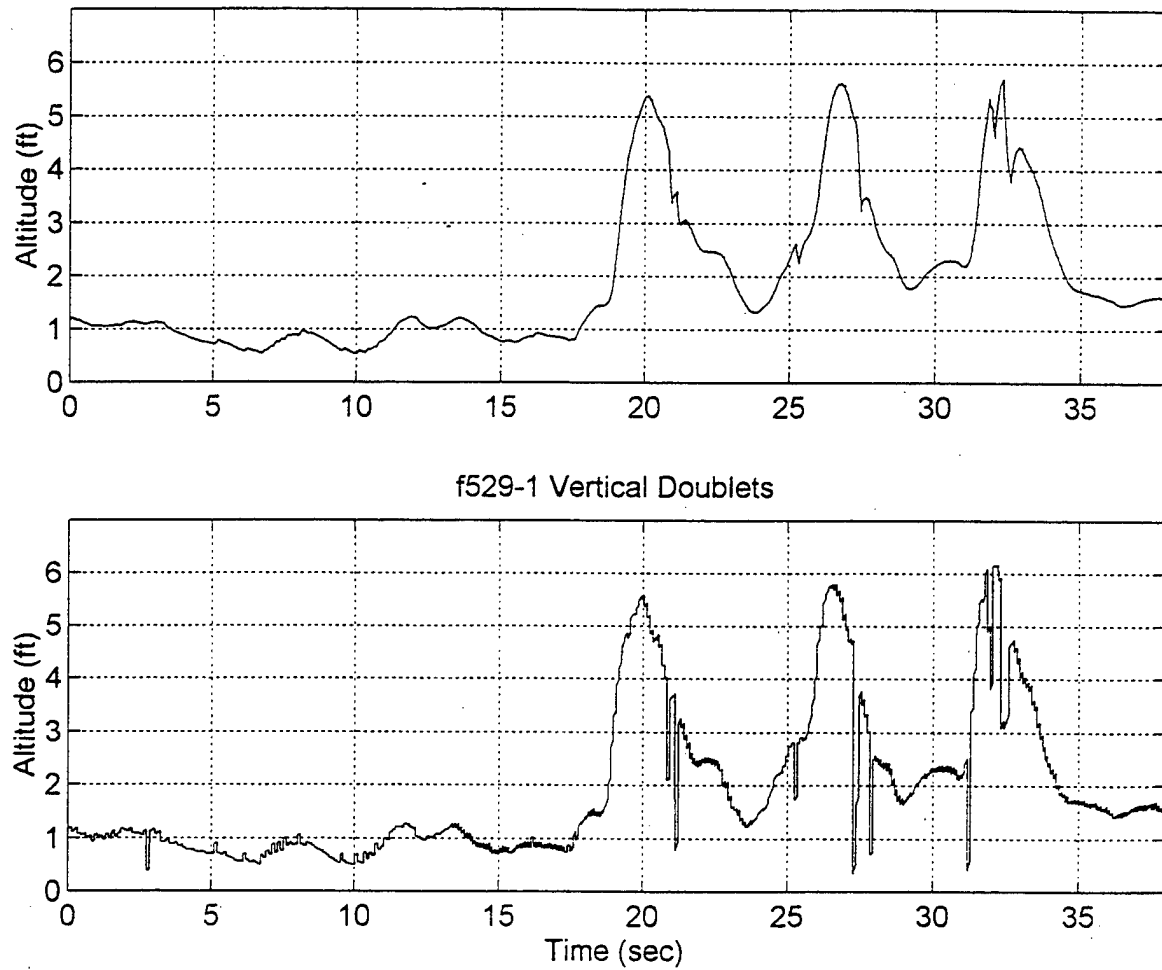


Figure G.1. SONALT Altitude During Vertical Doublets; Top: filtered, Bottom: raw

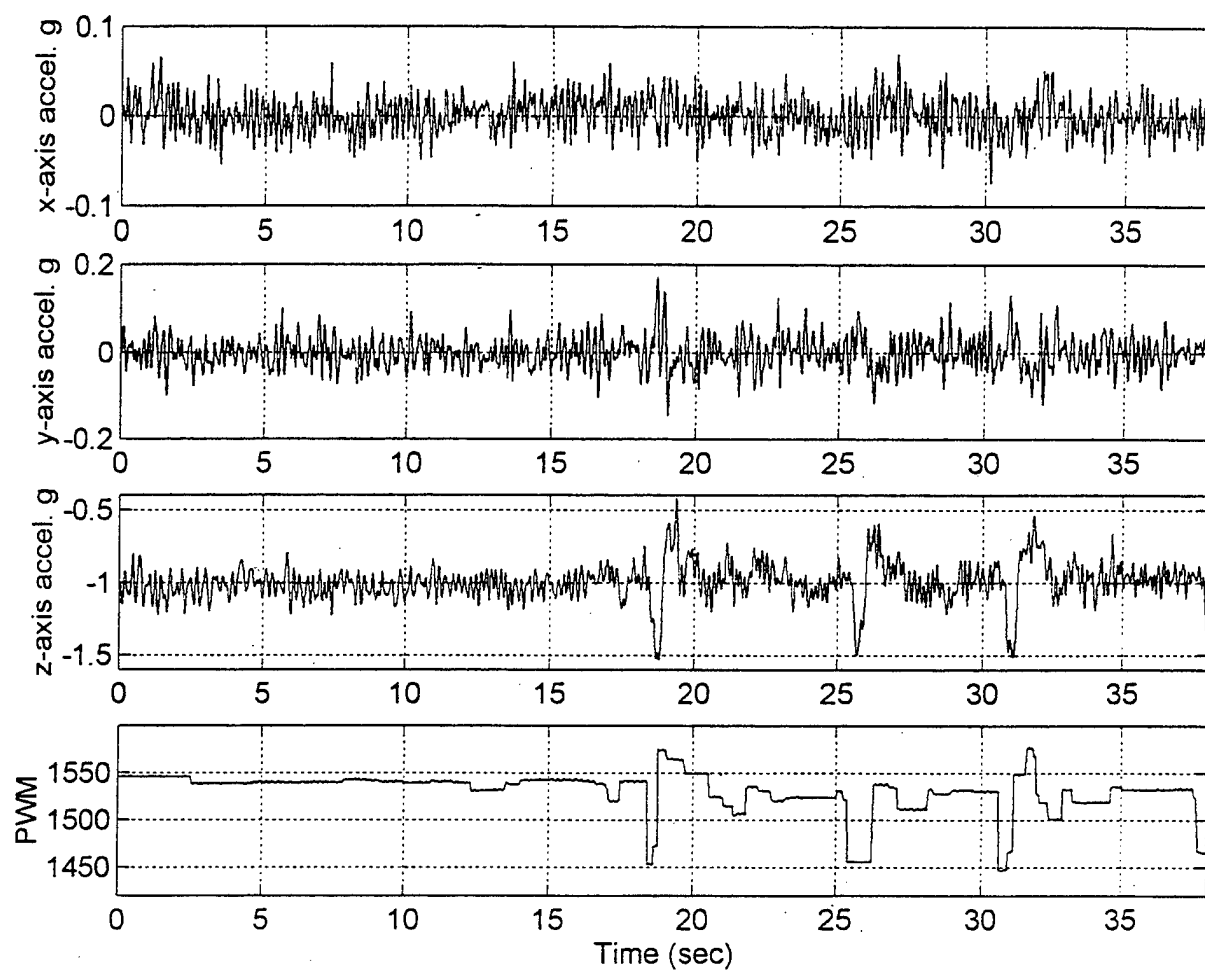


Figure G.2. Filtered Acceleration and Collective PWM Data During Vertical Doublets

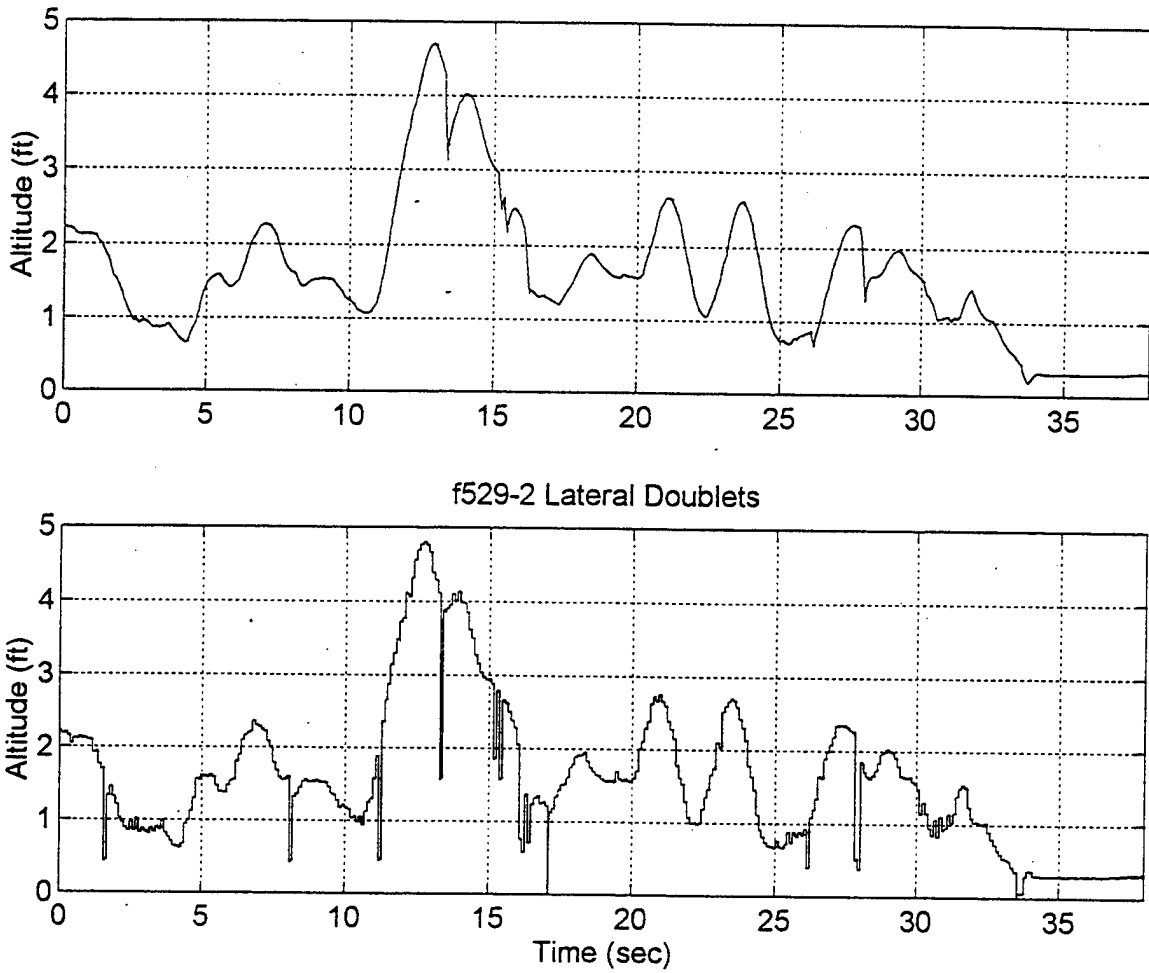


Figure G.3. SONALT Altitude During Lateral Doublets; Top: filtered, Bottom: raw



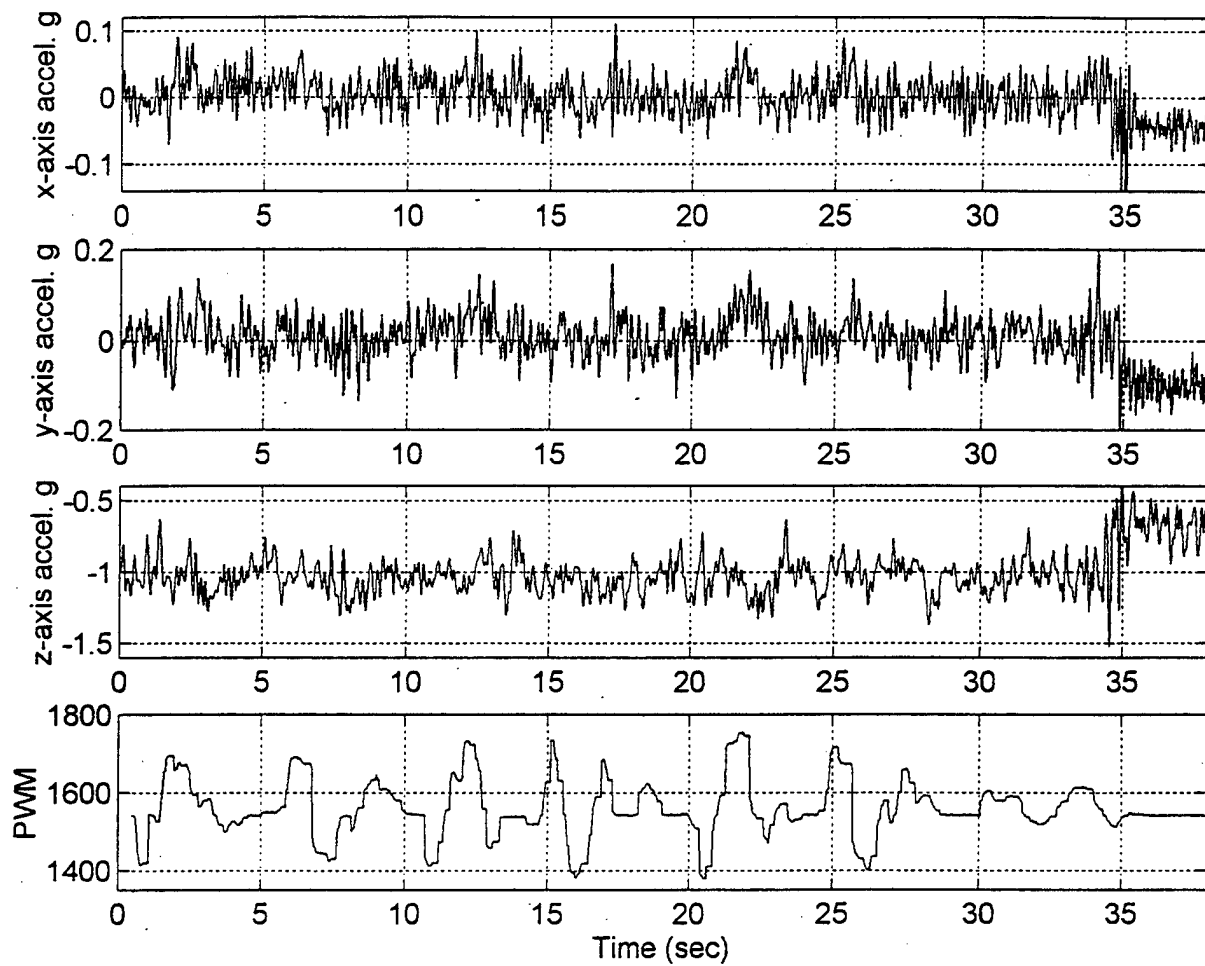


Figure G.4. Filtered Acceleration and Lateral Cyclic PWM Data During Lateral Doublets

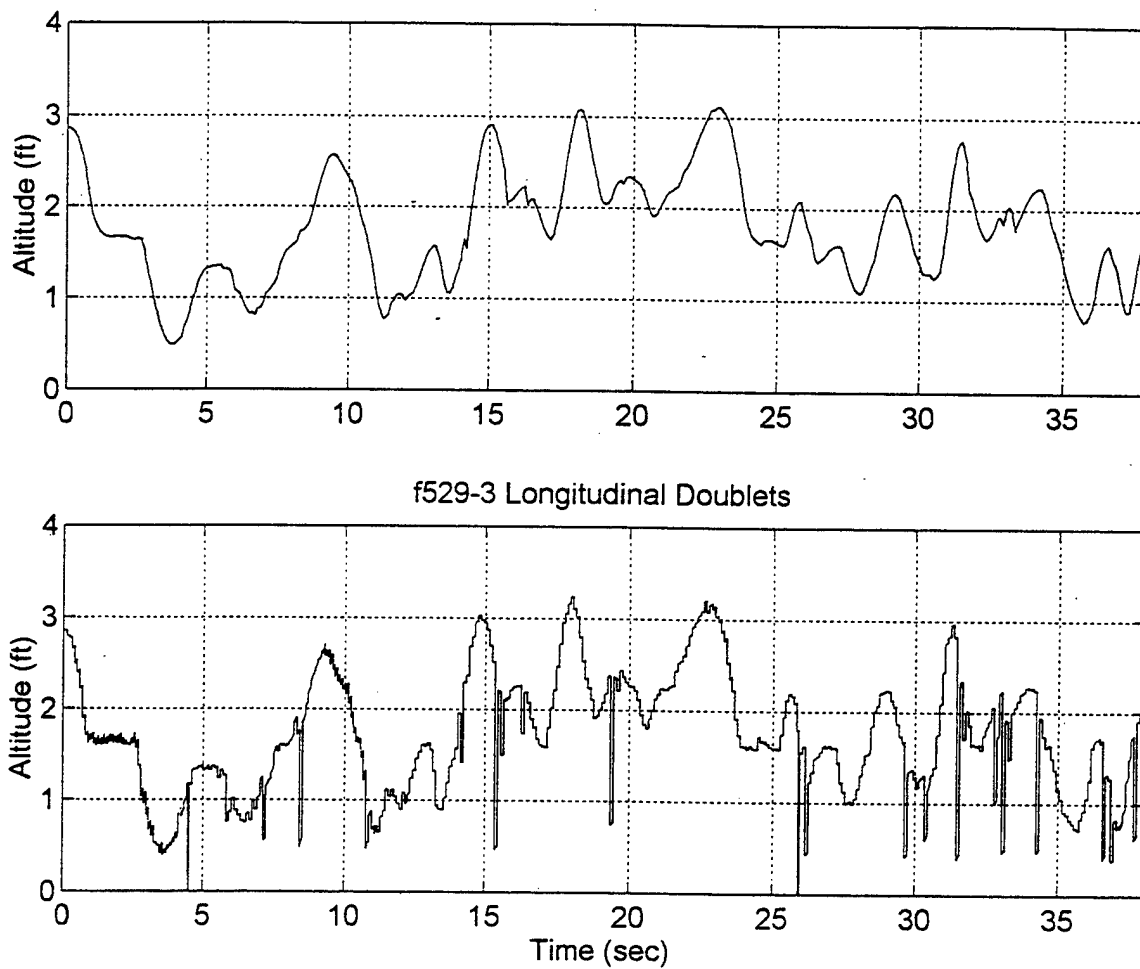


Figure G.5. SONALT Altitude During Longitudinal Doublets;  
Top: filtered, Bottom: raw

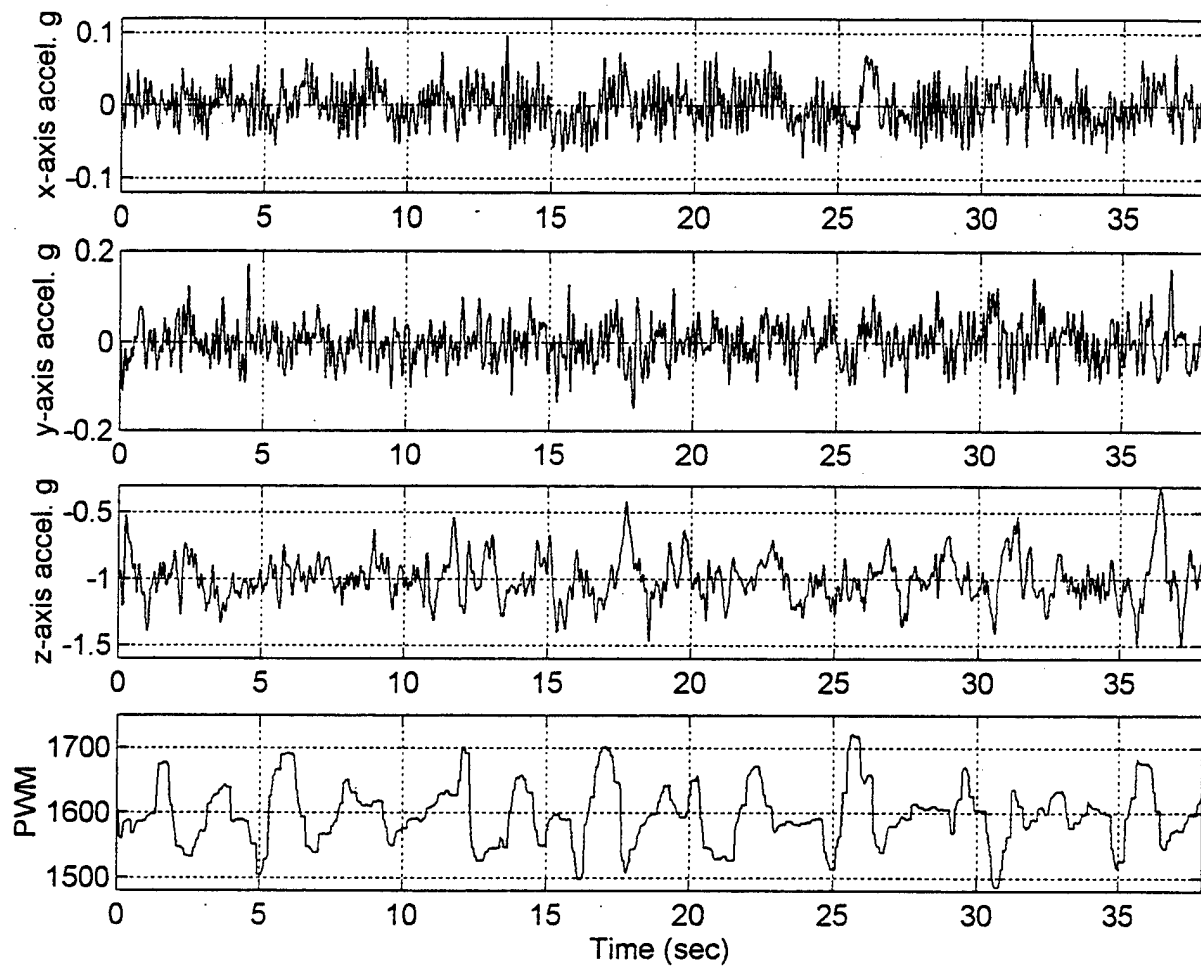


Figure G.6. Filtered Acceleration and Longitudinal Cyclic PWM Data During Longitudinal Doublets

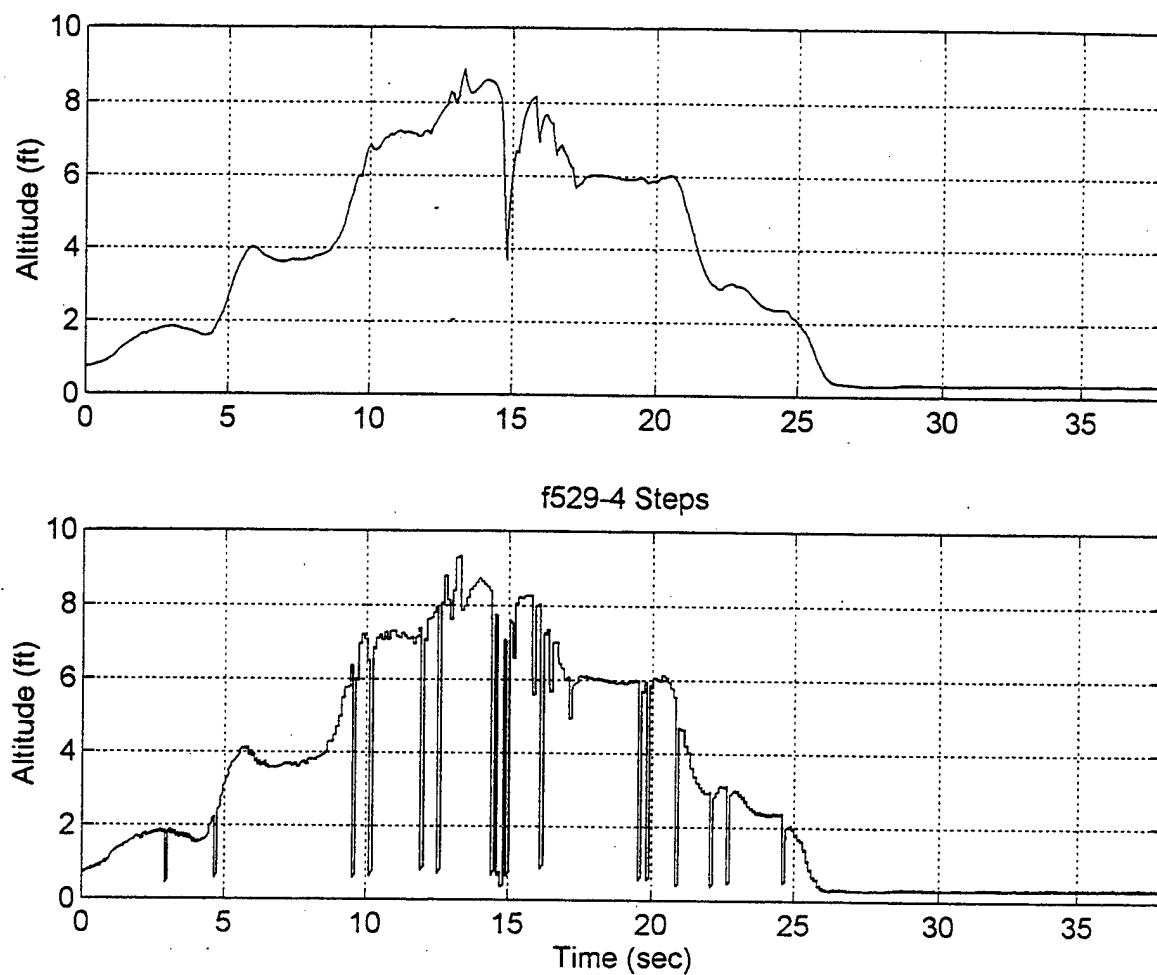


Figure G.7. SONALT Altitude During Vertical Steps;  
Top: filtered, Bottom: raw

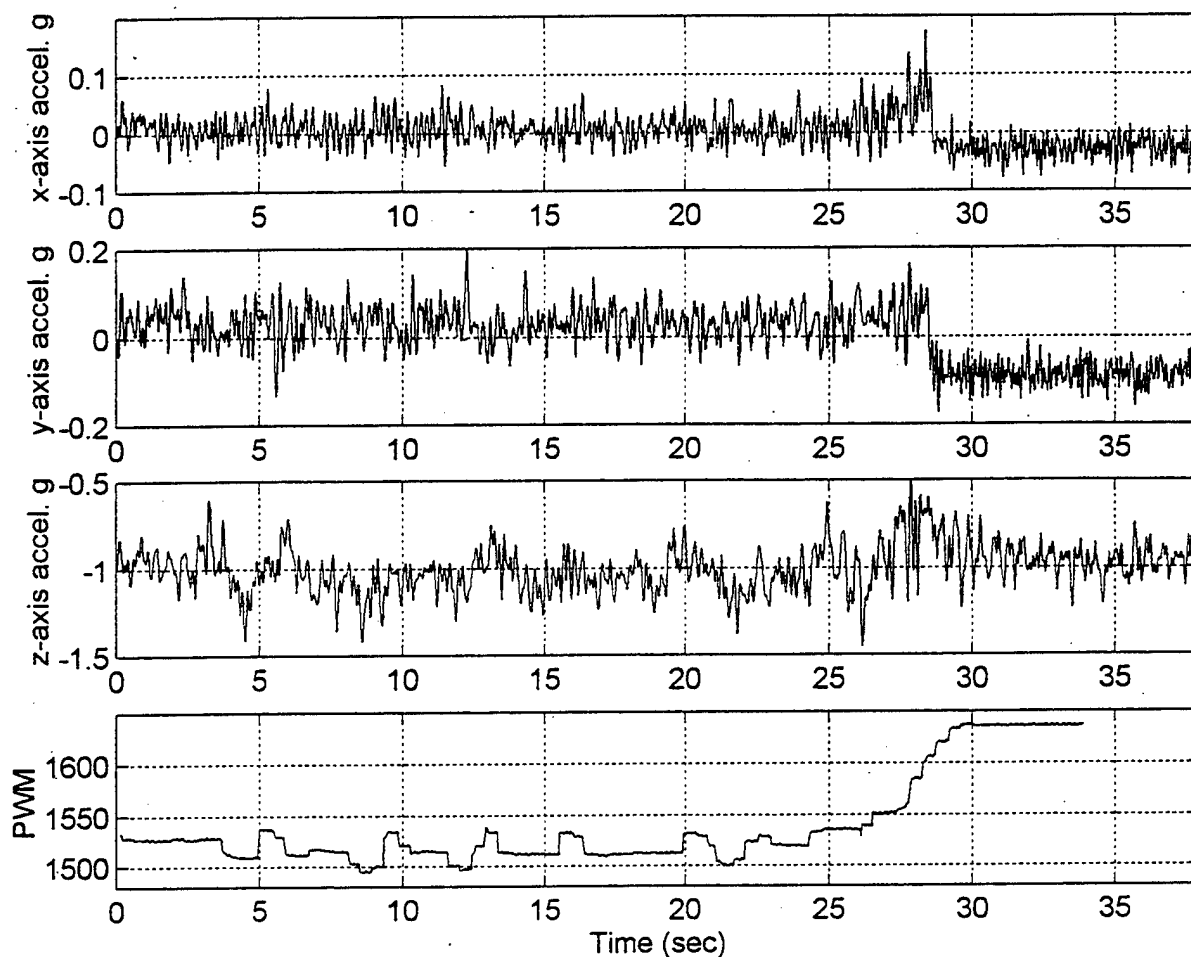
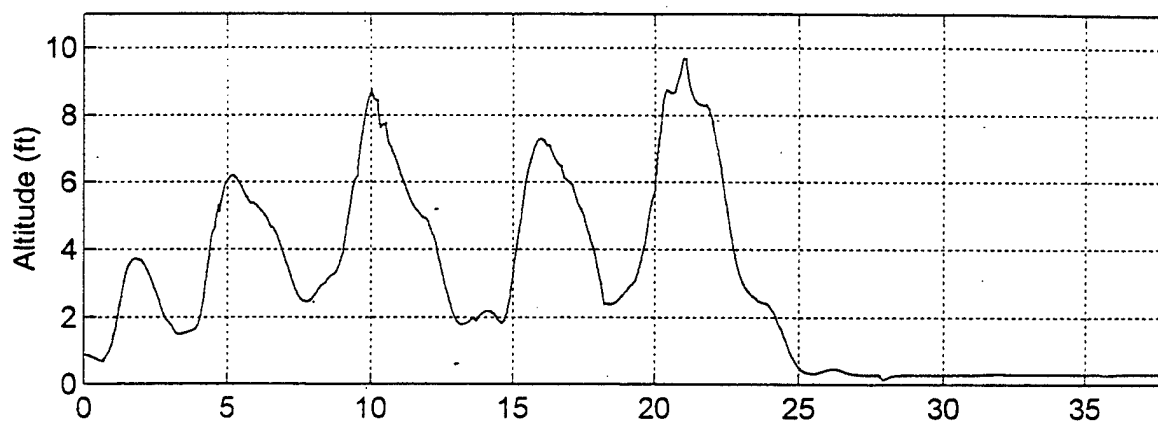


Figure G.8. Filtered Acceleration and Collective PWM Data During Vertical Steps



f529-5 Vertical Doublets

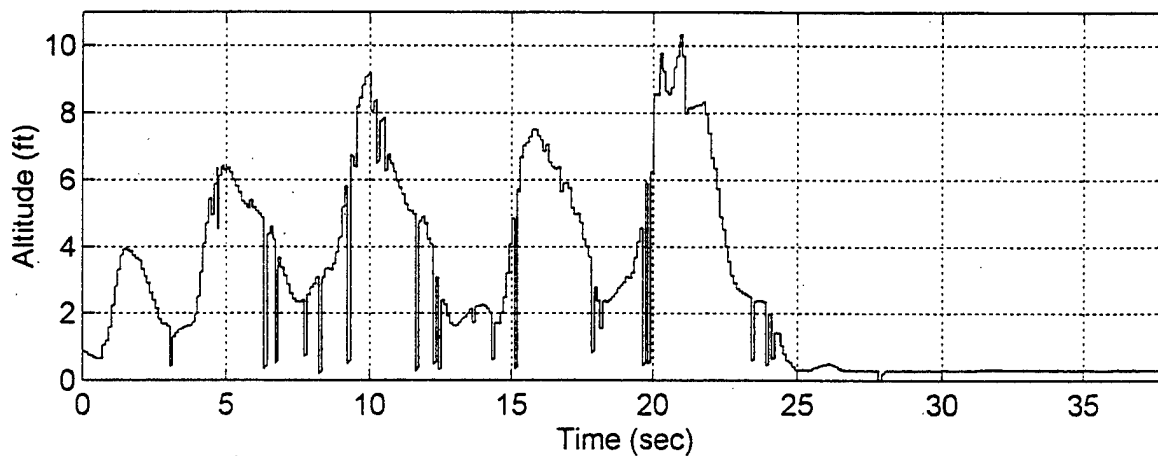


Figure G.9. SONALT Altitude During Vertical Doublets;  
Top: filtered, Bottom: raw

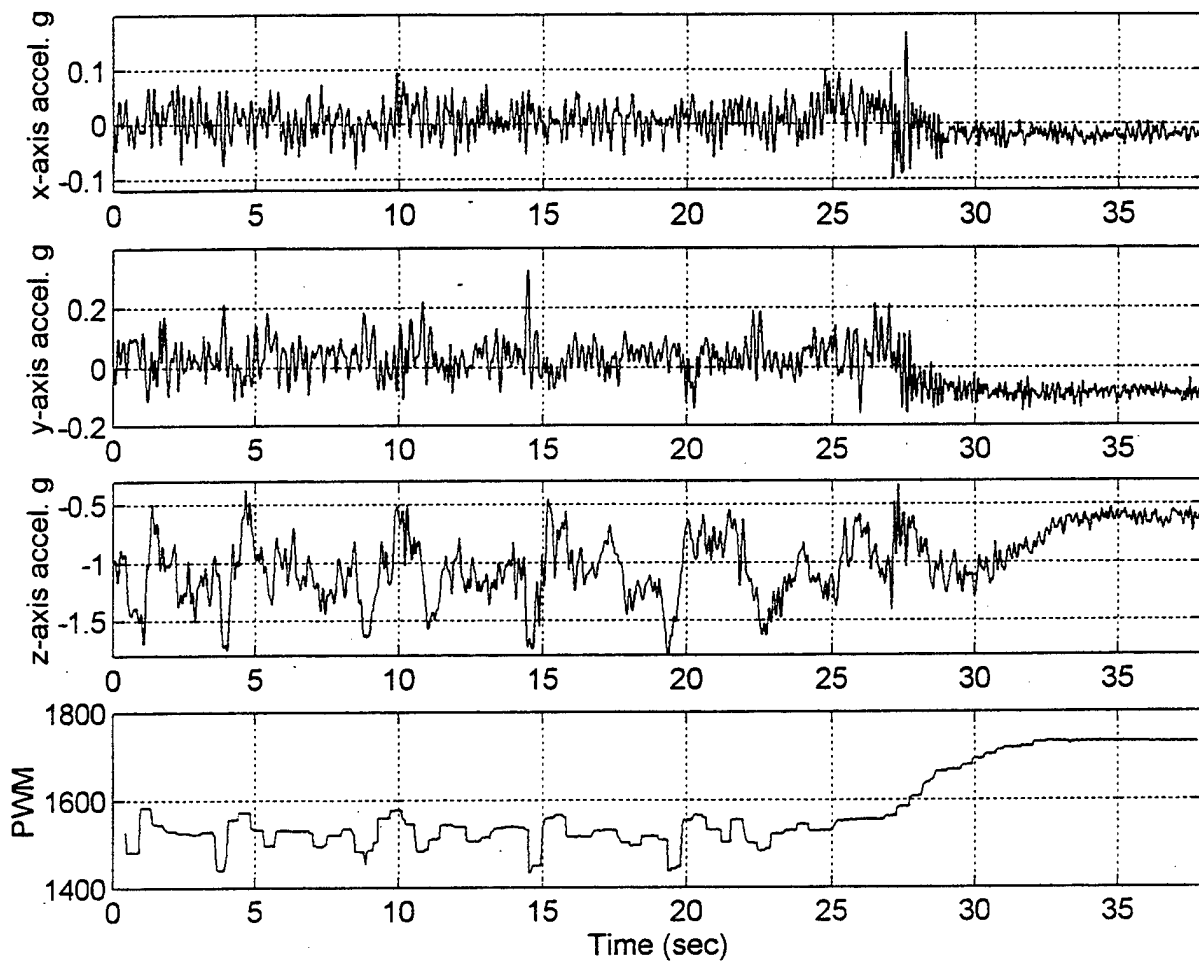


Figure G.10. Filtered Acceleration and Collective PWM Data During Vertical Doublets

```

t=linspace(0,38.46,7692);
% This code filters altitude data from the loaded file and creates a
% plot of the filtered data against time above the original data.
% 5/24/98 D.S. Greer

%load f2_523;
alt=f(:,4);
alt2=alt;
for i=2:size(alt)
    if alt(i)<1
        if alt(i-1)>1

            for j=i:i+25

                alt2(j)=alt(i-1)+(alt(i+26)-alt(i-1))/27*(j-i+1);

            end
        end
    end
    if i>8
        alt2(i)=mean(alt2(i-8:i));
    end
end

subplot(2,1,1)
plot(t,alt2,'r');grid
ylabel('Altitude (ft)')
axis([0,38,0,11])
subplot(2,1,2)
plot(t,alt,'b');grid
ylabel('Altitude (ft)')
xlabel('Time (sec)')
axis([0,38,0,11]);

```

Figure G.11. MATLAB Script for Digitally Filtering SONALT Data





## INITIAL DISTRIBUTION LIST

1. Defense Technical Information Center.....2  
8725 John J. Kingman Rd., STE 0944  
Ft. Belvoir, Virginia 22060-6218
  
2. Dudley Knox Library.....2  
Naval Postgraduate School  
411 Dyer Rd.  
Monterey, California 93943-5101
  
3. Dr. Russ W. Duren.....2  
Department of Aeronautics and Astronautics, Code AA/DR  
Naval Postgraduate School  
Monterey, California 93943-5101
  
4. Dr. Isaac I. Kaminer.....1  
Department of Aeronautics and Astronautics, Code AA/KA  
Naval Postgraduate School  
Monterey, California 93943-5101
  
5. Chairman.....1  
Department of Aeronautics and Astronautics, Code AA  
Naval Postgraduate School  
Monterey, California 93943-5101
  
6. Daniel S. Greer.....2  
1105 Leahy Rd.  
Monterey, California 93940